AERODYNAMIC CONFIGURATION DEVELOPMENT OF THE HIGHLY MANEUVERABLE AIRCRAFT TECHNOLOGY REMOTELY PILOTED RESEARCH VEHICLE

P. B. Gingrich, R. D. Child, and G. N. Panageas

Rockwell International
Los Angeles Aircraft Division
Los Angeles, California 90009

June 1977

Prepared for

NATIONAL AERONAUTICS AND SPACE ADMINISTRATION
Dryden Flight Research Center
Edwards, California 93523

1. Report No.	2. Government Accession No.	3. Recipient's Catalog No.
NASA CR-143841		

4 Title and Subtitle	5. Report Date
AERODYNAMIC CONFIGURATION DEVELOPMENT OF THE HIGHLY MANEUVERABLE AIRCRAFT TECHNOLOGY REMOTELY PILOTED RESEARCH VEHICLE	June 1977
	6. Performing Organization Code

7. Author(s)	8. Performing Organization Report No
P. B. Gingrich, R. D. Child, and G. N. Panageas	NA-76-865
	10. Work Unit No. 723-01-01

9. Performing Organization Name and Address	11. Contract or Grant No
Rockwell International Los Angeles Aircraft Division Los Angeles, California 90009	NAS4-2276
	13. Type of Report and Period Covered
12. Sponsoring Agency Name and Address	Contractor Report - Topical
National Aeronautics and Space Administration Washington, D.C. 20546	14. Sponsoring Agency Code H-972

15 Supplementary Notes

NASA Technical Monitor: Jerry L. Lockenour, NASA Dryden Flight Research Center

16. Abstract

The aerodynamic development of the highly maneuverable aircraft technology remotely piloted research vehicle (HiMAT/RPRV) from the conceptual design to the final configuration is presented. The design integrates several advanced concepts to achieve a high degree of transonic maneuverability. The purpose of this report is to present the analytical and experimental tools used in that development. The design was keyed to sustained maneuverability goals while other fighter-typical performance characteristics were maintained. Tests of the baseline configuration indicated deficiencies in the technology integration and design techniques. After substantial reconfiguring of the vehicle, and with improvements in the analytical methods, the subcritical and supersonic requirements were satisfied. Drag-due-to-lift levels only 5 percent higher than the optimum were obtained for the wind tunnel model at a lift coefficient of 1 for Mach numbers of up to 0.8. The transonic drag rise was progressively lowered with the application of nonlinear potential flow analyses coupled with experimental data.

17. Key Words (Suggested by Author(s))	18. Distribution Statement
Close-coupled canard Maneuverability Transonic flow	Unclassified - Unlimited Category: 02

19. Security Classif. (of this report)	20. Security Classif. (of this page)	21. No. of Pages	22. Price*
Unclassified	Unclassified	142	

For sale by the National Technical Information Service, Springfield, Virginia 22161

FOREWORD

The phase III HiMAT development was performed at the Los Angeles Aircraft Division of Rockwell International, Inc, with J. E. Kinnu serving as program manager. Contributors to the work reported here include: Configuration Aerodynamic Design - R. D. Child, G. N. Panageas; Linear Theory Design - K. M. Dunn, R. S. Nishida, G. A. Freeman; Transonic Design - P. B. Gingrich, T. P. Goebel, and E. Bonner.

Technical assistance by the following is gratefully acknowledged: W. F. Ballhaus and R. Bailey of NASA Ames Research Center; R. T. Whitcomb and W. P. Henderson of NASA Langley Research Center; T. G. Ayers of NASA Dryden Flight Research Center; and N. D. Malmuth and W. D. Murphy of Rockwell Science Center.

Page intentionally left blank

Page intentionally left blank

TABLE OF CONTENTS

LIST OF ILLUSTRATIONS

LIST OF ILLUSTRATIONS (continued)

LIST OF ILLUSTRATIONS (continued)

LIST OF ILLUSTRATIONS (continued)

LIST OF TABLES

AERODYNAMIC CONFIGURATION DEVELOPMENT OF THE HIGHLY MANEUVERABLE AIRCRAFT TECHNOLOGY REMOTELY PILOTED RESEARCH VEHICLE

By P. B. Gingrich, R. D. Child, and G. N. Panageas
Rockwell International
Los Angeles Aircraft Division
Los Angeles, Calif.

SUMMARY

The development of the highly maneuverable aircraft technology remotely piloted research vehicle (HiMAT/RPRV) from the conceptual design to the final configuration is presented to assess the technologies required to achieve a high degree of transonic maneuverability and to evaluate the state-of-the-art analytical methods which were utilized. The performance goals proposed by NASA for the advanced fighter concept were a sustained 8g turn at M = 0.9 and an altitude of 9144 m, and a mission radius of 300 n mi. Additionally, supersonic acceleration capability would not be compromised. Preliminary trade studies established a 7740 kg fighter baseline along with a 44% scale RPRV that would allow a low-risk demonstration of the advanced technologies. Tests of the baseline configuration indicated deficiencies in the technology integration and in the design techniques. After substantial reconfiguring of the vehicle, and with improvements in the analytical methods, the subcritical and supersonic requirements were satisfied. A high level of efficiency for subsonic conditions was realized with the linear theory optimization techniques and the variable camber system. Drag-due-to-lift levels only 5% higher than $1/\pi AR$ were obtained for the wind tunnel model at a lift coefficient of 1 for Mach numbers of up to 0.8. The transonic drag rise was progressively lowered with the application of nonlinear potential flow analyses coupled with experimental data. Projections for the fighter concept indicated a maneuvering performance of 7.3g at the design point.

INTRODUCTION

The examination of the technologies required for the next generation of fighter aircraft has been pursued in recent years with the objective of increasing maneuvering performance. Additionally, it was envisioned that an advanced fighter designed for superior transonic maneuverability would not compromise mission radius requirements or supersonic acceleration capability. With these

objectives proposed, NASA initiated a comprehensive program to evaluate high-maneuverability technologies, define advanced concepts, and to ultimately design and build a demonstration vehicle.

The highly maneuverable aircraft technology (HiMAT) program involved three phases. The first phase was concerned with the evaluation of various high-maneuverability technologies and the definition of preliminary designs which would best integrate the features of these technologies. In this phase, analytical studies and a review of experimental results relative to close-coupled canards, winglets, the jet flap, and variable camber systems formed a basis for evaluating various technologies and determining a configuration which would incorporate the positive interference effects associated with these concepts. In addition to the aerodynamic technologies, the initial HiMAT program phases considered propulsion, structures, and flight control system technologies that would, in the conceptual design, best meet the design objectives for enhanced maneuverability.

The second phase of the HiMAT program involved a more detailed analysis of the advanced technologies and a definition of a baseline advanced fighter concept. As part of the overall NASA program, an RPRV was defined to demonstrate the technologies embodied in the fighter. The RPRV is a scaled configuration which provides a low-risk, low-cost, test vehicle.

The third phase of the HiMAT development encompassed the detailed refinements to the baseline necessary to meet the transonic maneuver goal as well as provide acceptable low-speed, transonic cruise, and supersonic acceleration capabilities. This phase continued with the definition of the detailed RPRV structure leading to the construction of the test vehicle. The first part of this phase, the aerodynamic configuration refinement, is the subject of this report. An objective of the design process was to utilize the available theoretical design and analysis methods to their fullest extent in order to provide guidelines for future configuration developments and to minimize the wind tunnel test period. Throughout the design evaluation presented here, the successful as well as nonproductive approaches will be examined and an evaluation of the shortcomings of the theoretical methods will be discussed.

The first section presents an overview of the HiMAT/RPRV development. The specific performance goals to be considered along with the design constraints are presented. The baseline technology features are discussed to indicate their particular function and interactive effects. These concepts, close-coupled canard, jet flap, winglet, blended wing-body, variable camber system, reduced static stability, and design optimization techniques were defined on a preliminary basis in the early program phases. Modification of these concepts and even the analytical methods were required during the detailed

design/test cycle as knowledge was gained relative to the off-design characteristics of the various technologies and the requirements for efficient transonic operation. This evolution process is summarized in the first section and detailed in the subsequent discussion of the configuration development.

Detailed descriptions of the analytical methods and their function in the design process follow the HiMAT program summary. Next, the detailed design process is discussed. This consists of the linear theory initialization, the modifications for transonic flow through analytical and empirical means, and the effects of aeroelastic tailoring on the aerodynamic design. Characteristics of the evolved configuration are then presented to evaluate the overall success in meeting the design objectives.

NOMENCLATURE

a	Speed of sound
AR	Aspect ratio
ARC	Ames Research Center
B	Body
b	Span
C	Canard or Chord
CG	Center of gravity
$\bar{c}$	Mean aerodynamic chord
C_D	Drag coefficient
C_{D_L}	Drag due to lift coefficient
C_d	Section drag coefficient
C_L	Lift coefficient
C_l	Rolling moment coefficient

C_ℓ	Section lift coefficient
C_M	Moment coefficient
C_m	Section moment coefficient
C_n	Yawing moment coefficient
C_p	Pressure coefficient
C_p^*	Critical pressure coefficient
C_Y	Side force coefficient
D	Drag
e	Span load efficiency factor
H	Singularity strength
h	Altitude
INBD	Inboard
L	Lift or Body length
LRC	Langley Research Center
M	Mach number
NAAL	Rockwell low-speed wind tunnel
N_Z	Normal load factor
OUTBD	Outboard
PDR	Preliminary design review
POI	Preliminary operating instructions
P_S	Specific excess power
R_{e_c}	Chord Reynolds number

S, S_{REF}	Wing area
SEP	Separation
T	Thrust
TOGW	Takeoff gross weight
TWT	Rockwell transonic wind tunnel
t	Thickness
U, V, W	Velocity components
UDP	Unified distributed panel theory
V	Vertical stabilizer
W	Weight or Wing
X, Y, Z	Cartesian coordinates
α	Angle of attack
β	Angle of sideslip
γ	Ratio of specific heats
Δ	Increment
δ	Deflection or Thickness to chord ratio
δ^*	Displacement thickness
ϵ	Twist
η	Wing semispan fraction
η_C	Canard semispan fraction
θ	Polar angle
Λ	Sweep

Φ	Velocity potential
ϕ	Perturbation velocity potential

Subscripts

AVG	Average
c	Camber
cp	Center of pressure
DES	Design
l	Lower
max	Maximum
u	Upper
w	Wave
x, y, z	Partial differentiation with respect to X, Y, Z
α, β	Differentiation with respect to α or β
$\perp$	Perpendicular
∞	Free-stream conditions

HiMAT CONFIGURATION DEVELOPMENT

The objectives of the HiMAT program are outlined in order to indicate the advanced configuration concepts required to meet the aerodynamic performance goals. The baseline technologies that were selected as a result of analytical and experimental studies are presented along with a summary of the configuration development that refined the baseline concept.

Primary Design Objective

The primary design objective is to enhance the maneuverability of the advanced fighter concept to the point where a sustained 8g turn at $M_\infty = .9$, h = 9144m may be achieved while maintaining a 300 n mi mission radius

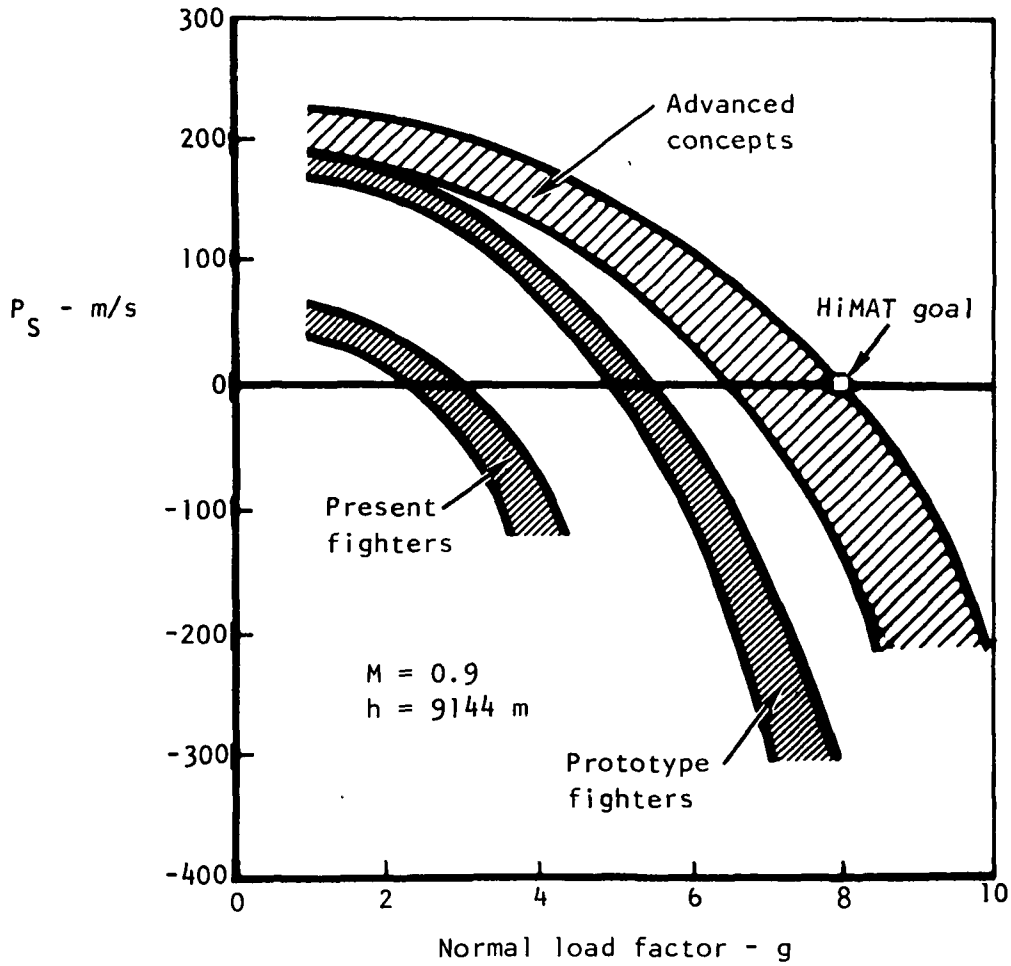

Figure 1. - HiMAT maneuvering performance objective.

capability. The relation of this steady-state maneuver goal to state-of-the-art fighter performance is illustrated in figure 1. To realistically achieve this goal requires high efficiency at high lift coefficients in order to decrease the slope of the P_S versus load factor relationship. The alternative brute force approach of increasing thrust-to-weight ratio or decreasing wing loading becomes untenable for this performance goal and is incompatible with the other design objectives including, in particular, the range requirement. Thus, the solution will require the examination, refinement, and proper integration of advanced technologies.

Design Requirements and Constraints

To achieve a practical design, all requirements must be properly balanced so that off-design performance is not severely degraded. In addition to the need for efficient subsonic cruise there is also a supersonic dash requirement. The critical design considerations are:

(1) Maneuver goal, 8g, $P_S = 0$ at $M_\infty = .9$, h = 9144m

(2) Efficient subsonic cruise, 300 n mi range

(3) Efficient supersonic cruise, wave drag $C_{D_W} = 0.02$ to 0.025

(4) Low-speed $C_{L_{max}} = 1.6$ to 2.0

(5) Stability and control with reduced static stability (adequate control must be provided, particularly near the flight envelope boundaries)

(6) Maximum Mach number $M_\infty = 1.6$

(7) Maximum load factor $N_Z = 12$

(8) 1974 propulsion technology level

The balancing of the first three considerations involved a compromise in wing loading between the maneuver requirement, low wing loading, and supersonic cruise requirement, high wing loading. The configuration sizing studies of phases I and II prescribed a wing loading of the order W/S = 2400 to 2650 N/m^2. For the maneuver condition, the requirement for high efficiency, increased L/D, at high lift coefficients, $C_L \sim 1.1$, provides a selection criteria for assessing the various high-maneuverability technologies.

Reference Technology Level

The high-maneuverability concepts associated with the configuration arrangement and the theoretical design and analysis methods are the technologies which are integrated into the overall design process to satisfy the mission objectives. A description of the baseline high-maneuverability technologies and the aerodynamic design methodology is presented in the following.

Configuration arrangement concepts. - All major high-maneuverability technologies were evaluated in phases I and II. The screening process identified those concepts which enhanced maneuvering performance and range while providing positive interaction effects when integrated into the configuration. These technologies are presented in table I along with the features that affect their utilization.

Close-coupled canard: The close-coupling effects of the canard have several benefits for achieving high lift efficiency as detailed in references 1 and 2. The canard-induced downwash on the wing, figure 2, results in a redistribution of the loading. The reduction of the inboard wing loading more than compensates for the upwash on the outer wing if the design is properly integrated. As a result of the load redistribution, for a given twist and camber, separation can be delayed for the highly loaded outer wing. For moderate lift coefficients, a corresponding wing without canard configuration could be designed for equal performance but at the expense of greater structural deformation. At lift coefficients where separation is present, the vortex lift of close-coupled canard systems can result in favorable induction effects which increase the lift above that of a weakly coupled system. Several investigations, utilizing a unique two-balance system, have shown the results of favorable wing-canard interference varying several configuration variables. The trend of these results (refs. 3, 4, 5, and 6) formed a solid foundation for the HiMAT development.

For the HiMAT application, some typical results for the effect of the canard on lift and drag are shown in figure 3. At lift coefficients where separation occurs on the wing, the flow for the wing-canard system is still attached. This must be qualified as noted previously, since a wing alone design could achieve similar performance but with increased structural deflection (twist) requirements. The same consideration holds for the drag, figure 3. This was a wing-canard design, the design lift being effectively higher than the wing alone configuration, so the results must be viewed in this context.

Some of the interactive aspects of the close-coupled canard relate to its function as a trimming surface. With a jet flap, the full potential of the super circulation effects can be realized without adverse trim requirements.

TABLE I. - BASELINE TECHNOLOGY

High-maneuverability design concepts	Technology features
Vortex lift	Blended wing-body/strakes Close-coupled canard
Reduced trim	Reduced static stability Self-trimming configuration Canard
Propulsive lift	Jet flap Flight propulsion control coupling
Optimized section contours	Supercritical airfoil Variable camber
Optimized twist	Composite materials
Reduced wetted area	Reduced static stability Winglet directional stability input

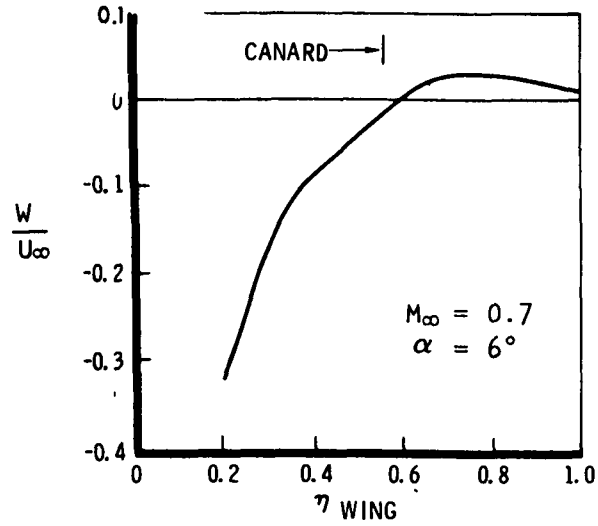

Figure 2. - Calculated canard downwash on wing plane.

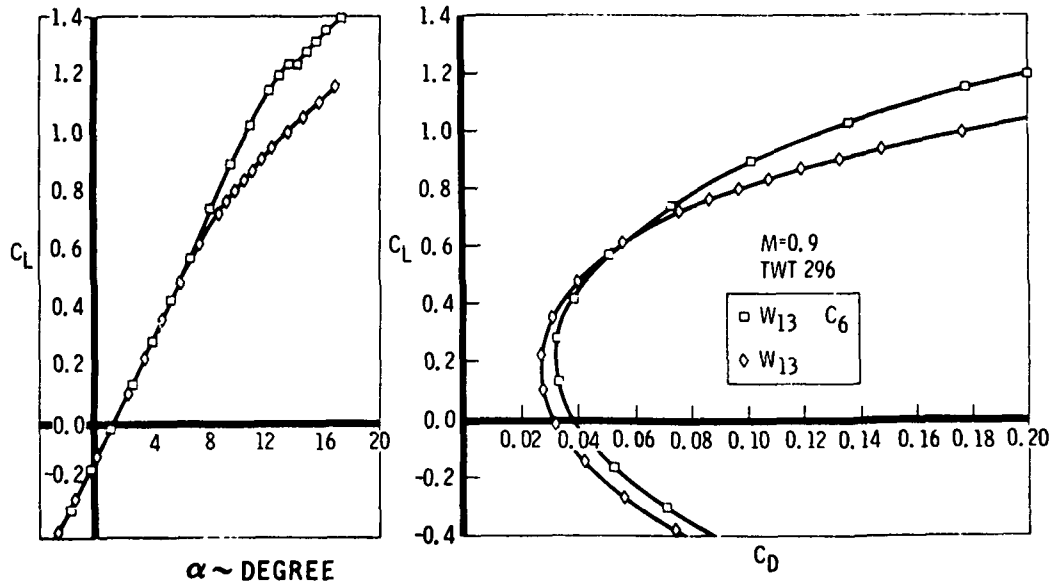

Figure 3. - Effect of close-coupled canard.

In conjunction with the wing or jet flap, the capability of direct lift exists. With canard dihedral, direct side force may be obtained with simultaneous rudder and canard elevon deflections. Interest in these aspects arose from the improved weapons aiming capability with direct lift and side force.

Winglets: The winglet simultaneously reduces the vortex drag while allowing reductions in vertical tail size and thus skin friction drag. The directional stability input is the foremost consideration since, for induced drag reasons alone, adding the additional area as wing tip extensions is more effective. The additional loading at the wing tip (figure 4) and on the winglet may be utilized to increase aeroelastic deformation to achieve the required twist. The benefit for reduced drag exists at lift coefficients where the reduced vortex drag compensates for the increased skin friction drag as shown in figure 4. The attractiveness of this concept at the transonic maneuver point is reduced unless the production of shock waves due to the wing-winglet interference can be minimized. However, throughout the flight regime, the directional stability input of the winglet will be effective. This input, illustrated in figure 4, allows reduction in the vertical tail size and consequently reduced skin friction drag.

Blended wing-body/strakes: The blended wing body is used in this context to provide a capability for incorporating vortex strakes between the body and wing proper. The strakes increase the vortex lift at high angles of attack, ultimately increasing the maximum lift. The nonlinear moment characteristics are adaptable to the jet-flap concept with regard to the associated control capabilities but otherwise these characteristics must be carefully integrated if reduced static stability is utilized.

Jet flap: The jet flap or two-dimensional nozzle can increase the high lift efficiency through localized supercirculation effects. For a partial span jet flap the increased inboard wing loading will delay the impact of separation associated with the outboard wing. The removal of the Kutta condition moderates the trailing edge recompression. Thus, the occurrence of strong shocks and separation can be reduced through proper integration of the jet flap into the design.

Reduced static stability: At a particular design point, the transonic maneuver condition for example, favorable trim requirements may be prescribed by designing the configuration to have negative static stability at subsonic conditions. Small trim drag may be maintained over the Mach number range and the skin friction drag is reduced through reductions in trim surface size. Adequate control must be provided at the boundaries of the flight envelope, in particular, at low speeds and high angles of attack where the manifestation of vortex lift nonlinearities is greatest.

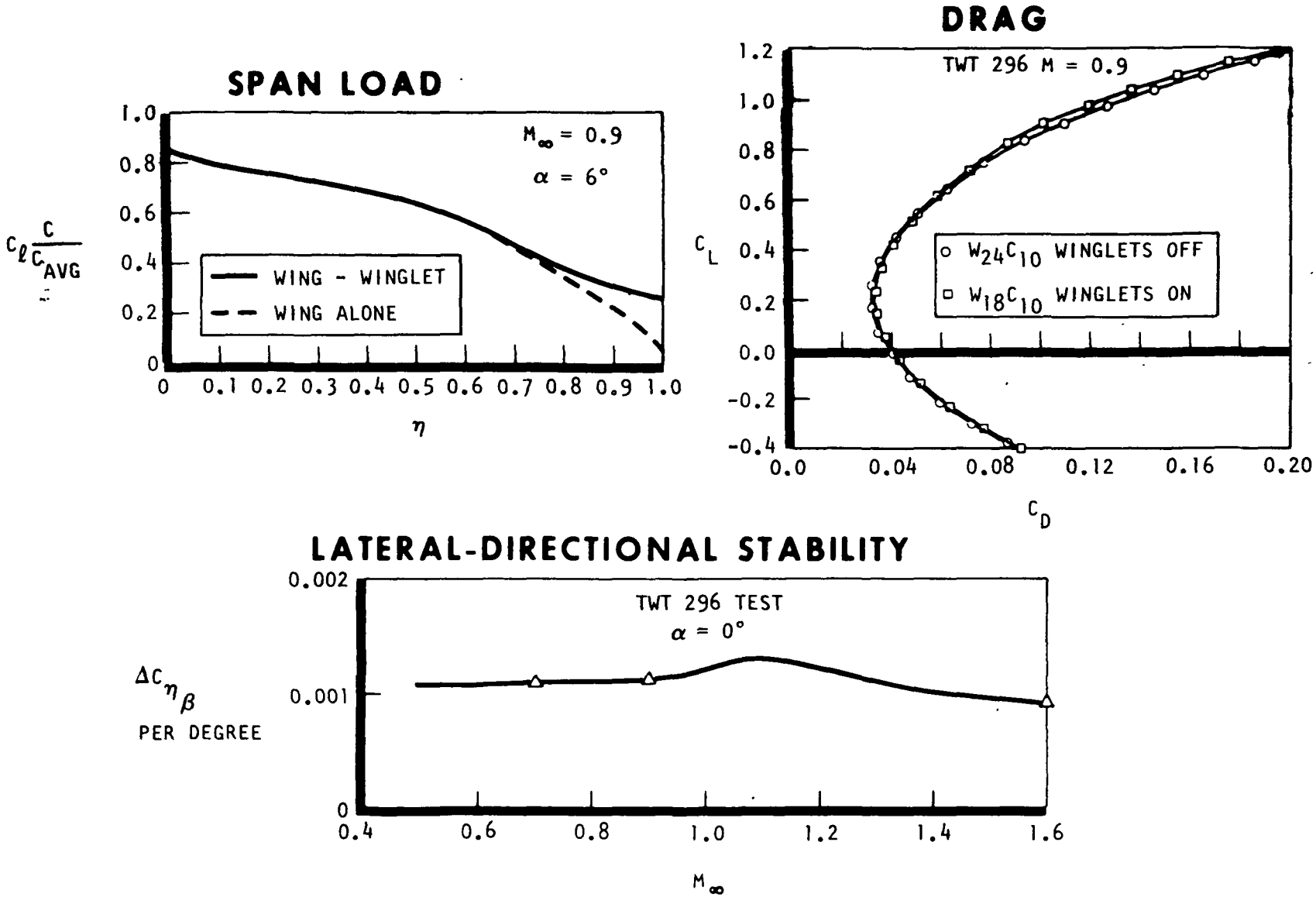

Figure 4. - Effect of upper surface winglet.

Variable camber system: Minimum drag due to lift may be obtained over a wide range of lift coefficients by a camber system which varies the design lift. This concept includes mechanical leading edge variable camber and aeroelastically tailored lifting surfaces as illustrated in figure 5. The aeroelastic effects are confined to prescribed deflections due to bending which, for a swept wing, produces a twist increment. The variable camber system attempts to reduce, at high loadings, the leading edge pressure peaks which result in separation, while maintaining a low cambered, thin section for optimum transonic and supersonic cruise.

Analytical design. - The analytical methods and optimization procedures are the technologies which transform the concept into the final configuration definition. The major aerodynamic analysis methods are summarized in table II with their principal capabilities and limitations and function in the design process. A more detailed description of these methods is presented in subsequent sections. The utilization of these analytical tools is the design technology which ultimately satisfies the mission requirements. A brief description of the design technology is presented for subsonic, transonic, and supersonic operation.

Subsonic design: Within the framework of linear theory, high efficiency is sought by minimizing:

(1) Vortex drag (optimum loading for a set of constraints)

(2) Separation (zero leading edge singularity at an appropriate lift)

(3) Trim drag (moment constraint/self-trimming configuration)

(4) Viscous form drag and drag divergence (controlled subcritical flow by prescribing an upper surface pressure distribution)

Transonic design: Controlled supercritical flow encompasses those techniques which minimize shock strengths and prevent shock-induced separation. Considerable progress has been made recently in the implementation of two-dimensional shockless or weak-shock flows. For general three-dimensional flows, the design philosophy is still in the developmental stages.

Supersonic design: The reduction of supersonic pressure drag is obtained with the following linearized theory optimization techniques:

(1) Inverse supersonic area rule (minimized wave drag through redistribution of volume)

(2) Drag-due-to-lift optimization (lifting surface inverse solution minimizing 0% suction drag with moment constraint)

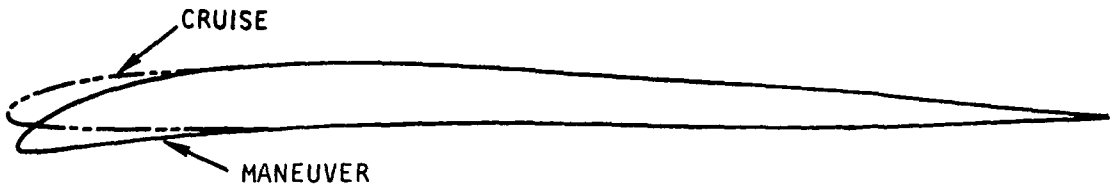

(a) LEADING EDGE VARIABLE CAMBER

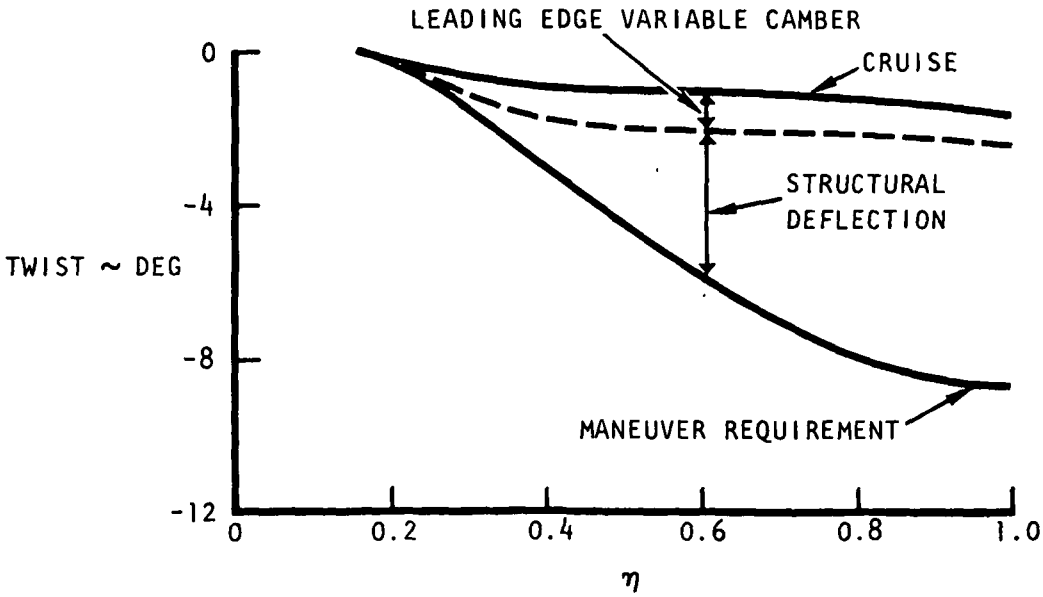

(b) AEROELASTIC TAILORING REQUIREMENTS

Figure 5. - Variable camber system.

TABLE II. - ANALYTICAL METHODOLOGY

Method	Capability and function	Limitations
Inviscid/linear theory Woodward distributed panel lifting surface theory (UDP)	Multiple surface, nonplanar design and analysis with body for subsonic or supersonic flow	Chord plane singularities
Slender body theory	Arbitrary cross section slender body analysis - Fuselage shaping to modify pressure distribution	Slender body approximation
Total pressure drag (supersonic area rule)	Lift, volume, and interference far field pressure drag - volume optimization for minimum wave drag	Slender body theory approximation
Inverse thickness	Derive thickness for specified velocity distribution	Chord line singularities, two-dimensional
Inviscid/nonlinear theory Bailey-Ballhaus transonic wing analysis	Transonic analysis of wing-body or wing-winglet configurations	Small disturbance, moderate shock sweep, limited nonplanar, and multiple surface capability
Transonic airfoil analysis Bauer code	Full potential transonic analysis - hodograph design solution	Isentropic
Transonic scaling	Derive airfoils from known solutions	Small disturbance
Viscous analysis Bradshaw turbulent boundary layer code	Tapered, yawed wing turbulent boundary layer analysis - finite difference solution	Quasi-three-dimensional
Transonic airfoil analysis (Bauer)	Transonic viscous/inviscid interaction	Two-dimensional integral boundary layer analysis, no laminar solution
Yawed wing analysis	Yawed wing laminar/turbulent boundary layer and conformal mapping/sweep theory analysis	Subcritical, integral methods

Configuration Evolution

The advanced fighter concept that evolved from the sizing and technology assessment studies is shown in figure 6. Constraints on the level of propulsion technology required that the demonstration vehicle (RPRV) be reconfigured with a standard axisymmetric nozzle. The baseline RPRV, a 0.44 scaling of the fighter concept, is shown in figure 6. The relationship between the fighter and RPRV performance is shown for the proposed configuration with and without the two-dimensional nozzle. The differences result from variances in thrust-to-weight ratio, wing loading, and Reynolds number. Thus, for example, the RPRV proposal with the axisymmetric nozzle had a maneuvering objective of $N_Z = 7.6g$, $P_S = 0$ at $M_\infty = 0.9$, $h = 9144m$. A refined analysis at the start of phase III set the performance goals contained within the preliminary operating instructions (POI) review. The increased configuration weight reduced the RPRV performance objective to $N_Z = 7.3$.

The important aspect to note is that the efficiency (drag due to lift) as a function of lift coefficient will be the same for the fighter concept and the RPRV. It is this technology that the program will demonstrate. The trimmed drag-due-to-lift goal is presented in figure 7. For the fighter, the 8g maneuver point corresponds to a lift coefficient of 1.1 including propulsive lift. The drag-due-to-lift goal at high lift coefficients is derived from the proposed fighter characteristics and flight condition. The goal requires the elimination of virtually all the drag rise normally associated with transonic, high-lift operation. Through a variable camber system, the high level of efficiency additionally was proposed to encompass the cruise point.

The major configuration modifications and associated design philosophy and test results are presented in figure 8. Notation for the wind tunnel models is presented in the appendix. The program and test schedule is shown in figure 9 as a frame of reference for the later discussion. The evolution from the phase II baseline (-17A) to the final preliminary design review configuration (-19) involved more than simply refining the design. Several planform modifications were required after analysis of the baseline (-17A) test results. Without the jet flap for control, the strakes were removed to reduce the nonlinear longitudinal characteristics. The refined linearized theory design process also indicated that the planform should be modified to produce a design which would meet the spanload constraints with a realistic structural arrangement. The resulting -18 design was vastly superior to the -17A baseline with regard to subcritical high-lift efficiency. The vortex lift characteristics were still not fully appreciated and the configuration required another major modification resulting in the -18A. The canard sweep was decreased and the wing planform modified.

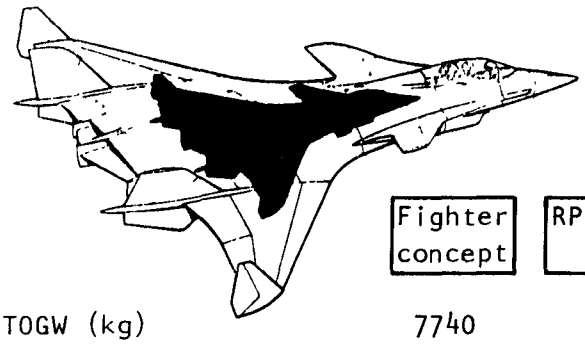

	Fighter concept	RPRV (proposal) 2-D nozzle	RPRV (proposal) standard afterbody	RPRV (POI) standard afterbody
TOGW (kg)	7740	1582	1503	1529
W_{FUEL} (kg)	1787	295	295	295
For M = 0.9, h = 9144 m				
W (kg)	6846	1435	1355	1386
W/S (N/m^2)	2423	2609	2471	2523
T/W	0.828	0.801	0.842	0.824
P_s @ 8g (m/s)	.6	.0	-35.7	-68.6
N_Z @ P_s = 0	8g	7.79g	7.60g	7.30g
Research time (min)		5.21	4.68	4.49

Figure 6. - Fighter/RPRV performance relationships.

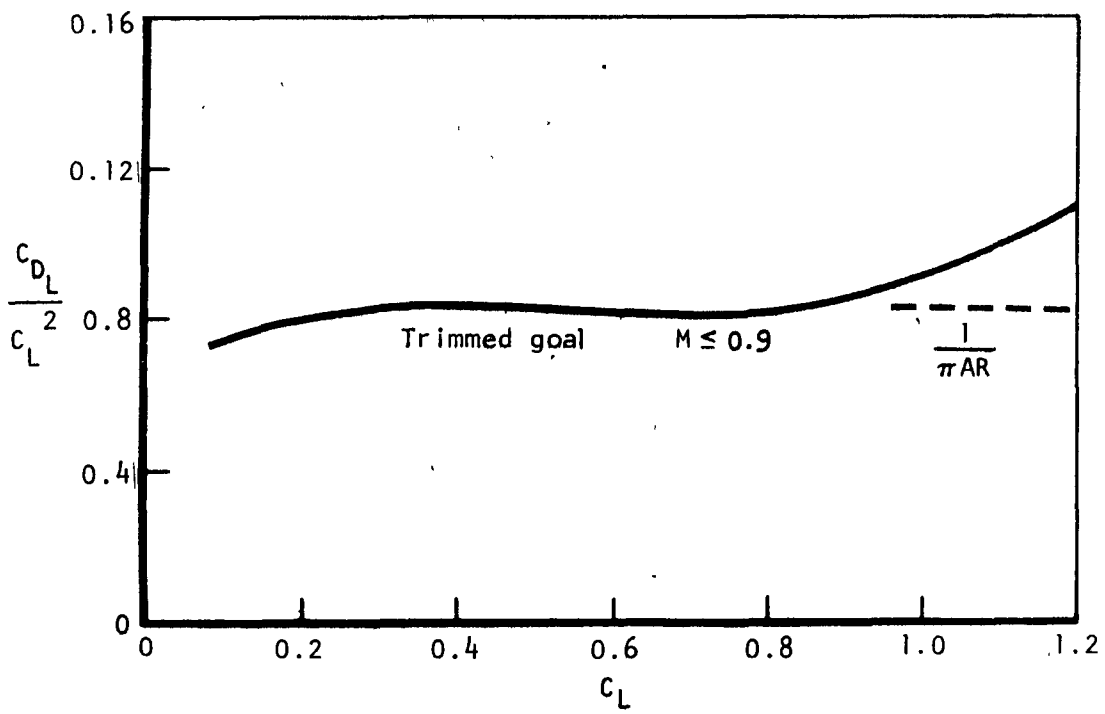

Figure 7. - Trimmed drag due to lift goal.

PHASE II ▼ PHASE III

Maneuver design

Configuration	-17A phase III baseline	-18 -31 W -41 C	-34W -42C	-18A -35W -44C	-36 W -44C (mod)	-39 W -44C (mod)	-310 W - 44 C (mod)	-310 W -48 C	-19 -310 W -48C
Design description	Wing alone optimum span load	Wing-canard constrained optimum span load Strakes removed	Wing-canard smoothed loading	Nonlinear 3-D wing design 55° canard	Outboard wing design Garabedian shockless airfoil 65-14-08	Scaled Garabedian section 70-11-06 Fuselage modification	Scaled LRC/Whitcomb airfoil 69-13-08	Outboard canard design, scaled LRC/Whitcomb airfoil	Lower surface winglets, larger vertical stabilizer
Test	LRC-721	ARC-156-1-14	ARC-156-1-14 TWT 296	TWT 296	TWT 296	TWT 296	TWT 296	TWT 296	TWT 296 TWT 304
Test configuration	$W_2\ C_M$	$W_3 C_2 B$	$W_7\ C_4\ B$	$W_{8,9}\ C_5\ B$	$W_{10}\ C_{5,6}\ B$	$W_{11-14}\ C_6\ B_2$	$W_{17,18}\ C_9\ B_2$	$W_{17,18}\ C_{10}\ B_2$	$W_{23}\ C_{10}\ B_2\ V_9$
Results and conclusions	High drag due to lift Nonlinear moment Body-canopy shock	Improved drag due to lift Leading edge separation - smoothed twist Linear moment Canopy shock reduced	Subcritical drag goal met Shock-induced separation on outboard wing, strong shock inboard	Inboard 70% wing shock weakened Outboard wing shock-separation	Transonic drag reduction Section off-design (M_∞)	Supercritical section off-design (lift) Transonic drag not affected by fuselage modification	Weak, swept shock at nominal design point	Outboard canard shock weakened Isobars unswept, marginal improvement in drag	Improved lateral-directional stability

Cruise development

Configuration	-18 -30 W -40 C	-18A -310 W -48C	-19 -310 W -48 C
Design Description	Constrained optimum span load	Design derived from maneuver configuration	Winglets, vertical
Test	ARC-156-1-14	TWT 296	TWT 296 TWT 304
Test configuration	$W_1\ C_1\ B$	$W_{19}\ C_{11}\ B_2$	$W_{22}\ C_{11}\ B_2\ V_9$
Results and conclusions	Cruise drag goal achieved	Drag-due-to-lift penalty at cruise C_L	Improved lateral - directional stability

Figure 8. - Configuration development.

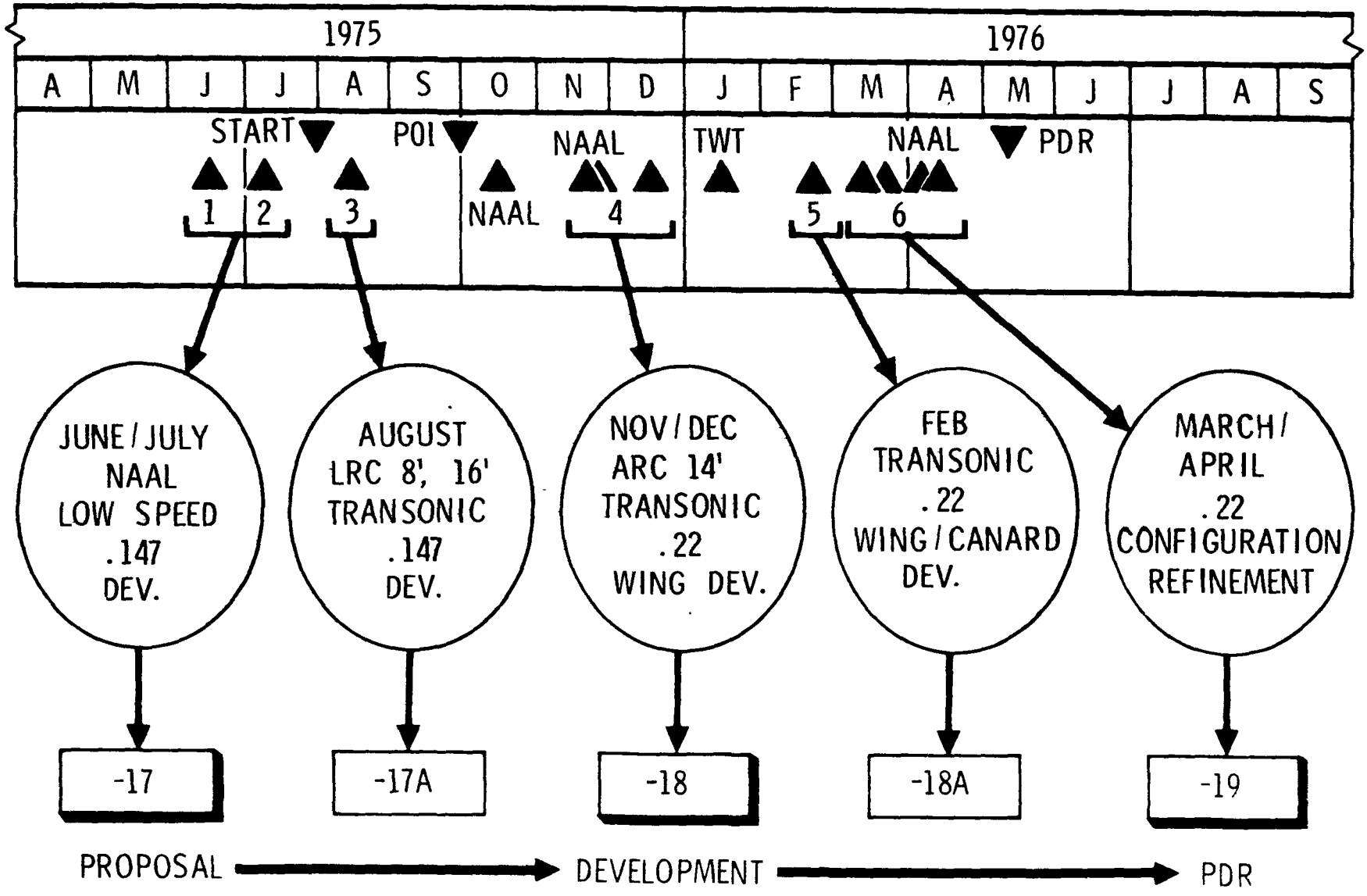

Figure 9. - Configuration/test evolution.

As indicated in figure 8, there then followed several design/test cycles to improve the transonic maneuver efficiency through refinements to the wing and canard sections.

As a result of the modifications which produced the -18A baseline, the lateral-directional stability characteristics were degraded. After correction of this situation by the addition of lower surface winglets and increased vertical tail volume, the -19 configuration was defined.

AERODYNAMIC DESIGN APPROACH

The optimization of the external contours is accomplished by a sequence of analytical design, test, and redesign phases. The basic aerodynamic method is linear theory because of the extensive development which has occurred over the past few years. Linearized theory methods are capable of analyzing or designing completely arbitrary nonplanar multiple surface configurations. The use of present day computers with their interactive and graphics capability allows numerous configuration modifications and optimizations to be evaluated in a short timespan at minimal cost. However, these methods have their limitations, as discussed in the following paragraphs, and must be supplemented with nonlinear theory and experimental data.

The HiMAT mission, which is a combination of subsonic cruise, a high degree of transonic maneuverability, and supersonic acceleration, requires the utilization of all these tools. The steps in the design process are:

(1) Design efficient subcritical and supersonic configuration with linear theory

(2) Test to determine the limitations and possible modifications of the theory to more closely achieve the goals

(3) Modify the contours with the nonlinear analyses to meet the transonic requirements

(4) Investigate the subsonic/supersonic consequences of the modifications

(5) Test the compromise configuration

The implementation of this procedure will be briefly described in the following sections, along with the features of the analytical methods and their limitations.

Analytical Methods

The principal analytical tools used in the HiMAT development were summarized in table II. In the following, a description of the theory, capabilities, and limitations of each method will be presented.

Linear theory.

Lifting surface theory: The primary linear theory design and analysis tool utilized is the unified distributed panel method (reference 7). This method solves the linearized small disturbance equation,

$$(1 - M_\infty^2)\ \phi_{xx} + \phi_{yy} + \phi_{zz} = 0$$

for arbitrary wing-body configurations by a superposition of chordplane singularities. Lifting effects are represented by constant vorticity panels. With linearized boundary conditions, a set of linear equations results which is solved for the singularity strengths. Thickness effects are represented by chordwise linearly varying source panels. The analysis is applicable to multiple-surface nonplanar configurations for subsonic or supersonic flow.

Wing-body solutions are obtained by superposition of an isolated slender body solution with a lifting surface/vortex shell representation. The isolated body perturbation velocities are included in the wing boundary conditions. A noncircular cylindrical vortex shell near the surface of the body is utilized to determine the wing carryover loading. The boundary condition on the interference shell, no normal velocity component, cancels lift and thickness inductions from the lifting surfaces.

The inverse lifting solution is obtained by specifying the net loads at the panel centroids and determining the boundary conditions by matrix multiplication. Problems where boundary conditions are given in one region and net loads are prescribed in the remainder can also be treated. Wing-body inverse solutions are obtained in this manner, where pressures are prescribed on the lifting surfaces with no normal flow on the interference shell.

Slender-body theory: A general slender-body analysis is used to predict surface and near-field flow properties for slender configurations of noncircular cross section in subsonic or supersonic flow. The solution is based on limiting solutions to the three-dimensional linearized small-perturbation equation. The total solution is composed of an axisymmetric result for a body of revolution of the same cross-sectional area and a crossflow solution, ϕ,

satisfying three-dimensional boundary conditions in the YZ plane. The cross-flow result is a solution of Laplace's equation:

$$\phi_{yy} + \phi_{zz} = 0$$

Conformal mapping theory is used to obtain the solution for noncircular sections.

The analysis is used to define flow characteristics for isolated bodies and fuselage induction effects on adjacent surfaces. As a design tool for isolated applications, body shaping, axially and circumferentially, is accomplished through an interactive mode to obtain satisfactory pressure gradients.

Supersonic pressure drag analysis: The techniques used to evaluate total pressure drag are the supersonic area rule and an extension which includes volume, lift, and interference drag (reference 8). The spatial singularities which are a solution to the linearized equation of motion are reduced to a series of equivalent lineal distributions by application of the cutting plane concept. The three-dimensional distribution is surveyed longitudinally at fixed roll angles by the oblique plane. The drag is then evaluated with slender body theory,

$$C_{D_w} = \frac{1}{4\pi^2 S} \int_0^{2\pi} \int_0^L \int_0^L H'(X_1,\theta)\, H'(X_2,\theta)\, \ln|X_1 - X_2|\, dX_1 dX_2 d\theta$$

where H is related to the equivalent lineal singularity strength and is the sum of the volume (source) and lift singularities.

Arbitrary configurations are composed of volume elements and lifting surface elements. The latter solution is obtained with the distributed panel theory. The total solution thus includes the drag due to lift, volume, and interference. For conditions of light loading, the interference is often neglected and thus the analysis may be reduced to the supersonic area rule. Preliminary wave drag estimates are generally made with this approximation.

In the design mode, the supersonic area rule theory is used to minimize wave drag for given volume, area, and wing thickness constraints. The geometry is perturbed by a set of harmonic functions. Lagrange's method for extremal problems with constraints is applied to the resulting expression for wave drag. The set of linear equations is then solved for the perturbation coefficients that minimize the drag.

Inverse thickness design: A two-dimensional inverse thickness solution based on chordline source singularities is used to derive airfoil thickness distributions for prescribed pressure distributions. Three-dimensional thickness solutions, based on the distributed panel theory with chordwise linearly varying sources are possible, but the procedure has not been automated.

Nonlinear theory.

Transonic wing analysis: The method used to analyze transonic characteristics is the classical small disturbance relaxation solution developed by Ballhaus and Bailey (reference 9). The small disturbance potential equation

$$\left((1-M_\infty^2) - (\gamma+1)\frac{M_\infty^2}{U_\infty}\phi_x\right)\phi_{xx} + \phi_{yy} + \phi_{zz} = 0$$

is solved by a mixed elliptic-hyperbolic, fully conservative relaxation algorithm applied to a finite difference approximation. The boundary conditions are linearized and applied on the wing chord plane. These linearizations restrict the solutions to those conditions (angle of attack) and regions of the wing (away from stagnation points) where the small disturbance formulation is applicable.

The solution is obtained in a rectangular XYZ space grid. For swept, tapered planforms a shearing and stretching transformation is available to assure adequate grid density for the entire configuration. The original formulation is applicable to planar, single surface simulations. According to reference 10, the small disturbance formulation is not capable of capturing highly swept shocks, and additional terms are required in the governing equation.

Transonic airfoil analysis: The inviscid transonic airfoil analysis developed by Garabedian and Korn (reference 11) solves the exact potential equation of motion for steady, irrotational flow

$$\left(a^2 - \Phi_x^2\right)\Phi_{xx} - 2\Phi_y\Phi_x\Phi_{xy} + \left(a^2 - \Phi_y^2\right)\Phi_{yy} = 0$$

by an iterative nonconservative finite difference numerical solution. The computational plane is derived from the physical plane by mapping the region external to the airfoil to the interior of a unit circle.

Transonic similarity scaling: The von Karman-Spreiter (reference 12) transonic similarity rule is useful as a design tool in obtaining airfoils for

a given transonic application from known airfoil data. The similarity rule, in a form proposed by Krupp (reference 13) is

$$K_1 = \frac{1 - M_\infty^2}{M\delta_\infty^{2/3}} \qquad K_2 = \frac{C_\ell M_\infty^{3/4}}{\delta^{2/3}}$$

In a design where two-dimensional data can be appropriately used, for example, a swept, moderately tapered wing, the available airfoil sections may not meet the design requirements. However, known airfoils may be scaled to obtain sections more closely matching the design condition. The scaled airfoil transonic characteristics are analyzed with the method of reference 11 and further modifications can be made (reference 14 for example) to achieve the desired design pressure distribution.

Viscous analysis. - No fully three-dimensional inviscid/viscous interactive solutions are presently available. Thus, for three-dimensional pressure distributions, a viscous calculation provides only qualitative results. The analysis is confined to estimating potential separation problems due to adverse pressure gradients and shock-boundary layer interactions for transonic flows. For the design case however, the inviscid/viscous interaction may be accounted for if the displacement thickness is removed from the wing sections. The design pressure distribution must produce attached flow.

A quasi-three-dimensional turbulent boundary layer analysis developed by Bradshaw (reference 15) is applicable to swept, tapered wings where the isobars coincide roughly with the wing generators. The method solves the momentum and turbulent shear stress equations in two coordinate planes with a finite difference scheme.

Viscous transonic airfoil interaction calculations are obtained with the method developed by reference 16. This analysis combines the previously described transonic inviscid solution with a two-dimensional Nash-MacDonald integral boundary layer analysis. The off-design characteristics of airfoil sections that are candidates for application to swept wings are analyzed with this method using simple sweep theory in conjunction with viscous independence. The analysis is not strictly applicable to the swept case so results are utilized in a qualitative manner.

A viscous yawed wing analysis is utilized to analyze inviscid/viscous interactions for swept wings in subcritical flow. The analysis combines integral laminar and turbulent boundary layer solutions with a conformal mapping solution which defines the inviscid flow. The analysis is also used to define initial conditions at transition for the Bradshaw turbulent boundary layer analysis.

Aerodynamic Design Process

The configuration design is initiated with a linearized theory inverse solution using guidelines relative to drag-due-to-lift optimization and upper surface pressure distributions. The design is then analyzed off design to assess the viscous characteristics and the maintenance of isobar sweep. Refinements are made based on this analysis. The transonic characteristics are then examined to establish the strength, location, and sweep of shocks and their impact on boundary layer separation. Modifications are then initiated through a trial and error process to reduce the shock strengths.

A flow diagram of the design process that evolved for the HiMAT configuration is shown in figure 10. Test cycles are shown where verification is required due to a lack of adequate theoretical capability or where the methodology is not sufficiently general and must be used interactively with experimental results.

Linearized design. - The goal of the subcritical design is to minimize drag due to lift at a given C_L, subject to constraints on the pitching moment (minimization of trim drag) and section lift (minimization of viscous form drag, separation).

The drag due to lift optimization proceeds by determining an optimum loading (constant downwash in the Trefftz plane) and then distributing the chord load such that there is no leading edge singularity, and the configuration is trimmed. There are any number of chordwise loadings that satisfy these conditions, which in general may be expressed by

$$C_{p_l} - C_{p_u} = \sum A_N \sin N\theta, \quad \theta = \cos^{-1}\left(1-2\frac{X}{C}\right).$$

This form produces no leading edge singularity and guarantees that the 0 and 100% suction drag polars are tangent at the design lift. Usually only two or three terms in the series are used; the first and second coefficients determined by the section lift and moment, respectively. The third independent of C_ℓ and C_m provides an additional degree of freedom to alter the pressure distribution.

An additional variable relates to the spanwise variation of the chordwise center of pressure. The centers of pressure must be such as to satisfy the total moment constraint for the given loading, but are otherwise arbitrary. To obtain a smooth spanwise camber and twist variation the center of pressure variation is initialized by that obtained from the additional load distribution and then adjusted by a constant to satisfy the trim requirements. For a given set of loadings, the boundary conditions are obtained from the inverse solution, then integrated to produce the twist and camber.

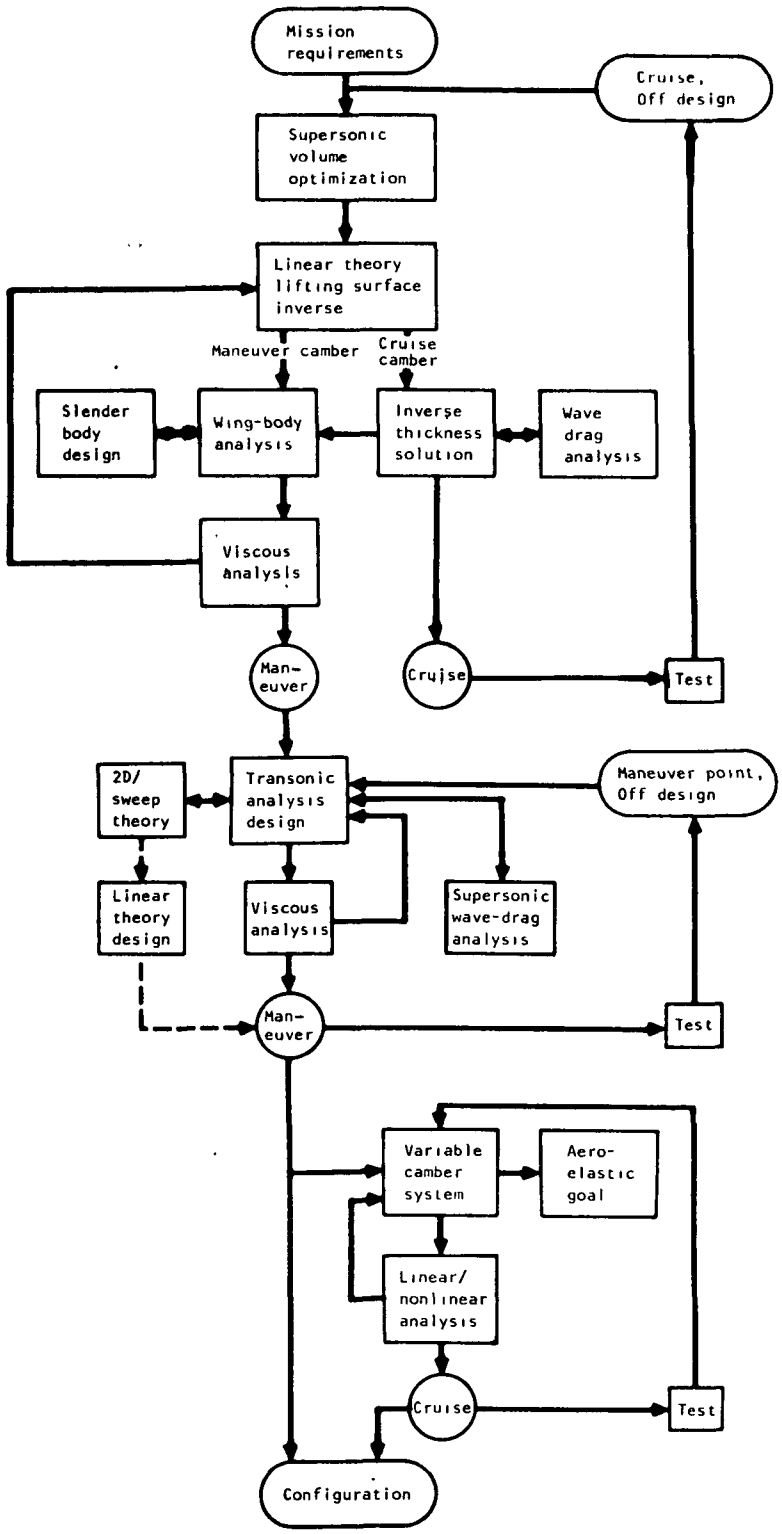

Figure 10. - Aerodynamic design process.

For efficient operation at high-lift coefficients, the design lift is usually selected at some intermediate value. The philosophy is that, through proper design, leading edge suction can be maintained well above $C_{L_{DESIGN}}$. Further, the resulting camber is structurally practical and results in efficient operation above and below the nominal design point. The spanload may require constraints in order to limit the section lift at off-design conditions. In this case, the span load is prescribed and the drag penalty monitored as the design cycle proceeds. The optimum and 100% suction drag is not coincident at the design point but the 0 and 100% suction drag polars will be tangent at the design lift.

For a wing-body configuration, the optimum cannot be implemented because the interference shell loading cannot be prescribed independently of the loading on the wing. This restriction is usually of minor consequence for the body-width-to-span ratio under consideration. The approach, then, is to prescribe a loading on the lifting surfaces which is similar to the solution obtained without the slender body. Once the loading is given, the inverse solution is obtained. After removing the isolated body perturbations from the total boundary conditions, the wing camber is derived.

For a given twist and camber, a thickness distribution may be derived for a prescribed upper surface pressure distribution. The pressure distribution criteria is the primary consideration for subcritical/transonic operation, although for a configuration with a supersonic cruise point, consideration is given to minimize wave drag due to volume. For subsonic cruise with swept, moderately tapered wings the thickness is typically derived to produce a flat-top upper surface pressure distribution which maintains subcritical flow normal to the isobars at the design condition. This type of distribution delays drag rise in comparison to peaky type distributions.

The thickness is derived by selecting a design point for which an upper surface pressure distribution is prescribed and calculating the contribution to the velocity due to lift (twist and camber) and, in some instances, wing-body interference. With an inverse solution, the thickness is obtained for the specified net velocity increment.

The thickness is typically derived for the cruise condition. For a variable camber system with transonic cruise and maneuver design points, the thickness could be derived for some intermediate condition. However, as an initialization, the cruise point is appropriate since experience has shown that linear theory methods are satisfactory for a lightly loaded condition where wing thickness is necessarily small based on wave drag considerations. The upper surface pressure distribution for some maneuver condition could be specified if it was known, a priori, that this produced a satisfactory transonic flow.

For configurations with a supersonic requirement, the supersonic far field drag analysis (reference 8) is used to optimize the volume distribution for minimum wave drag. This design process establishes the body area distribution and the initial lifting surface thicknesses prior to the detailed subcritical design phase. This phase involves trade studies between structural constraints, fuel volume, and wave drag.

For supersonic operation, a minimization of drag due to lift may be accomplished with the linear lifting surface analysis (reference 7) to define twist and camber. This could be used in conjunction with the transonic maneuver design to establish the variable camber requirements. For the HiMAT configuration this was not done, the transonic cruise point being used instead. For the supersonic design point, the camber and twist are obtained from an optimization which minimizes the 0% suction drag subject to total moment or spanwise distribution of chordwise center of pressure constraints, or both.

Linearized analysis. - A linearized theory analysis phase is conducted to establish the off-design characteristics. This analysis provides information for trade studies so that all the subcritical and supersonic design goals may be achieved.

The pressure distribution is calculated for subcritical, high-lift conditions for the maneuver configuration. The addition of lift and thickness should produce swept isobars and chordwise pressure variations without excessive leading edge peaks or aft adverse gradients. Some leading edge peak is expected since the design lift was selected at an intermediate value. If the viscous analysis indicates leading edge separation, the design lift can be increased. If the thickness and lift solutions indicate unsatisfactory performance (for example, steep gradients near the trailing edge), the design process is reinitiated. There are several paths that may be followed. The chord load shape for the high-lift condition (maneuver configuration) could be modified, keeping the thickness fixed. Second, the cruise chord load shape could be modified, thus varying the required thickness for a given upper surface pressure distribution. Finally, a combination of these options may provide the best compromise.

For a subsonic design, the supersonic performance is monitored during the subcritical design phase to verify that the wave drag due to lift and volume are within acceptable limits. Otherwise, these analyses provide results for further compromises between the subsonic and supersonic operation. The drag due to lift is analyzed with the distributed panel theory (reference 7) and wave drag due to volume with the supersonic area rule. The supersonic far field analysis of reference 8 is utilized to evaluate the total pressure drag including interference between volume and lift. The lift contribution is

obtained from the analysis of reference 7. The compromises between subsonic and supersonic operation are typically confined to wing thickness modifications in the detailed subsonic and transonic design phases.

The linearized design initiation is shown in the first stage of the design process of figure 10. The linearized maneuver condition design established a practical starting point for later modifications. That is, many design possibilities can be rapidly investigated to assure a reasonable structural arrangement which satisfies at least the subcritical design conditions. The test cycle at this stage need only consider the cruise design to evaluate the configuration stability and control characteristics and transonic and supersonic cruise performance. If deficiencies are present, the configuration is modified before substantial transonic design and analysis efforts are expended.

Transonic characteristics. - The next step in the design process is to analyze the transonic characteristics of the configuration to determine the position and strengths of shock waves, and the probability of boundary layer separation. Ideally, a complete analysis would consider either a small-disturbance or full potential inviscid solution for a nonplanar, multisurface configuration, coupled with a viscous interaction. At present, the calculation efficiency of a small disturbance formulation, relative to the full potential equation, usually dictates its use for analysis and particularly design applications. In either case, a viscous/inviscid interaction model does not exist so that viscous calculations are utilized principally in a qualitative manner. For the HiMAT configuration, a further complication arises because the nonlinear code does not have a multiple surface capability. Thus, the analysis is limited to wing-alone solutions.

Transonic design. - Based on the initial analysis at transonic conditions, the configuration planform and sections are modified to meet the design goals of weak, swept shocks. This is an iterative process where modifications are made and the design reanalyzed. With the present small disturbance formulation, an accurate assessment of the magnitude of wave drag cannot be made. The design proceeds qualitatively. That is, shock strengths are minimized to avoid boundary layer separation. If the planform does not facilitate the elimination of unswept shocks, they are admitted, but restricted to the trailing edge region where their effect on the boundary layer will be minimal.

Ideally when a satisfactory inviscid solution is attained at the design point the displacement thickness would be calculated for the design pressure distribution and removed from the inviscid contour. For the configuration under examination here, the final design pressure distribution cannot be determined because the canard is omitted. Thus, with the available methods, an analytical/test iteration is required to assess the impact of the canard on the transonic design.

The design criteria for the upper surface pressure distribution are summarized as follows:

(1) For highly tapered regions, a triangular pressure distribution with peak near the leading edge and a gradual recompression to the trailing edge is selected. The intent is to maintain a constant supercritical Mach number normal to the isobars. One or more shocks may exist at or near the design point but they will be weak if the basic shape of the design pressure distribution is retained and the isobars are swept roughly along the generators.

(2) Approaching the centerline or wing-body intersection where the critical condition is nearly constant along the chord (isobar sweep of 0 degrees) a return to a flat-top distribution will be more desirable. This would prevent strong shocks and adverse boundary layer interactions near the forward part of the wing. This may require the acceptance of a moderate strength shock near the trailing edge.

(3) For swept, moderately tapered regions, a two-dimensional supercritical airfoil design philosophy is appropriate if the wing is designed for roughly infinite yawed wing conditions in the region of interest. Current highly loaded supercritical sections are characterized by a flat or small adverse pressure gradient in the forward part and followed by either (a) a shockless recompression such that there is no separation or (b) a weak shock, subcritical flat-top region, and steep adverse gradient. The latter may have a small region of trailing edge separation. The former philosophy is the optimum at a specific design point, while the latter approach is less sensitive to off-design conditions. Section data, sweep theory, the transonic similarity rule, and the Bauer code are used to initialize the transonic design modifications for regions where the aforementioned criteria can be met.

The limitations inherent in the transonic analysis method forced the adoption of several alternate and supplementary paths as indicated in figure 10. Sweep theory and the available supercritical airfoil data and analysis methods were used, with a linear theory implementation, to bypass the restrictions of the three-dimensional transonic wing analysis. The analysis/test iteration was required to account for viscous effects and the inability to simulate the entire configuration.

Modifications to Analytical Methods

In the course of applying the design procedure, certain deficiencies were noted. Some applied to the overall efficiency of the design process while others resulted from the particular requirements of the HiMAT configuration.

A description of the deficiencies encountered and the corrections made is given below. Areas where further development of the analytical capability is required are examined in the later sections.

Linear theory. - The time involved in obtaining a subsonic optimization limited the number of design conditions and variables that could be surveyed. To increase the efficiency of the design process, existing separate programs and concepts were integrated into the distributed panel lifting surface theory. The additions and extensions are summarized as follows:

(1) An optimum loading solution with constraints by the method of Lagrange multipliers was incorporated. Provision was made for specifying an arbitrary loading in an interactive manner.

(2) The capability to constrain the moment for multisurface configurations was added. Previously this step was done manually.

(3) The chord load calculation was incorporated with an interactive capability to modify the shape for a given section lift and moment.

These modifications allow the twist and camber to be derived in one step. Thus, the solution can be examined and parameters varied in an efficient manner.

Nonlinear theory. - The Bailey-Ballhaus code was originally applicable to a single surface. For the HiMAT configuration, the presence of the wingtip fin and the canard presented complications. A wingtip fin was incorporated as a first step. The simulation was limited to the X-Z plane. Efforts to simulate a wing-canard configuration were continued. Recent progress in this respect has been reported in reference 17.

The planform geometry of the HiMAT wing required the capability for analysis of a leading or trailing edge that was curved or segmented, or both. As a result, a spline fit was incorporated into the calculation of the transformation metric.

Flexible Wing Design

The last phase in the design establishes the incremental deformation necessary to meet two or more design conditions. The maneuver design, being the primary design condition, is held fixed. It is then necessary to determine the best cruise definition within the variable camber concept. After the modifications are made to the maneuver design for satisfactory transonic flow, the cruise design must be determined by iteration since there is no direct approach

for the constraints associated with the maneuver shape. When a suitable cruise definition is obtained, the aeroelastic goals may be set. The iterative process requires a linear or nonlinear potential flow analysis, or both, to examine the possible cruise designs which will produce a near optimum span load distribution and a satisfactory upper surface pressure distribution.

SUBCRITICAL DESIGN

Wing Alone Design

This section describes efforts directed toward the HiMAT design which were initiated prior to phase III. A wind tunnel model with a variable camber system and close-coupled canard was designed in order to acquire basic data and gain experience relative to the design process for highly loaded configurations. The modifications and extensions to the linear theory design method, described under "Linear Theory," were made as a result of the findings of this effort. The design philosophy was essentially unchanged, but the implementation required several separate steps to arrive at a twist and camber definition.

Initial attempts at designing a wing-canard configuration were not successful. To arrive at a structurally feasible twist and camber usually requires several iterations. The time involved in selecting a load distribution, solving for the trimmed condition, and deriving the camber prevented a thorough examination of all variables. An alternate approach was to design for a weak wing-canard interaction. That is, the canard is treated solely as a trimming surface. The wing is constrained to carry all the load at the design point by being self-trimming.

An optimum loading may be implemented by assuming the wing and canard are coplanar. Then, the loading may be distributed in any manner between the surfaces. With all the loading on the wing and the moment constrained, $C_{M_{CG}} = 0$, the twist and camber may be derived such that all the design criteria are satisfied.

The extent to which the design remains optimum depends upon the selection of the canard. With an arbitrary geometry (camber), the canard may be deflected for minimum additional lift and moment. Optimum canard camber may be determined from a mixed solution where boundary conditions are given on the wing and pressures (identically zero) on the canard. This latter design will then be in the set of optimum solutions although the required camber may prove impractical. In either instance, since these are restricted solutions, the off-design characteristics must be carefully monitored.

Cruise design. - The -17A RPRV is shown in figure 11. A planform simulating the wing, strake and wingtip fin is shown in figure 12. The optimum loading (valid also with an in-plane canard) is shown in figure 13. A chordwise center of pressure $(X/C)_{cp}$ spanwise variation similar to that for the add load was selected and adjusted to satisfy the moment constraint. The restricted solution (wing alone) resulted in forward center of pressure locations and thus higher net loads near the leading edge. The twist and a typical camber distribution derived for this loading are shown in figures 14 and 15, respectively.

An upper surface pressure distribution was selected, based on maintaining subcritical flow normal to the isobars up to $M_\infty = 0.93$. For the assumed flat-top distribution the required thickness distribution was calculated. Since the velocity due to lift was high near the leading edge, a thickness distribution with small leading edge radius evolved (figure 16). For supersonic cruise this type of thickness distribution is advantageous and since the transonic cruise pressure distribution requirements are met there was no reason to further alter the cruise design.

The maneuver camber for a design lift coefficient of $C_L = 0.5$ was simply scaled from the cruise wing camber by the ratio of the design lift coefficients. Thus, the optimum span load will result at the intermediate design point ($C_L = 0.5$). The twist and camber were modified to limit the section lift on the outboard wing to $C_\ell \sim 1$ for $C_L = 1$. Maneuver twist and camber are presented in figures 17 and 18.

At this point a variable camber system was not considered for the canard. An uncambered canard, similar to standard weakly coupled trim surface arrangements was selected. The problem of setting the proper incidence for operation with either the cruise or maneuver wings, or both, was not addressed. Since the system is, in fact, highly coupled, the performance could be severely degraded. Later analysis of both the cruise and maneuver systems indicated that, as a result of not integrating the canard properly into the design,

(1) The 0% and 100% suction drag polars for the complete configuration were not tangent,

(2) The maneuver design lift was effectively lower than prescribed,

(3) The high peak pressures and small leading edge radius would promote separation on the outboard wing, and

(4) The configuration was not self-trimmed.

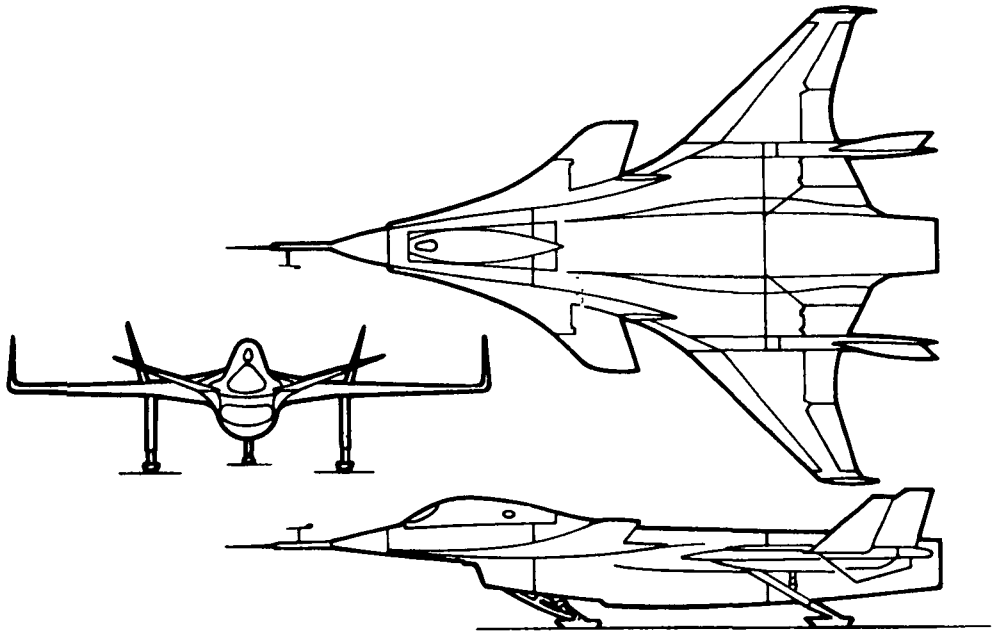

Figure 11. - RPRV, -17A.

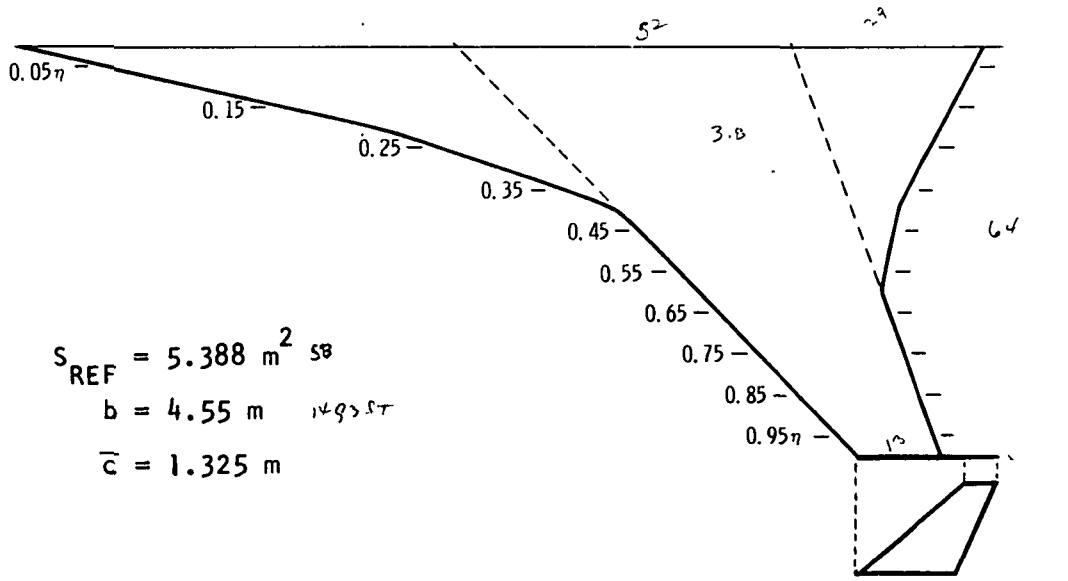

Figure 12. - RPRV wing planform, -17A.

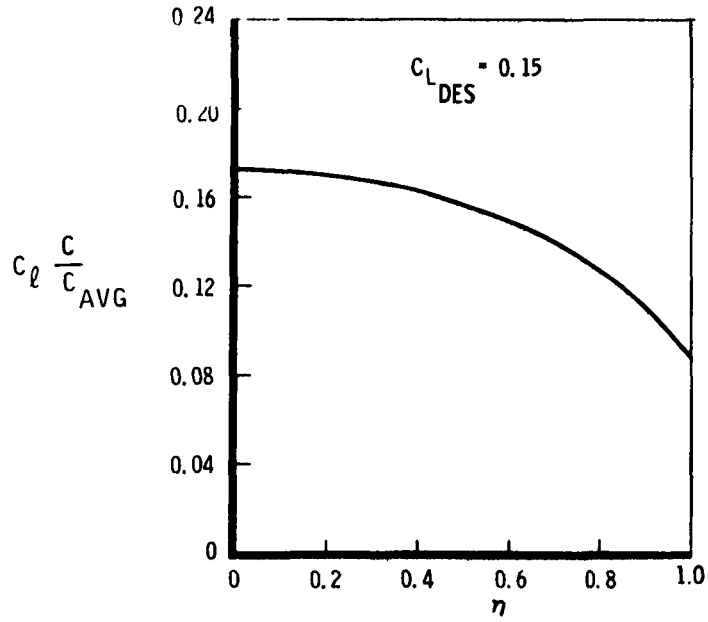

Figure 13. - Wing optimum spanwise load distribution, -17A.

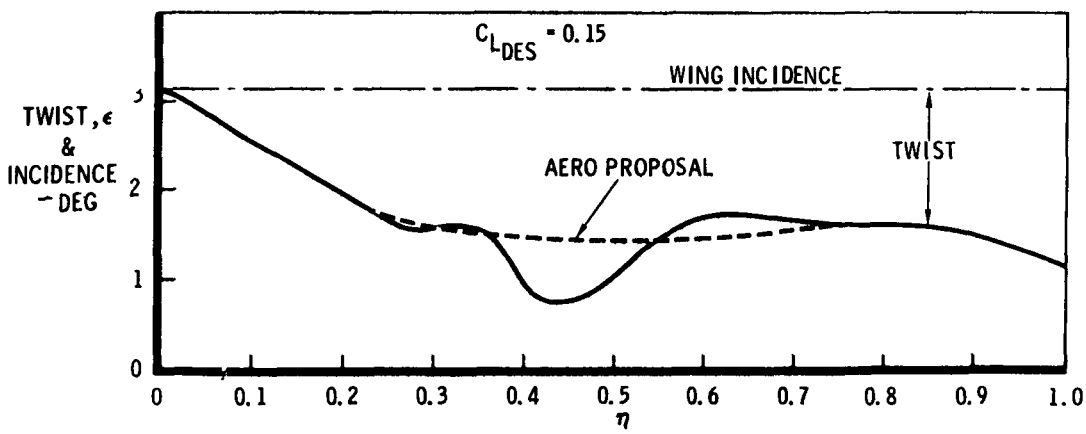

Figure 14. - Optimum twist and incidence distribution, -17A.

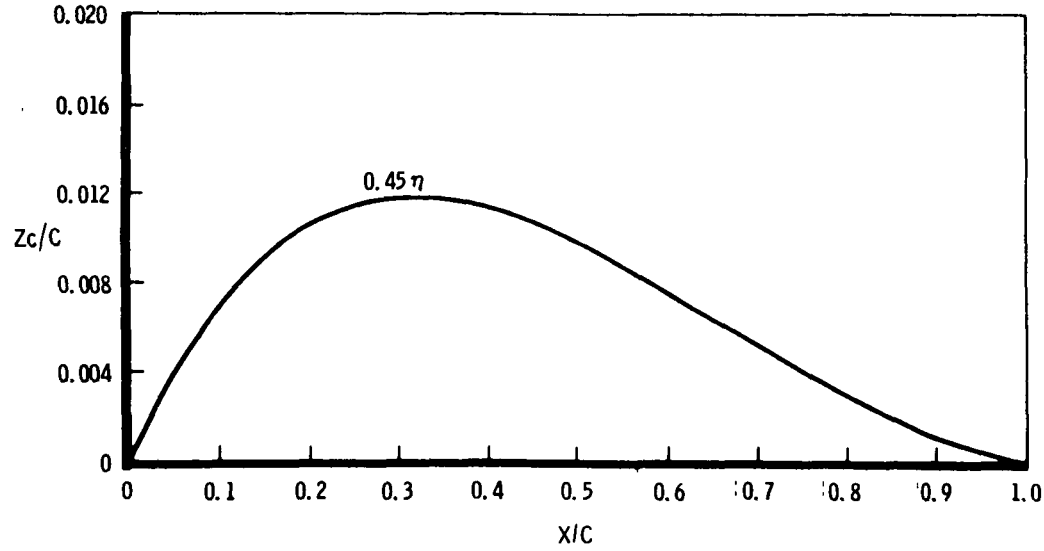

Figure 15. - Typical wing camber distribution, -17A cruise wing.

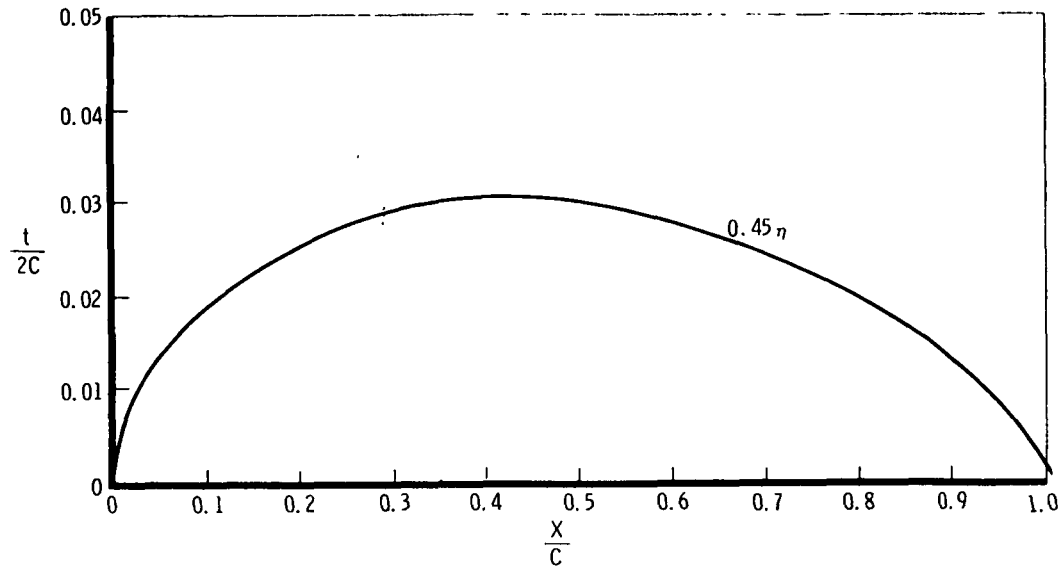

Figure 16. - Typical wing thickness distribution, -17A cruise wing.

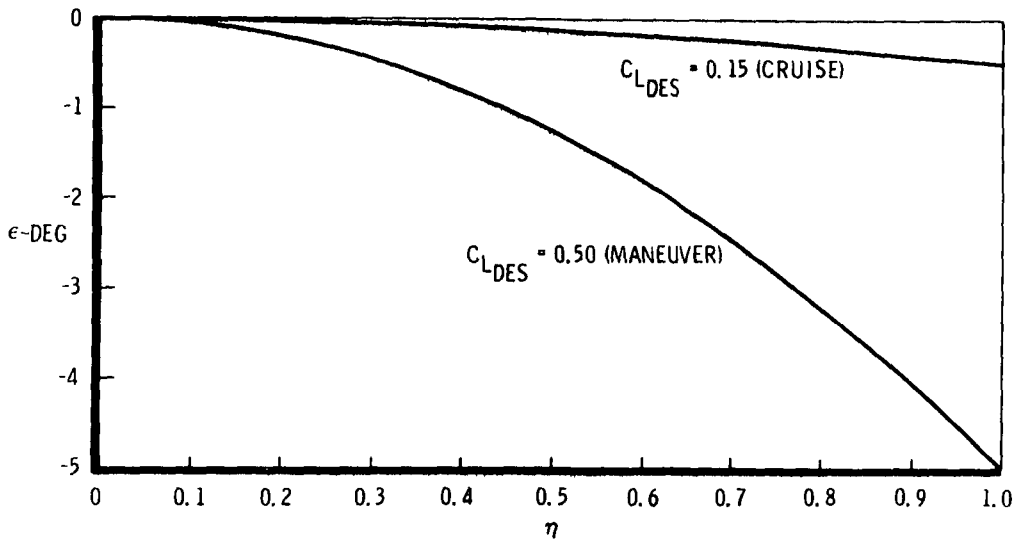

Figure 17. - Spanwise twist distribution, -17Λ.

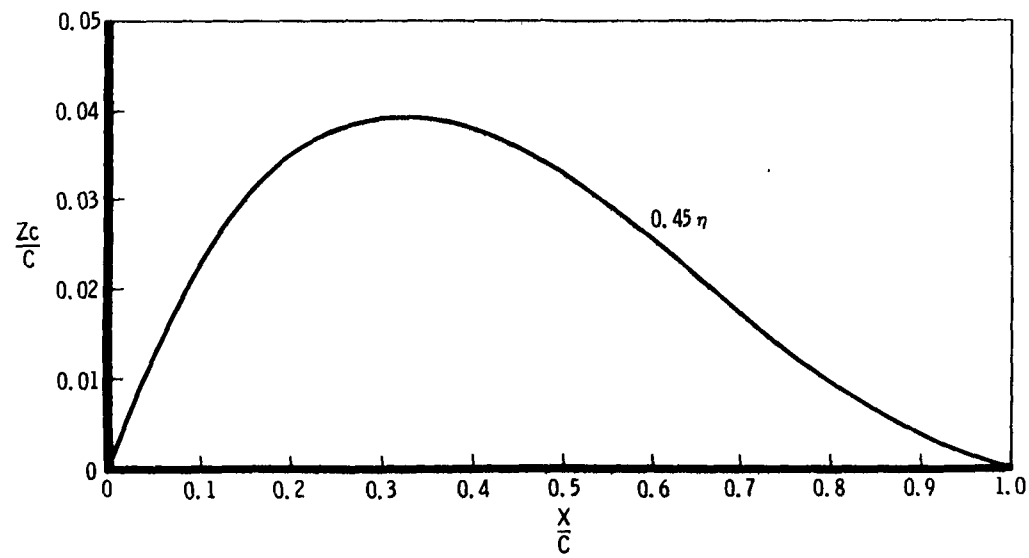

Figure 18. - Typical wing camber distribution, -17Λ maneuver wing.

Test results. - A 0.147-scale model of the configuration designated -17A was tested in the LRC 8-Foot Transonic Pressure Tunnel. The data presented are used to illustrate those aspects pertinent to the subcritical design process. Lift, moment, and drag due to lift for the maneuver wing are shown for subcritical conditions. Drag due to lift was evaluated by removing the estimated skin friction drag based on flat plate turbulent skin friction and standard form factor corrections. Comparisons with a linear theory analysis are also presented.

The nonlinear moment characteristics (figure 19) result from the wing and canard strakes, as indicated by data for the strake input. The strakes produced a vortex lift but negligible net load due to the effect of the close-coupled surfaces. The drag due to lift (figure 20) is indicative of the neglect of the canard interaction. In figure 21 drag due to lift factors are compared for canard on and off. Noting that this was essentially a wing alone design, the performance for the canard-off configuration meets the design objective for moderate C_L. The total drag at $C_L = 1$ is shown as a function of Mach number in figure 22 and indicates unsatisfactory maneuver performance relative to the design goal. Flow visualization studies indicated a strong shock in the canopy region, in addition to those on the wing and canard.

Conclusions. - The experience with the design process and the results of the wind tunnel test are summarized below. The major area of concern is the wing-canard interaction and the basic wing design. The -17A design resulted in a loading that was incompatible with the design objectives with the following adverse effects:

(1) Without the zero leading edge singularity constraint at a reasonably high lift coefficient, the leading edge peaks that developed on both the wing and canard resulted in premature separation. An additional factor in this regard was the arbitrary modification of the wing twist and camber in an attempt to limit the outboard wing section lift.

(2) The section lift on the outboard wing was not sufficiently constrained.

(3) The total configuration trim requirement was not met.

(4) The small leading edge radius resulting from the thickness derivation is inappropriate if an intermediate design lift is selected. Such a thickness distribution still may be applicable if the lift where the twist and camber are derived is sufficiently close to the primary design point ($C_L \sim 1$).

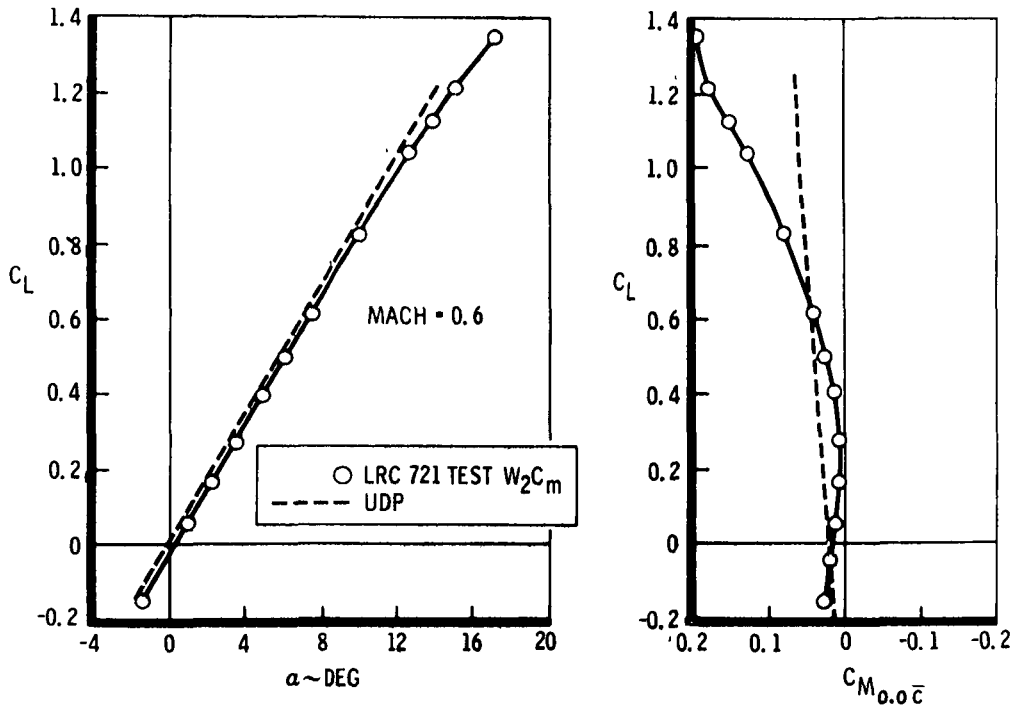

Figure 19.- Maneuver configuration longitudinal characteristics, -17A.

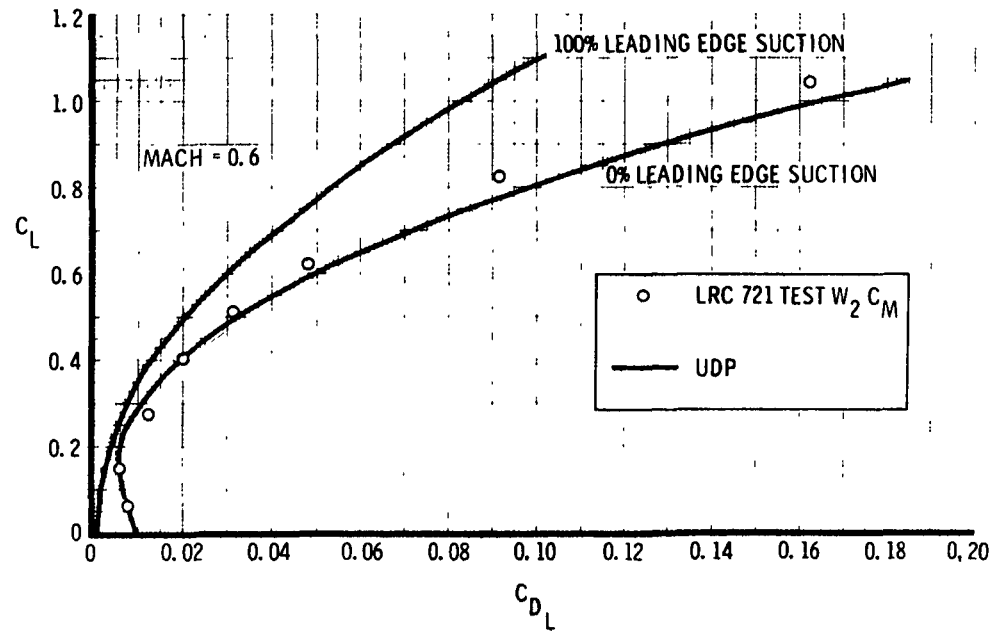

Figure 20.- Maneuver configuration (-17A) drag due to lift.

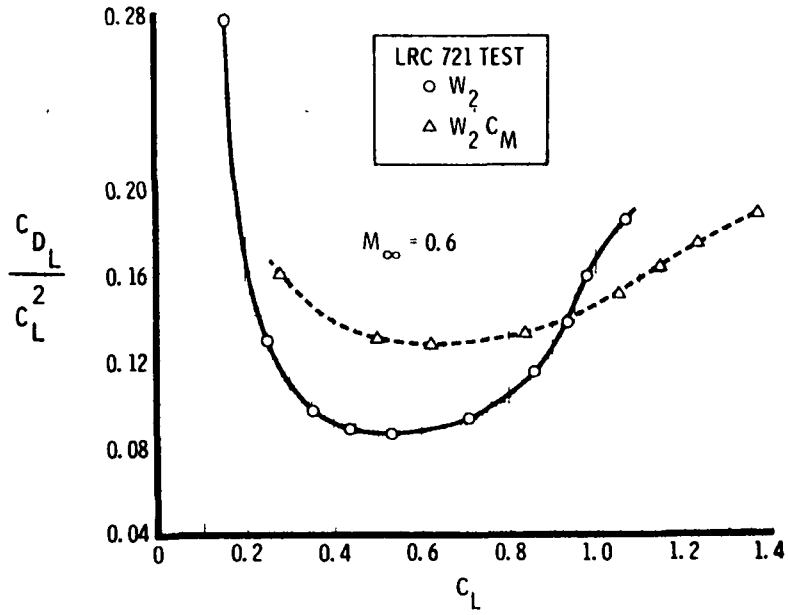

Figure 21. - Effect of canard on maneuver configuration (-17A) drag due to lift.

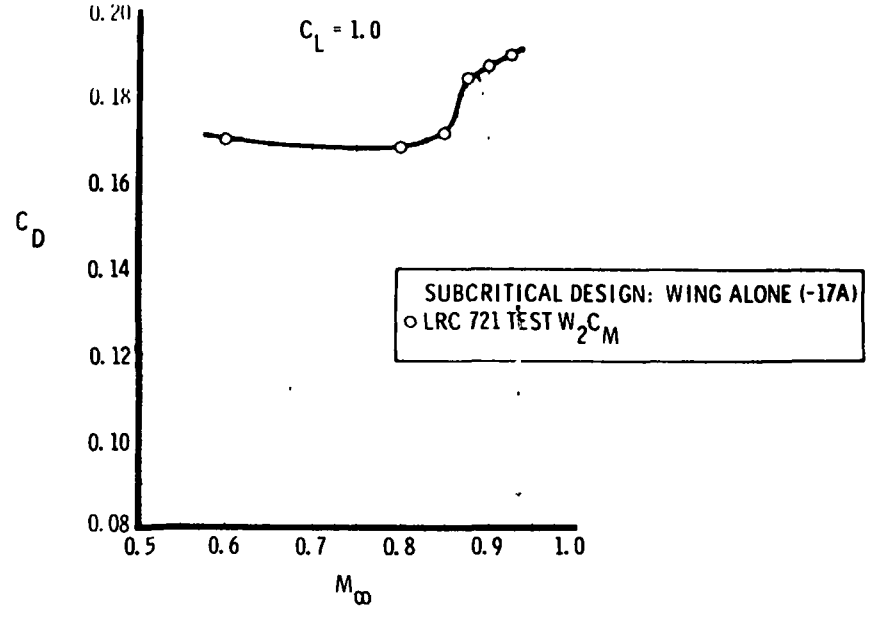

Figure 22. - Maneuver configuration drag rise.

A refined subcritical drag-due-to-lift optimization is capable of alleviating these problems. Additional actions required were to alter the stability variation due to the wing-body blending and strakes and to minimize the forebody pressure gradients.

Wing-Canard Design

Shortly after the initial design attempt, modifications to the linear theory design methods were made as noted previously. The design iterations involved in the second cycle are described in the following:

Objectives. - The overall objective was to optimize the drag due to lift for the entire configuration and set guidelines for this process for a close-coupled canard vehicle. The design goals utilized initially were:

(1) Twist and camber resulting in zero leading edge singularity at the design lift for both maneuver and cruise configurations

(2) Nearly optimum loading

(3) Trimmed configuration, including wing and canard loading, at the design lift

(4) Satisfactory thickness distribution (leading edge radius)

(5) Acceptable maneuver configuration upper surface pressure distribution at high loadings (spanload constraints)

The subcritical design points at $M_\infty = 0.7$ were $C_L = 0.5$ and 0.15 for the maneuver and cruise configurations, respectively. Additionally, the section lift would be limited to $C_\ell < 0.75$ for $C_L = 1$.

Design iterations. - A considerable number of solutions were evaluated with the modified design programs since the process was fully automated and used in an interactive mode. Attention was concentrated initially on the maneuver condition. Some preliminary calculations were made to determine the effect of the canard downwash on the wing twist and camber requirements for various loadings. Returning to the baseline -17A (figure 23) an optimum

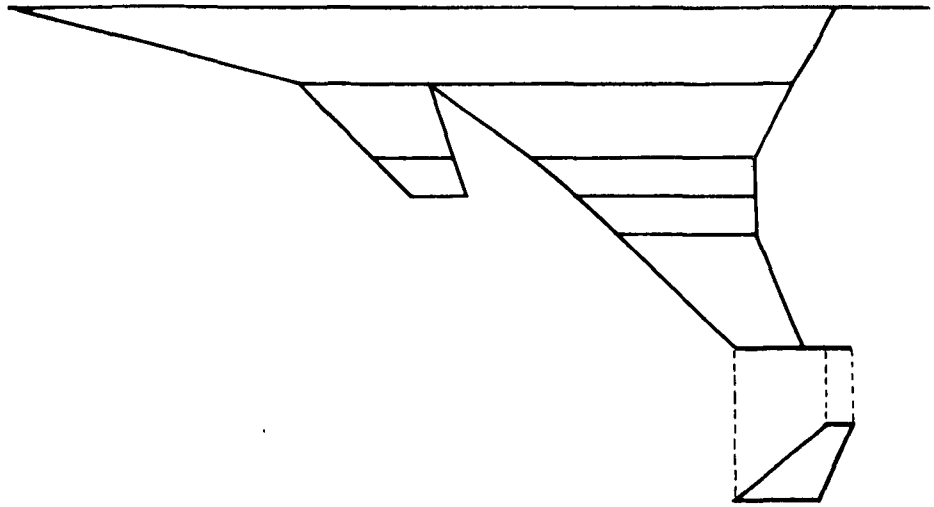

Figure 23. - HiMAT/RPRV planform, - 17A.

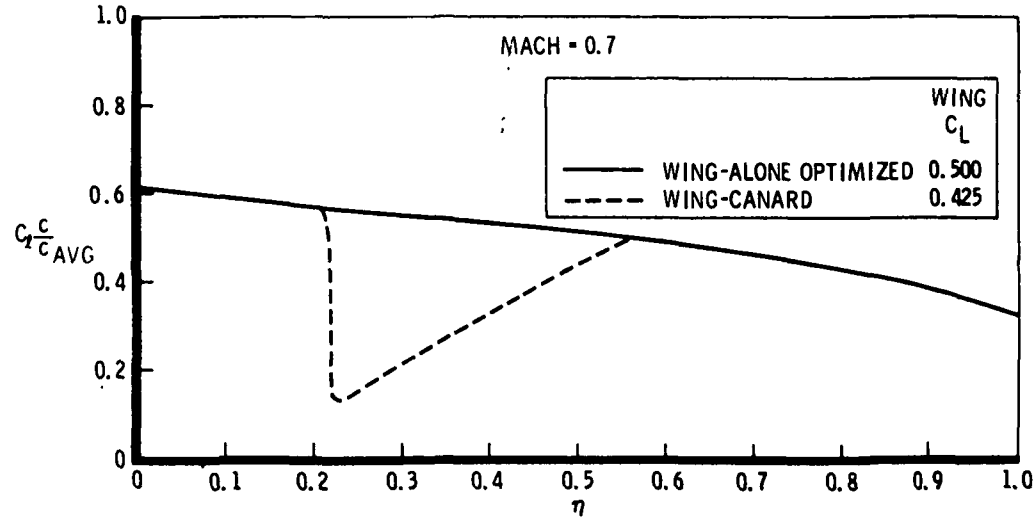

Figure 24. - Wing spanwise load distribution.

coplanar loading was calculated and the camber was derived for wing alone and wing-canard configurations. For the latter, an arbitrary load was removed from the wing (figure 24). The wing twist distributions (figure 25) illustrate the compensation required to counteract the canard downwash. With the same lift distribution, the effect of 20° canard dihedral was to decrease the peak downwash and upwash values resulting in the twist requirement shown on figure 25. The twist distributions for this example would of course not be considered in practice and indicate how the optimum loading may not be feasible. For additional wing-canard loadings the results indicated that the mutual interaction should be further dampened by increasing the vertical spacing of the surfaces.

Improved controllability at low speeds required the modification of the nonlinear moment characteristics of the strake arrangement. The wing strake and wing-body blending were deleted and the canard attachment point was moved inboard. The simulation is shown in figure 26. This was an interim configuration and for reference purposes it will be designated here as the -30Λ wing and -40Λ canard. Efforts to obtain a practical maneuver camber satisfying the design constraints were initiated with the calculation of the optimum loading. For the nonplanar configuration the wing-canard load distribution is now determinate. The load distributions for the optimum condition and the required wing twist are shown in figures 27 and 28, respectively. One of the design requirements was a limitation on the section lift. In figure 29 the boundary for $C_\ell = 0.75$ at $C_L = 1$ is compared with the results for the optimum. In the derivation of the optimum span load, constraints may be imposed for any number of surfaces. The outboard third of the wing was constrained to a lift coefficient equal to that corresponding to the design boundary of figure 29. With the canard constrained to $C_L = 0.075$, the wing span loads and twist distributions are shown in figures 27 and 28. The constraint process was successful in limiting the section lift at the wingtip (figure 29). However, the twist required (figure 28) to unload this region was impractical.

To obtain a smoother wing twist, the large variations in span load were eliminated. This was accomplished with two modifications. First, to reduce the outboard wing section lift and lift curve slope, the chord was extended. This allowed a higher design load to be specified. Second, loading was transferred from the inboard wing to the canard. The canard modifications were based on the following compromises:

(1) To eliminate possible unfavorable interference where the canard and wing overlapped, the canard trailing edge attachment point was moved forward.

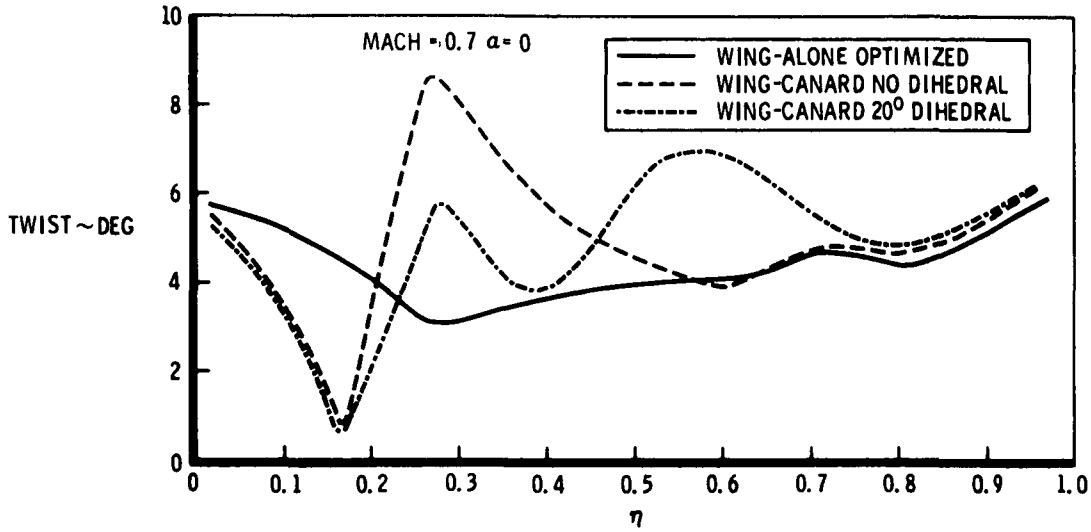

Figure 25. - Wing spanwise twist distribution.

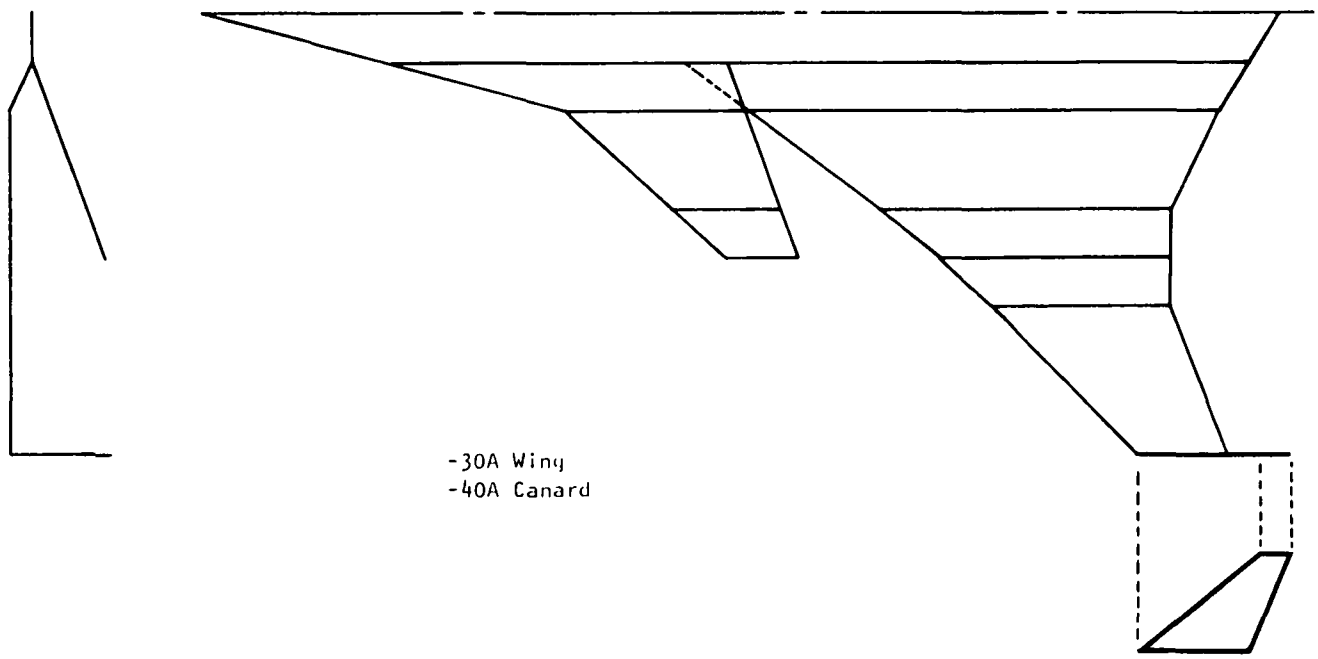

Figure 26. - HiMAT RPRV planform.

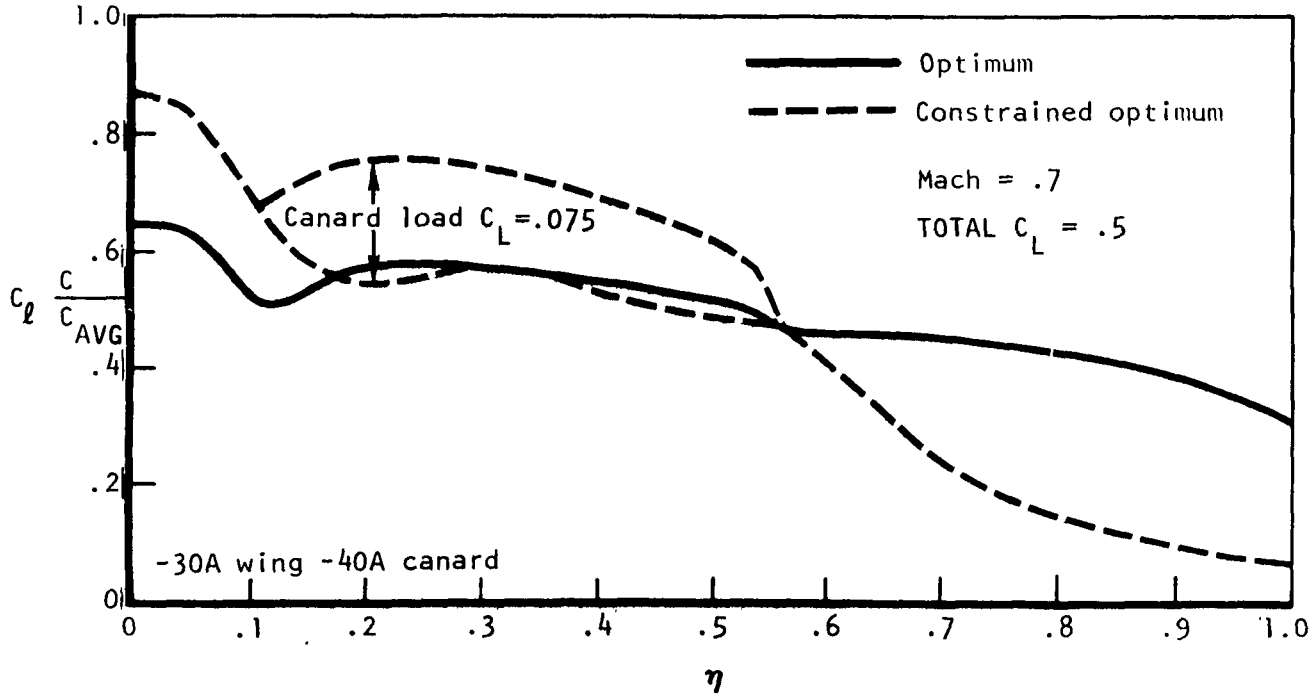

Figure 27. - Wing-canard spanwise load distribution.

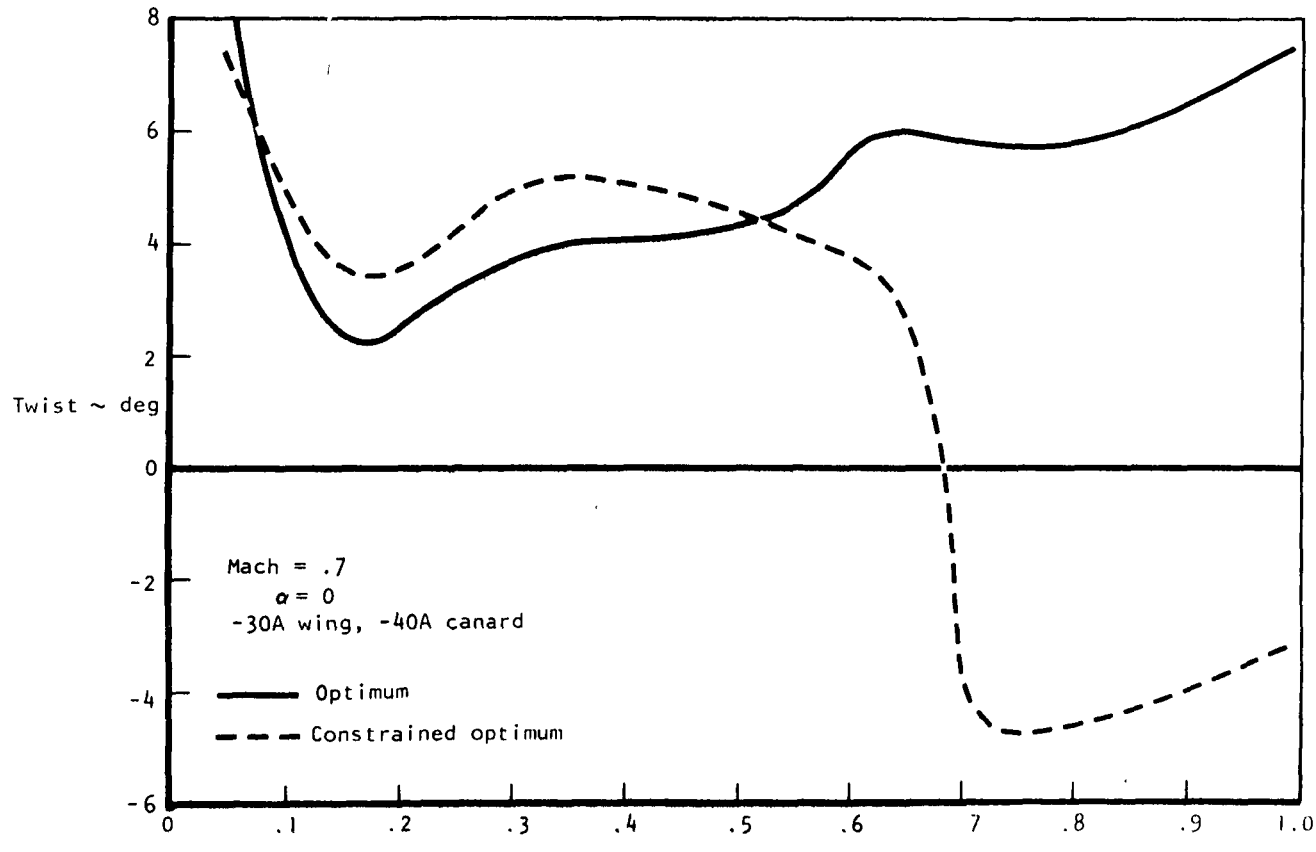

Figure 28. - Wing spanwise twist distribution.

(2) The canard sweep was changed to maintain approximately the same stability levels for the forward position and increased area.

(3) In an attempt to reduce the nonlinear moment at moderate lifts but retain the vortex lift concept at higher lifts, the canard strake was removed and the canard leading edge sweep was increased to 63°.

These revisions are shown in figure 30.

A constrained optimum span load was calculated with 30% of the design load on the canard and the wing load constrained as before. The load and twist distributions are shown on figures 31 to 34. As a result of the more even load distribution, the wing twist is smoother relative to earlier results. In deriving the solution, the following parameters were monitored:

(1) Drag-due-to-lift penalty resulting from constraints, and

(2) Chord load shape.

The chord load distribution must be such that acceptable upper surface pressure distributions result at and above the design point (C_L = 0.5). Since the chordwise load shape is primarily a function of $(X/C)_{cp}$, a spanwise distribution of $(X/C)_{cp}$ is prescribed so that the isobars are properly swept.

The wing twist distribution was smoothed as noted in figure 33. At some span stations the zero-singularity requirement will not be met at the design point. The net effect on drag due to lift was negligible. However, this compromise produced a leading edge peak on the outboard wing. The section lift constraint was met on the outboard wing, but was not met on the canard tip. This was a compromise in an effort to produce a smooth wing twist and camber. When trimmed at C_L = 1, the canard section lift exceeded only slightly the design constraint.

Cruise wing. - A similar design was obtained for the cruise condition, C_L = 0.15. The outboard wing loading was not constrained. To achieve compatibility in camber shape the same load balance was assumed, that is, 30% of the total lift was placed on the canard (figure 35). This constraint resulted in only a 0.0003 vortex drag penalty relative to the optimum. The wing and canard twist are shown in figure 36. The cambers were similar in shape to the maneuver configuration but they could not be obtained geometrically from the maneuver camber by deflection of the leading edge. Therefore, over most of the wing, the cruise camber slopes were replaced by the maneuver values for the center chordwise region. An analysis indicated no drag-due-to-lift penalty. The design cruise and maneuver camber distributions for η = 0.5 are shown in figure 37 along with the modification for the cruise wing.

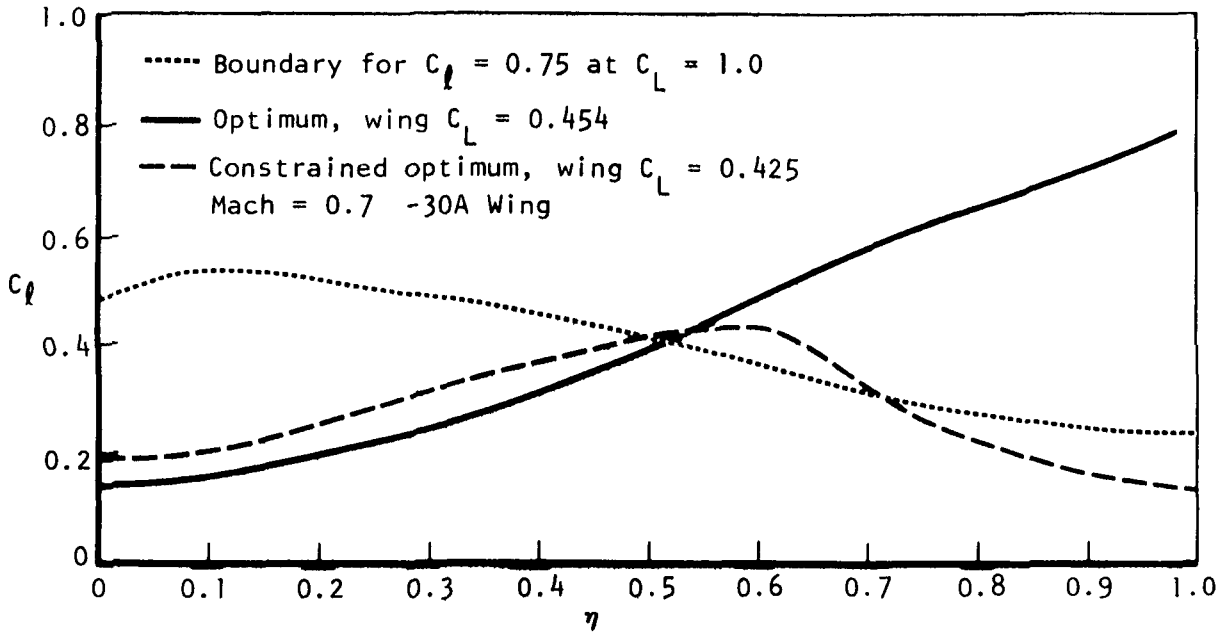

Figure 29. - Spanwise variation of wing section lift.

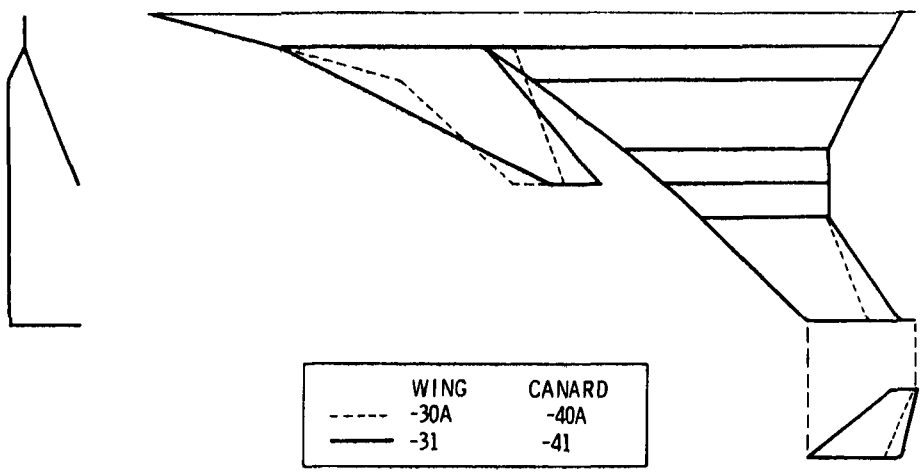

Figure 30. - HiMAT/RPRV planform.

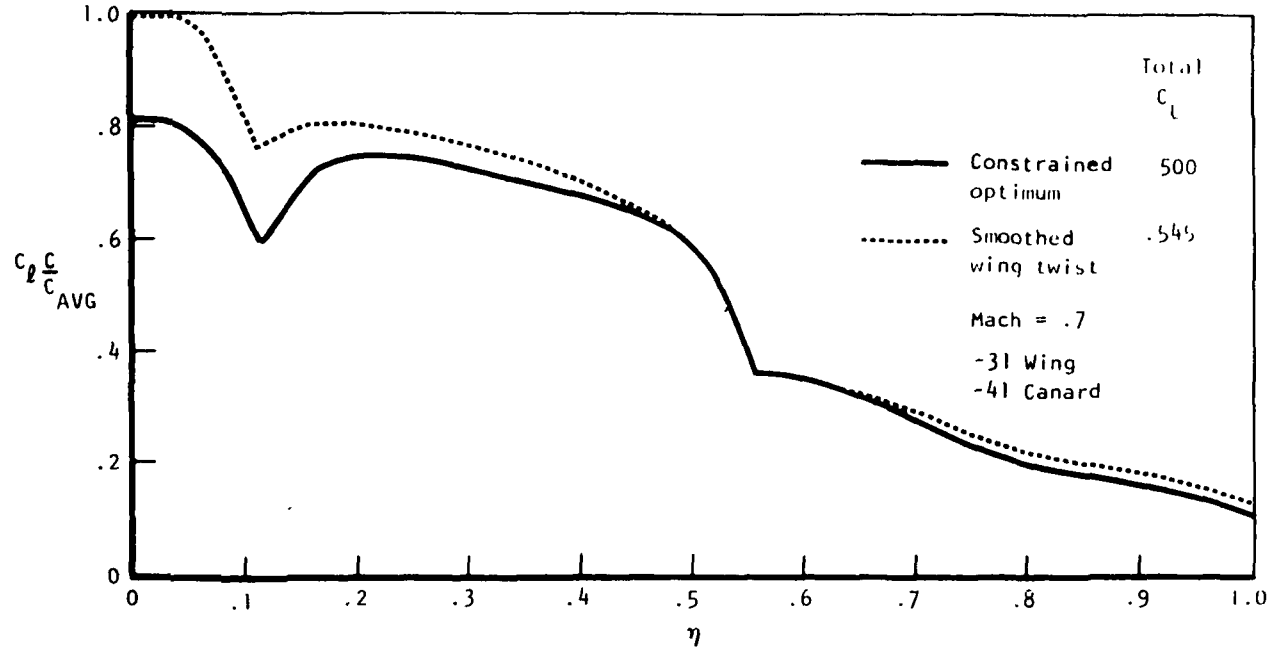

Figure 31. -1 Wing-canard spanwise load distribution.

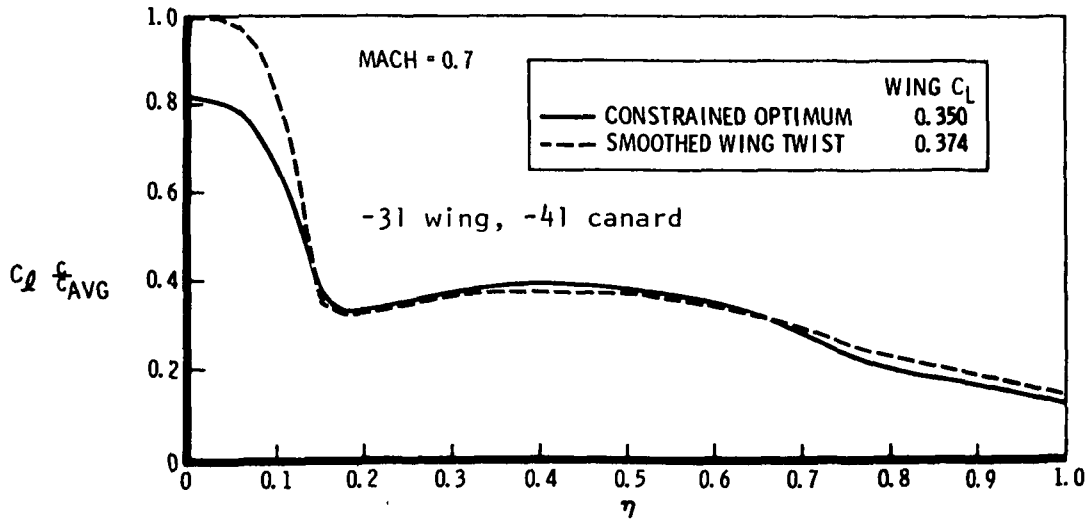

Figure 32. - Wing spanwise load distribution.

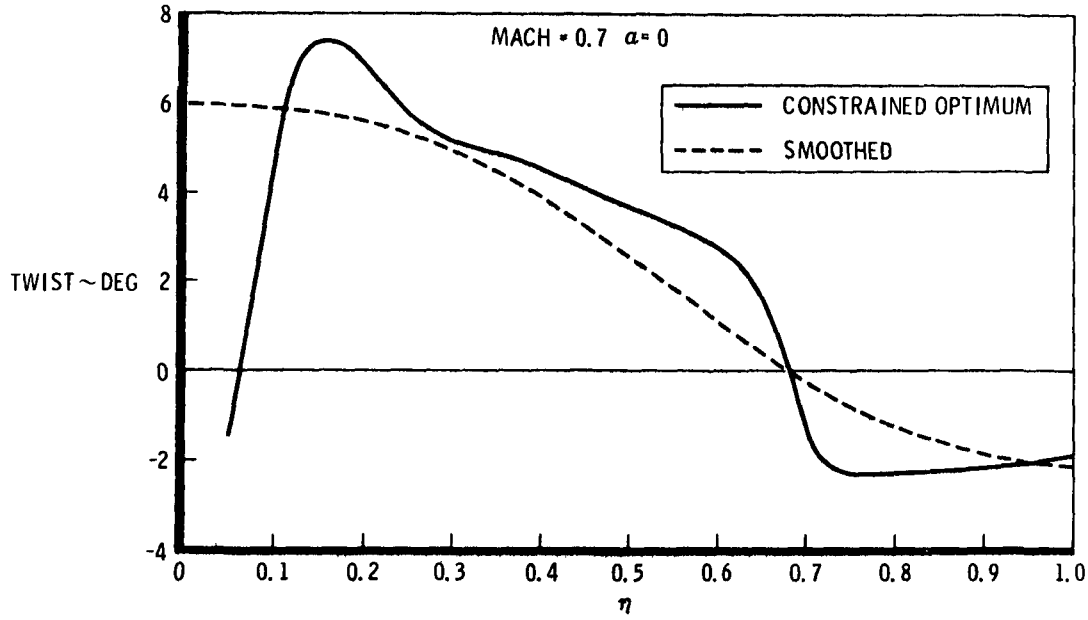

Figure 33. - Wing spanwise twist distribution.

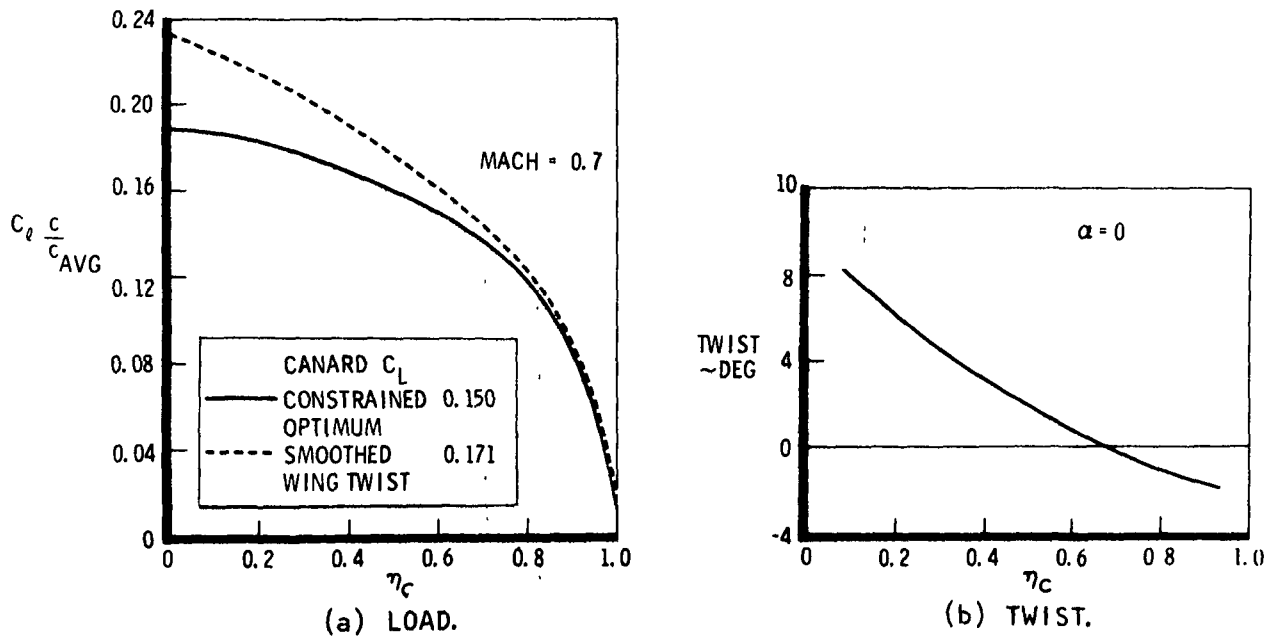

Figure 34. - Canard spanwise distributions.

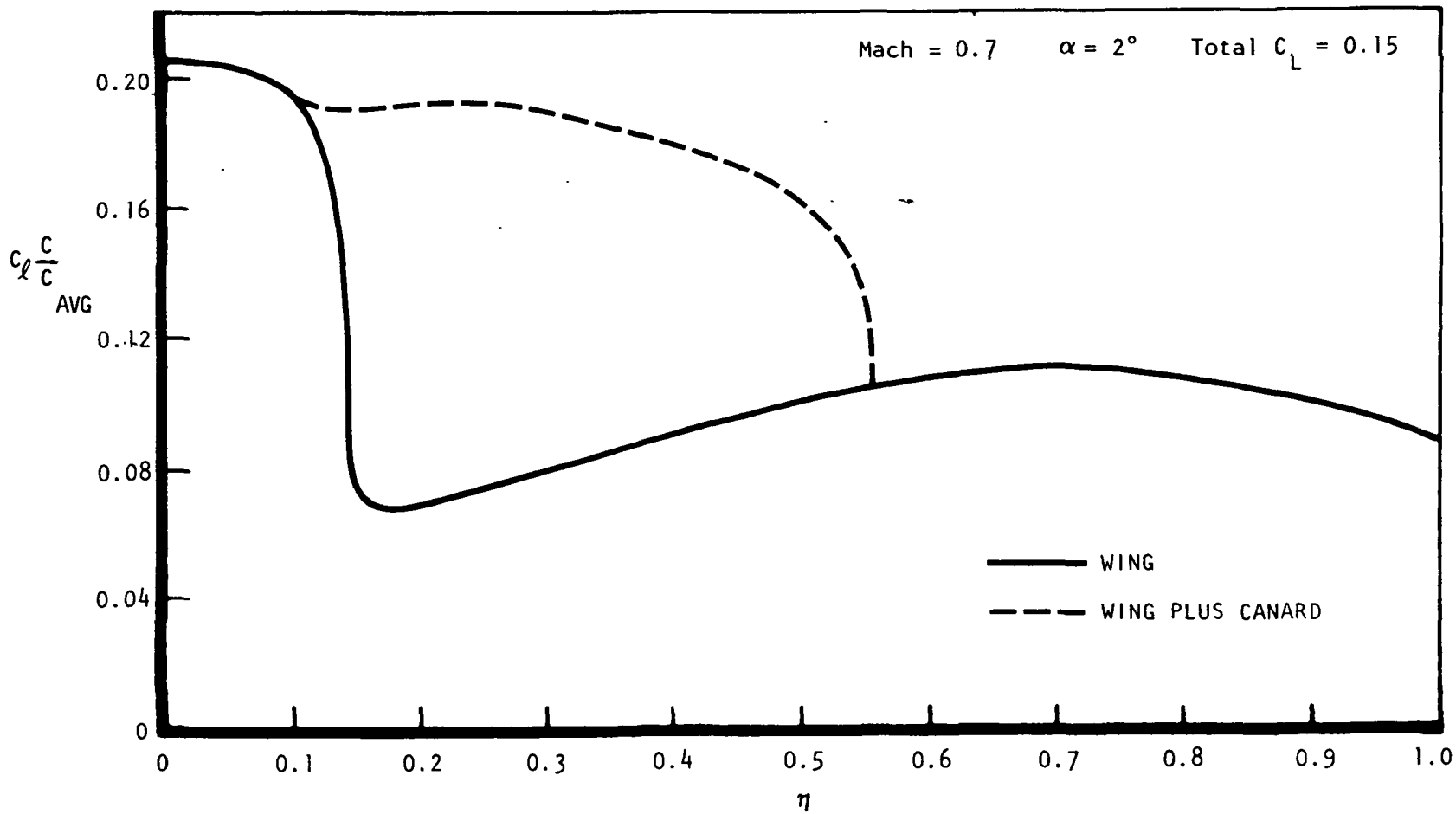

Figure 35. - Spanwise load distribution for cruise configuration.

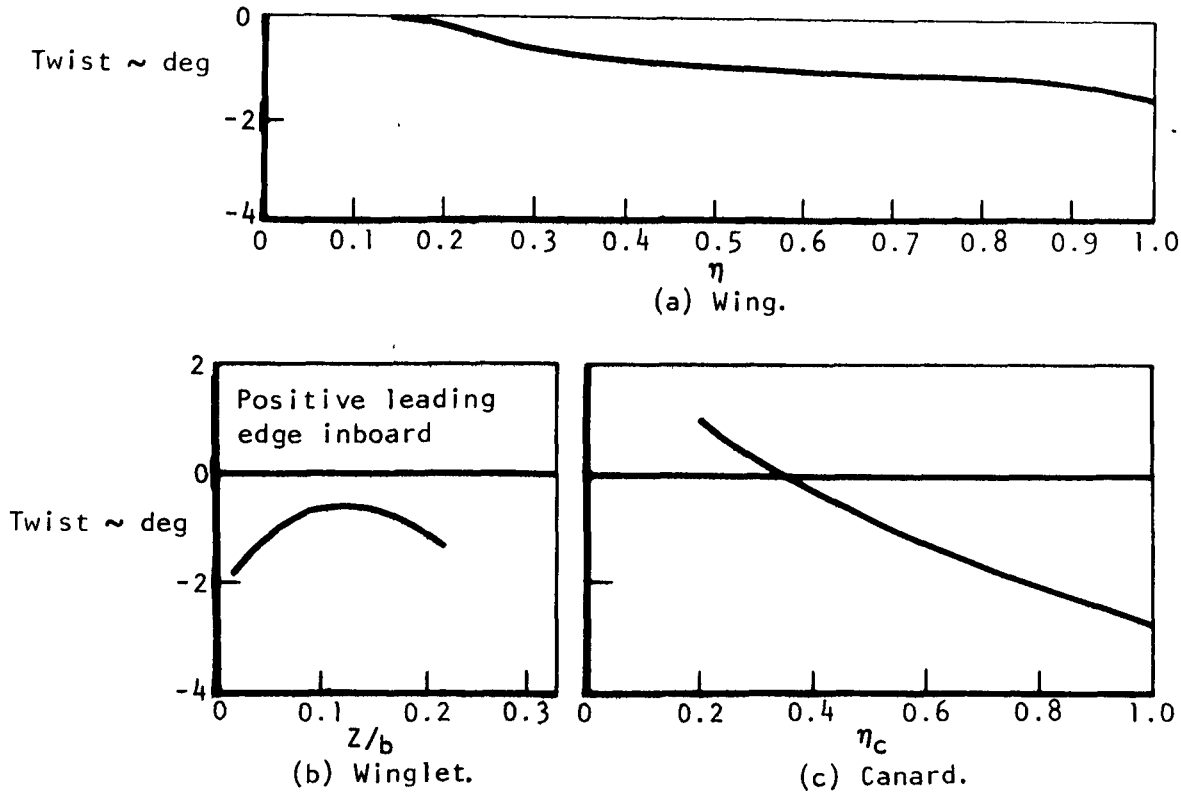

Figure 36. - Cruise configuration twist distributions.

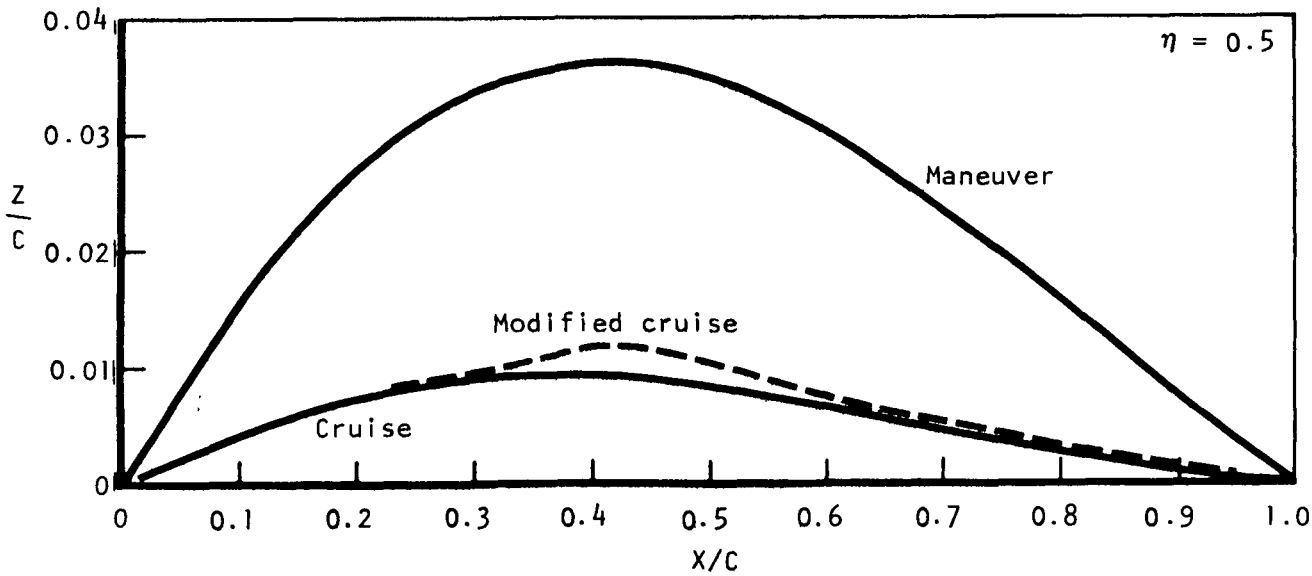

Figure 37. - Wing variable camber system requirements.

Thickness derivation. - The thickness distributions were derived for the cruise condition using the linear theory design guidelines. The assumed upper surface pressure distribution is shown in figure 38 along with a typical chordload shape and the resulting thickness distribution. The importance of properly prescribing the chordload shape is illustrated by the comparison with the -17A results. The improved leading edge will minimize the development of pressure peaks at off design.

The thickness distributions for the inboard wing are shown in figure 39. To reduce the supersonic pressure drag, a thinner section was designed based on a compromise between a flat-top upper surface pressure distribution and the associated wave drag due to volume (figure 39). The revised thickness distribution was also selected to produce a triangular type pressure distribution such that the local isobar sweep was slightly higher than the wing generator sweep in the forward wing region.

Lifting surface analysis. - The maneuver sections were constructed and analyzed at $M_\infty = 0.7$ for a range of lift coefficients. For $C_L = 0.88$ the wing and canard upper surface pressure distributions are shown in figure 40. In general the desired isobar sweep has been achieved and the aft gradients are moderate. As noted previously, as a result of smoothing the twist, the outboard wing exhibits a leading edge pressure peak. A yawed wing viscous calculation predicted transition due to cross flow instability near the leading edge but no separation of the turbulent boundary layer.

For comparison, the results for the -17A configuration, at a lower lift of $C_L = 0.78$, are shown in figure 41. The superiority of the revised design is indicated by the overall reduction in adverse pressure gradients. For subcritical flow, no additional problems are indicated from this analysis of the maneuver sections. The remaining problems, alluded to previously, are the excessive section lift on the canard and the leading edge singularity resulting from the smoothing of the twist. Efforts were initiated to correct these deficiencies as explained in subsequent sections.

Fuselage modifications. - The forebody and canopy regions were revised in an attempt to weaken the adverse pressure gradients, which produced shock-induced separation at the transonic design point. The objective was to reshape the forebody maintaining approximately the same longitudinal area distribution for wave drag considerations and weakening the growth of pressure peaks in the region of the canopy. Any adverse effect in this region is increased due to carryover loading from the canard. This carryover loading was evaluated for the equivalent body of revolution to establish where the interference would be greatest. The arbitrary slender-body analysis was then used to determine, by

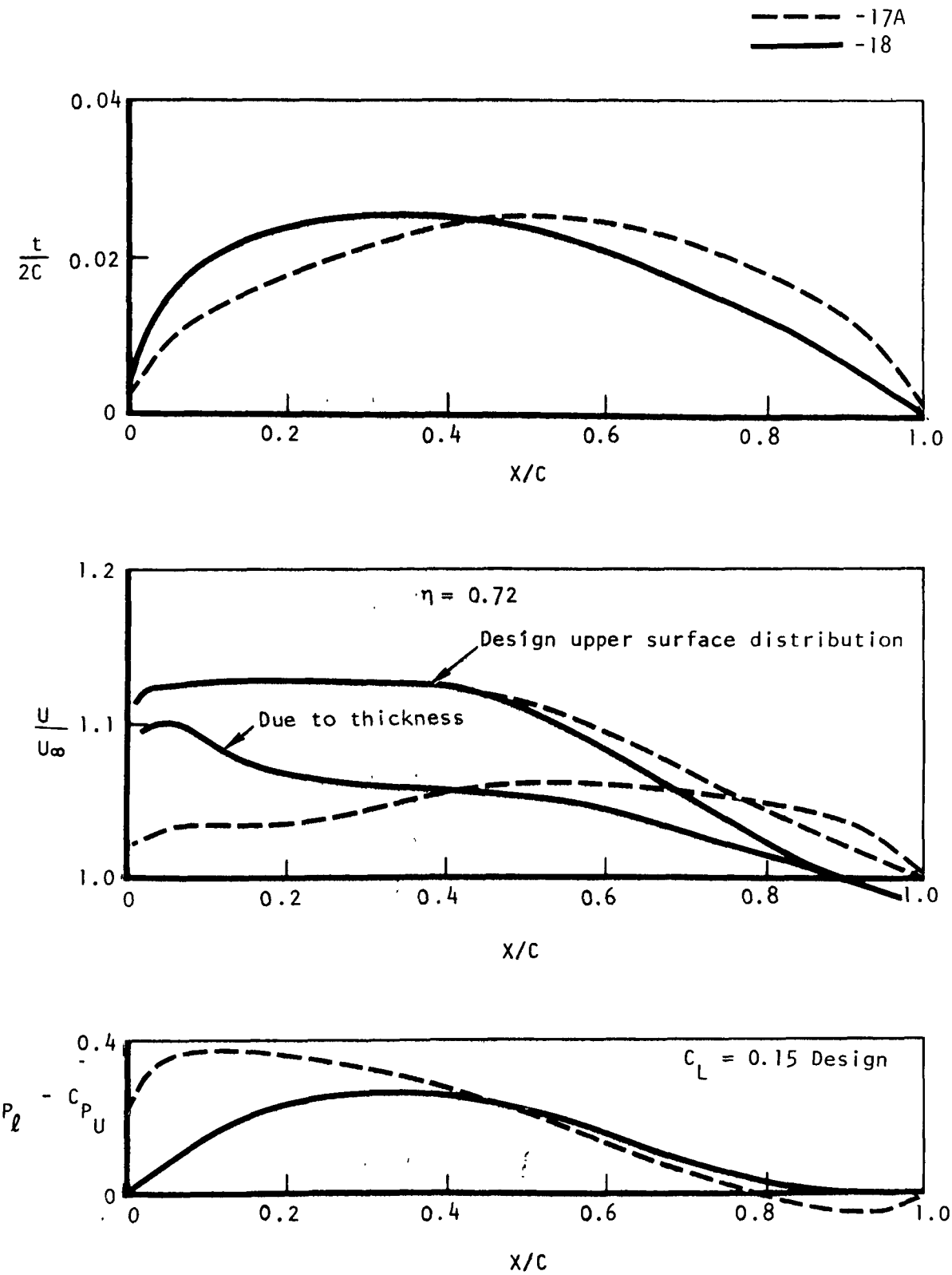

Figure 38. - Derivation of thickness distribution.

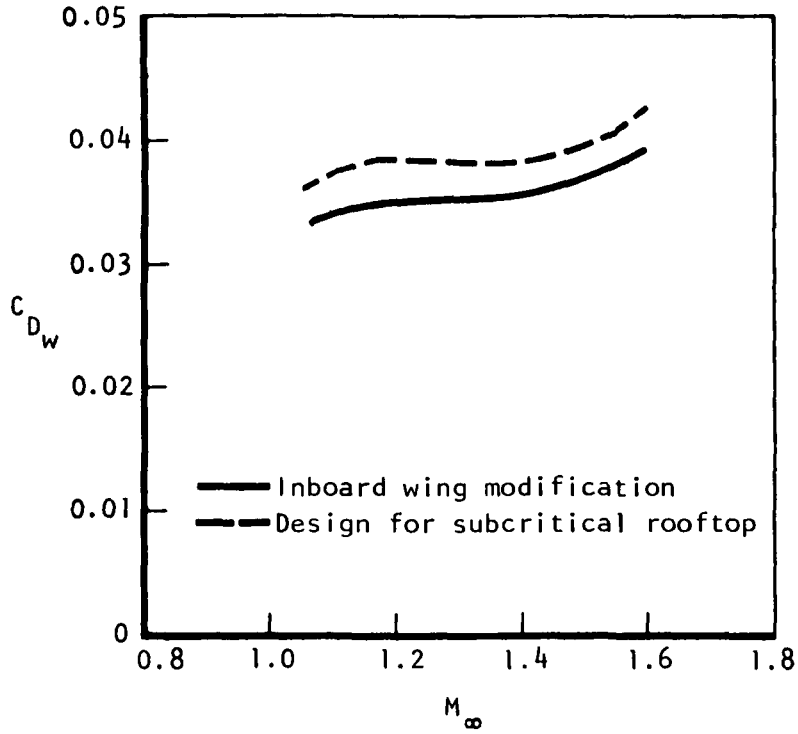

(a) Wave drag.

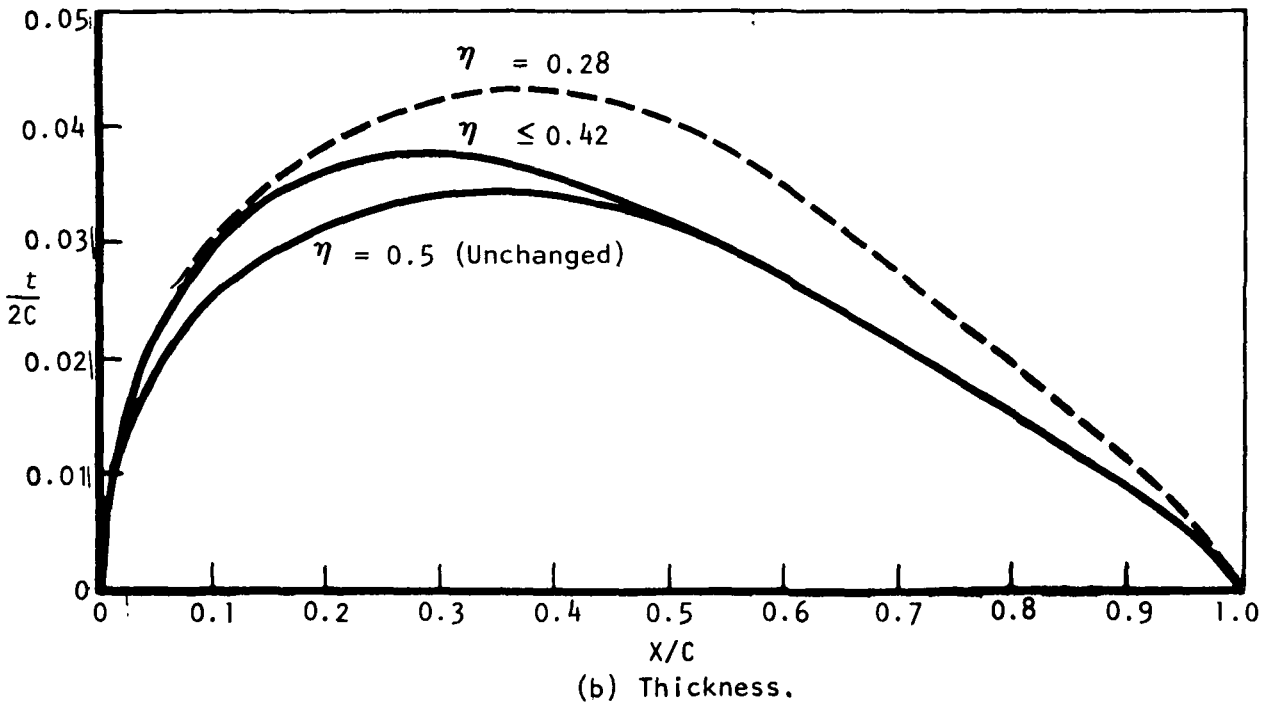

(b) Thickness.

Figure 39. - Inboard wing modification to reduce wave drag.

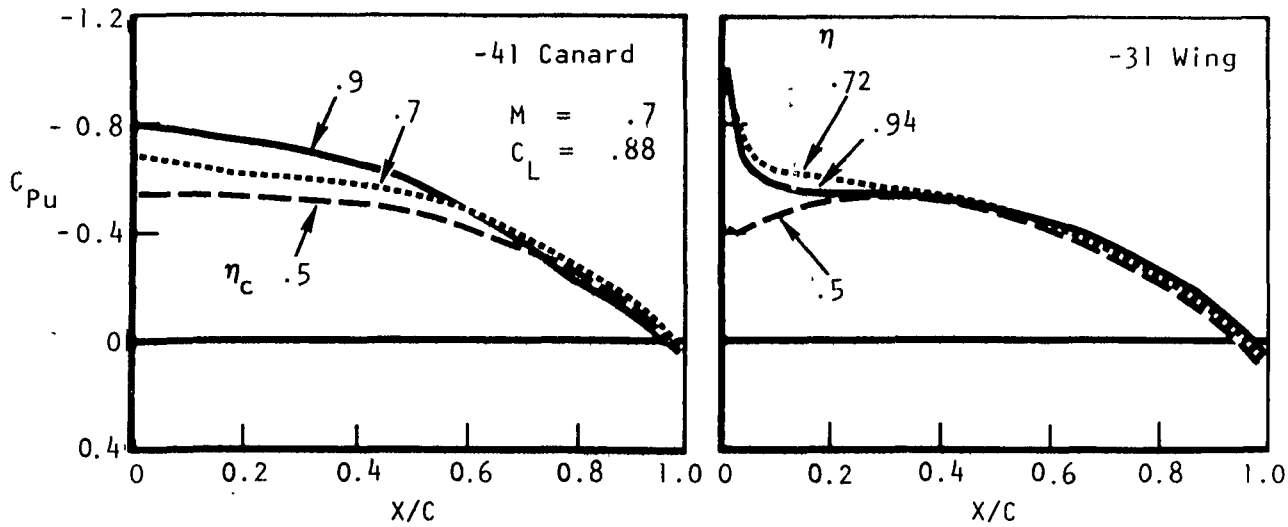

Figure 40. - Maneuver configuration (-18) upper surface pressure distributions - linear theory.

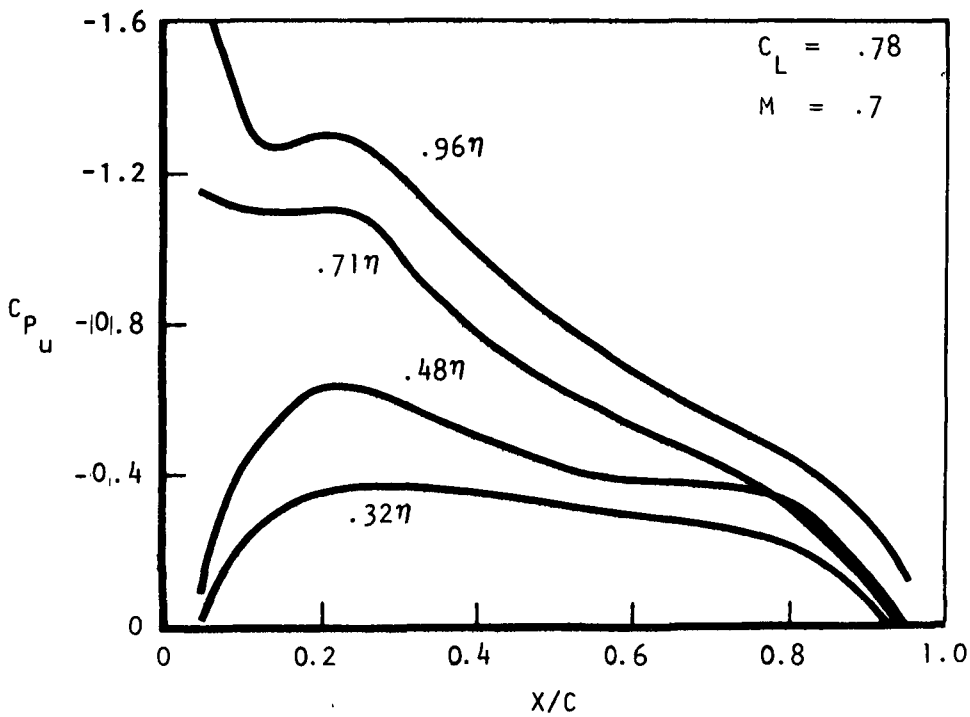

Figure 41. - Calculated -17A maneuver wing upper surface pressure distribution, wing-canard configuration.

iteration, a suitable forebody geometry that would limit the growth of peak pressures with angle of attack. In this way, the longitudinal adverse gradients would be reduced.

The original -17A and the revised cross sections at X/L = 0.25 are shown in figure 42. At this station the carryover interference was largest. The extent of the reduction of the upper surface velocities is shown in figure 42 and indicated that the adverse gradients will be substantially reduced.

Test analysis. - The maneuver and cruise designs referred to as the -18 configuration (figure 43) were tested to determine both low speed and transonic characteristics. Discussion of the cruise wing characteristics will be deferred to a later section but the transonic, M = 0.9, drag-due-to-lift goal was met at the cruise lift coefficient.

Results for the maneuver configuration at subcritical conditions, M = 0.6, are presented in figures 44 and 45 along with theoretical estimates. Lift and moment are shown in figure 44. The moment reference point is the leading edge of the mean aerodynamic chord, $\bar{c}$, while the center of gravity used in the design was $0.07\bar{c}$ aft. The fact that the analytical model was not trimmed at the design C_L is due to the smoothing of the twist distribution. The difference between predicted and experimental moment resulted from some discrepancies in the model design twist and camber. Of importance, though, is the reduction of the nonlinear moment for the intermediate lift range.

Drag due to lift is shown in figure 45. The improvement relative to the -17A configuration is indicated by comparing these results with figure 20. For the -18, at high lift, leading edge suction is lost due to separation on the canard or the outboard wing, or both. The drag due to lift is, however, still 30% lower than the previous configuration because the polars are tangent at the prescribed design lift.

At the transonic design point (M = 0.9, C_L = 1) there was appreciable drag rise resulting from an unswept shock on the inboard wing and shock-induced separation on the outboard wing. However, the body-canopy shock was substantially weakened.

Conclusions. - The major conclusion was that the subcritical design process was successful in reducing the drag due to lift by:

(1) Constraining the span load

(2) Maintaining the tangency of the 0% and 100% suction drag polars

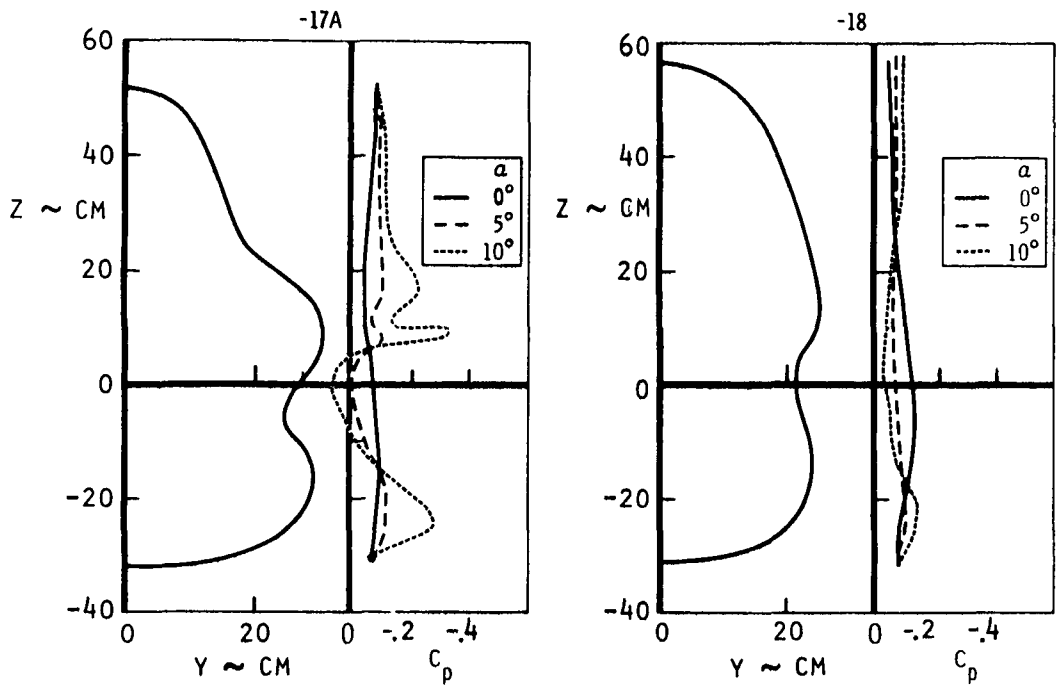

Figure 42. - Forebody circumferential pressure distribution X/L = 0.25.

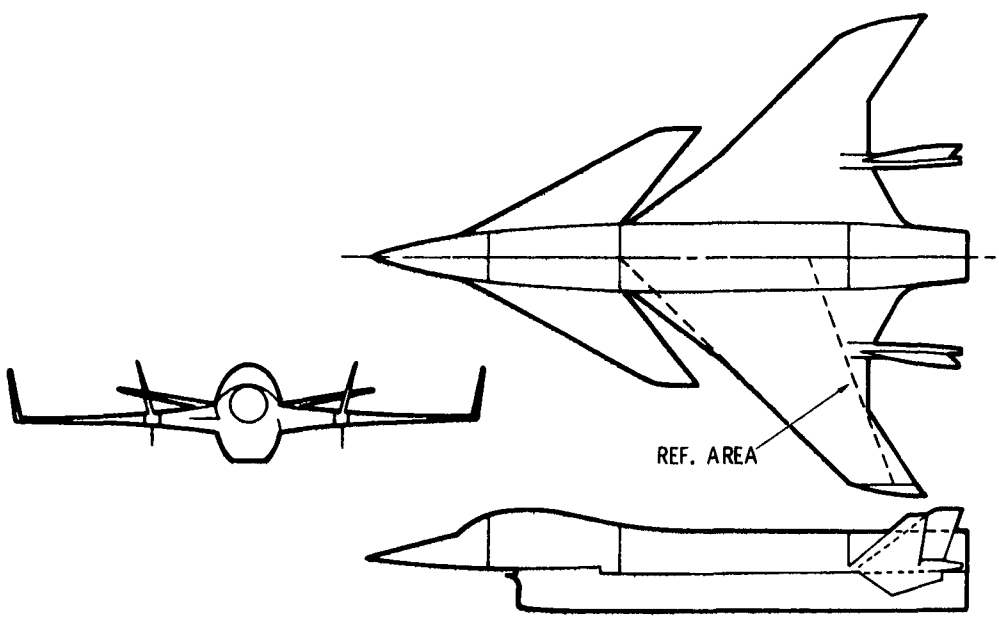

Figure 43. - RPRV wind tunnel model, -18.

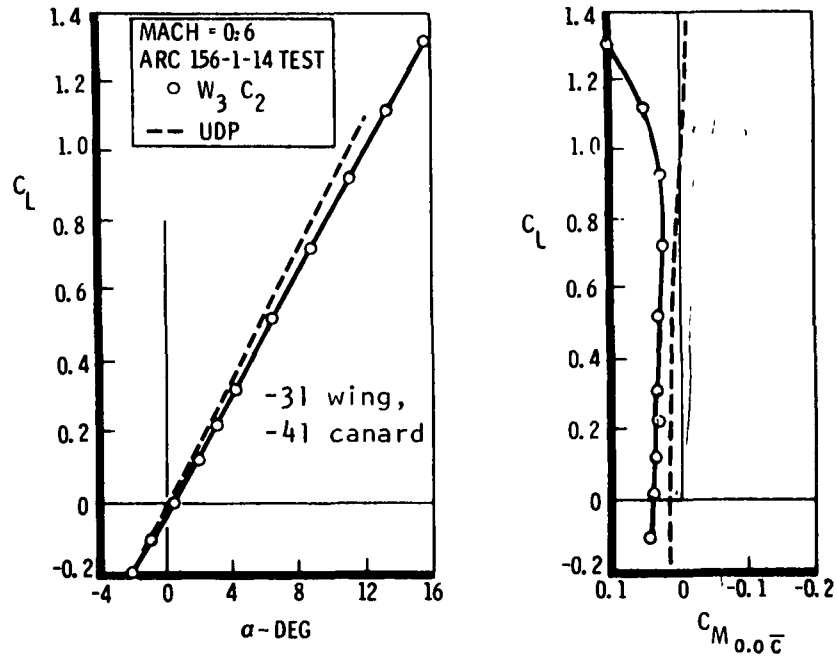

Figure 44. - Maneuver configuration longitudinal characteristics.

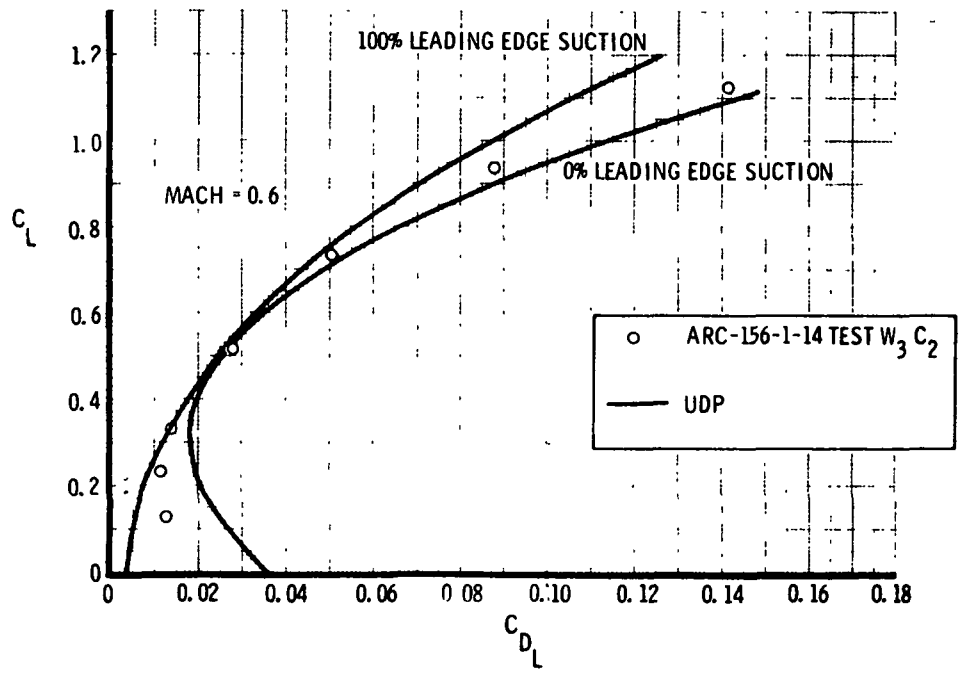

Figure 45. - Maneuver configuration drag due to lift.

(3) Providing a sufficient leading edge radius to accommodate the difference in the required ($C_L \sim 1$) and design (0.5) lift coefficients

The loss in efficiency at higher lifts may be corrected by constraining the canard lift and eliminating the leading edge peak on the outboard wing. Redesign of the twist/loading distributions will also restore the self-trimming capability. The unsatisfactory characteristics at transonic speeds were not surprising since no modifications were made to the design for this operating range.

Revised Subcritical Design

Objective and implementation. - The objectives of the second subcritical wing-canard design cycle were to examine the various wing-canard loading combinations which would meet the section lift requirements and to derive a twist and camber that did not require modification. To accomplish both objectives the constrained optimum solution was not used directly. Instead, the loading was prescribed at each span station so that all constraints would be met. For the inboard wing, where section lift constraints were not required, the loading was adjusted and the camber examined in an iterative cycle.

Design iterations. - The span load/camber iteration was initiated with the load distribution resulting from the first -18 design. To satisfy the section lift constraints, load was shifted from the canard to the wing. The loading on the inboard wing was varied until a smooth twist and camber resulted. The revised wing-canard loading is shown in figure 46 and the corresponding twist distributions are presented in figure 47. Since the design twist was not compromised, the leading edge singularity does not occur at the intermediate design point and is weakened at the maneuver point in comparison to the previous design.

For the revised design, the moment constraint was relaxed to provide favorable transonic trim requirements. At the design lift, $C_L = 0.55$, the configuration was trimmed at 0% $\bar{c}$, forward of the actual center of gravity. The revised load and moment balance resulted in maximum wing cambers which were considerably larger than the original design. To provide compatibility with the cruise configuration, the solution was actually obtained at $M_\infty = 0.9$. For linear theory the span load shape is essentially independent of compressibility. The penalty in 0% suction drag at subcritical conditions was small, as will be shown subsequently.

The twist and maximum camber distribution for the revised wing (-34) are compared to the previous results in figures 48 and 49. Note that the

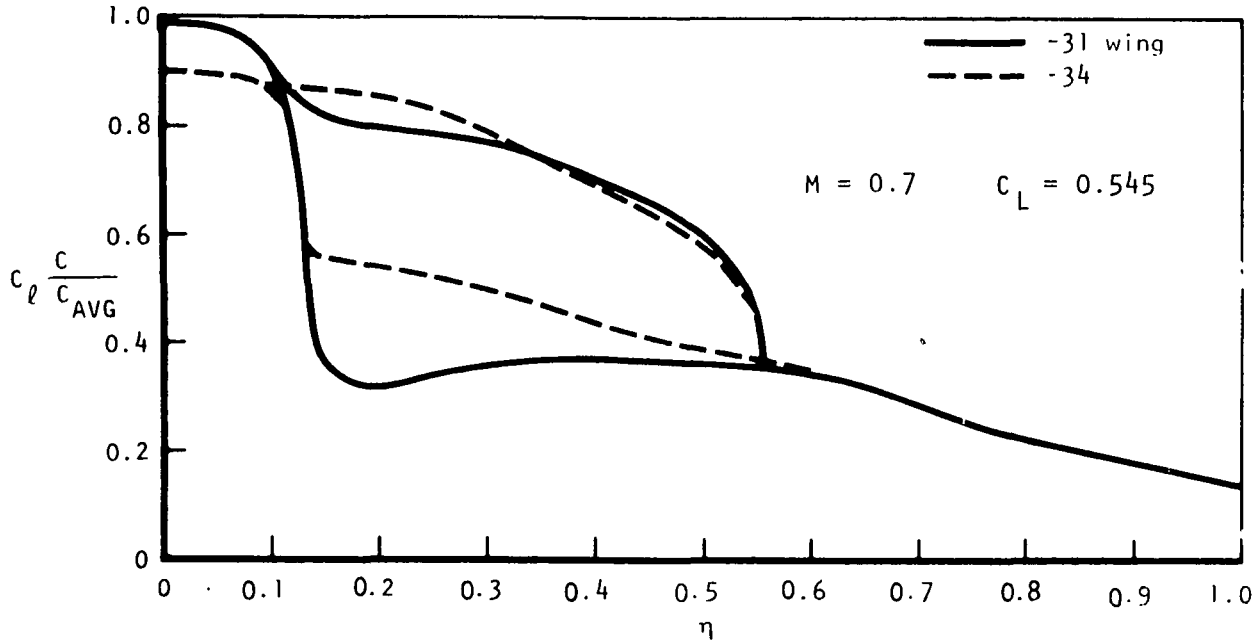

Figure 46. - Modified spanwise load distribution.

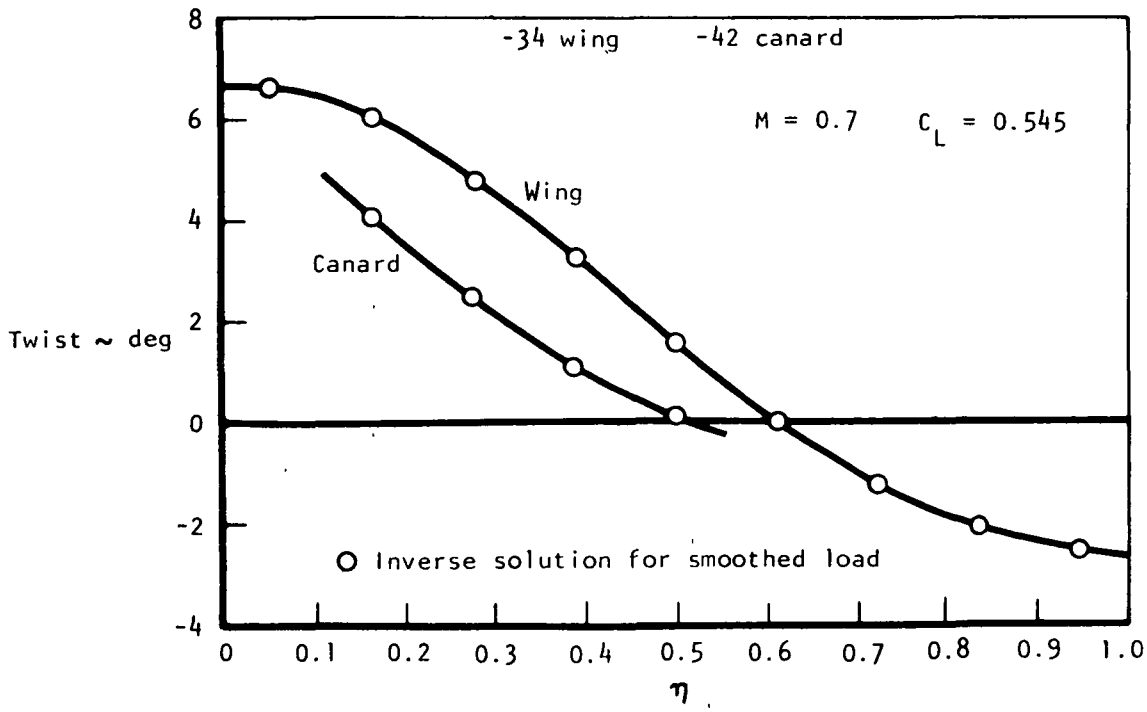

Figure 47. - Modified maneuver configuration twist requirements.

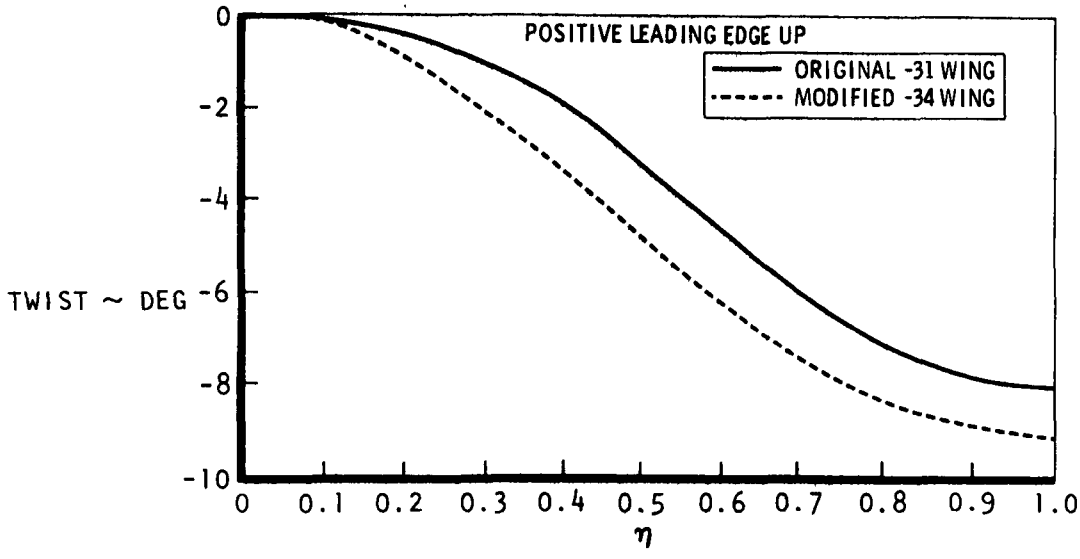

Figure 48. - Spanwise variation of wing twist.

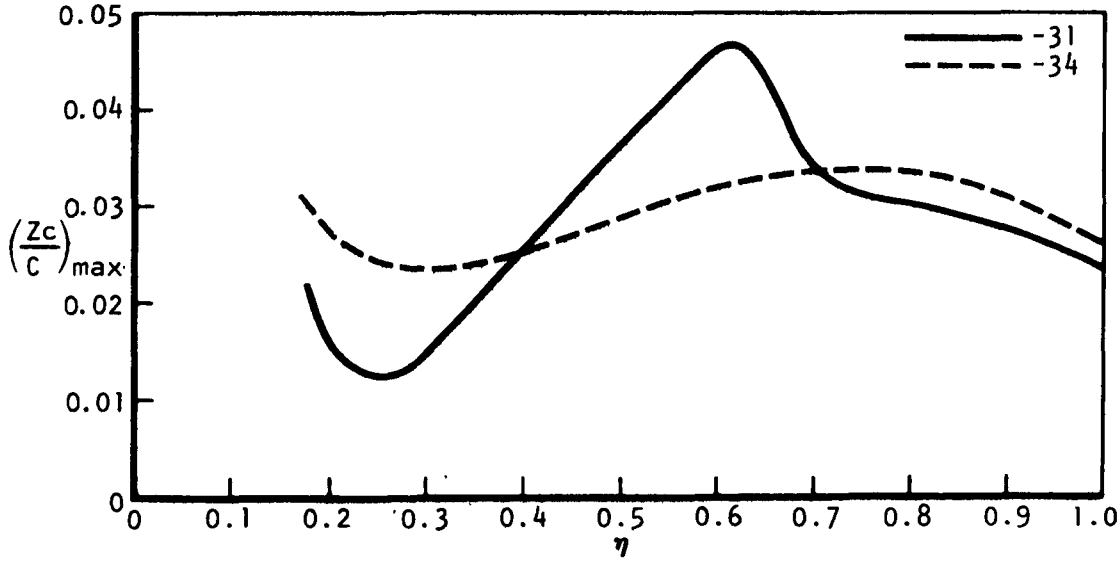

Figure 49. - Wing maximum camber.

spanwise camber distribution has also been smoothed due to the revised loading. The corresponding results for the canard are shown in figures 50 and 51.

Test analysis and comparison with theory. - The 0.22-scale model of the -18 configuration was modified and tested in the Ames 14-Foot Transonic Wind Tunnel. Longitudinal characteristics at subcritical conditions, M = 0.6, are shown in figures 52 and 53. A linear theory lifting surface analysis was made with the measured model coordinates. The agreement with the experimental lift and moment (figure 52) is quite satisfactory. Drag due to lift is shown in figure 53. The increase in the 0% suction drag relative to the previous configuration (figure 45) is small. Of more importance is the reduction in vortex drag (100% suction) resulting from the improved span load shape. The increased efficiency at high lifts results from the canard section lift constraint and the improved upper surface pressure distribution on the outboard wing.

The untrimmed drag rise characteristics of the first -18 configuration and the revised design are shown in figure 54. The revised configuration meets the subcritical design goal but, as expected, both subcritical wing-canard designs are deficient at the transonic design point. The oil flow results for the transonic maneuver condition (figure 55) indicate shock-induced separation on the outboard wing and canard and an unswept shock near the trailing edge of the inboard wing.

Conclusions. - The test results confirm the validity of the design process for subcritical flow for high lift, high efficiency operation. As a measure of the total efficiency achieved reference is made to figure 53 where the flat plate drag-due-to-lift factors $1/\pi AR$ and $1/C_{L\alpha}$ are compared with the test data. Of course for a nonplanar configuration the optimum is $1/\pi ARe$ where $e \sim 1.3$ for the HiMAT design. This optimum, though, can only be realized at high loadings to the extent separation can be eliminated. The subcritical design now provides a basepoint from which further modifications can be made for supercritical flow. The subcritical design process cannot be expected to yield satisfactory designs for low aspect ratio, highly loaded configurations operating in the transonic range. However, this process provides an effective means of initializing the design.

Wing-Body Interference

The subcritical design was obtained with the body simulated as a lifting surface. The alternative is to replace this lifting surface with a slender body and an interference shell located near the surface of the actual body. Some of the consequences of this alternative will be examined in the following paragraphs.

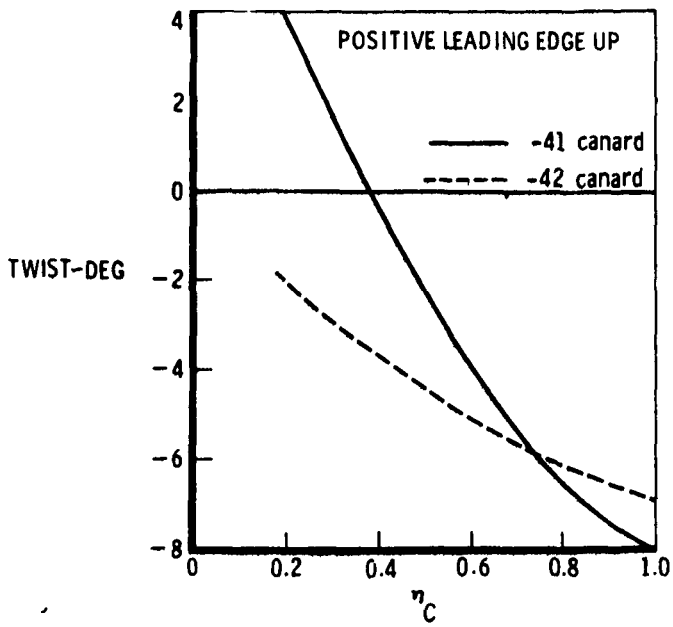

Figure 50. - Spanwise variations of canard twist.

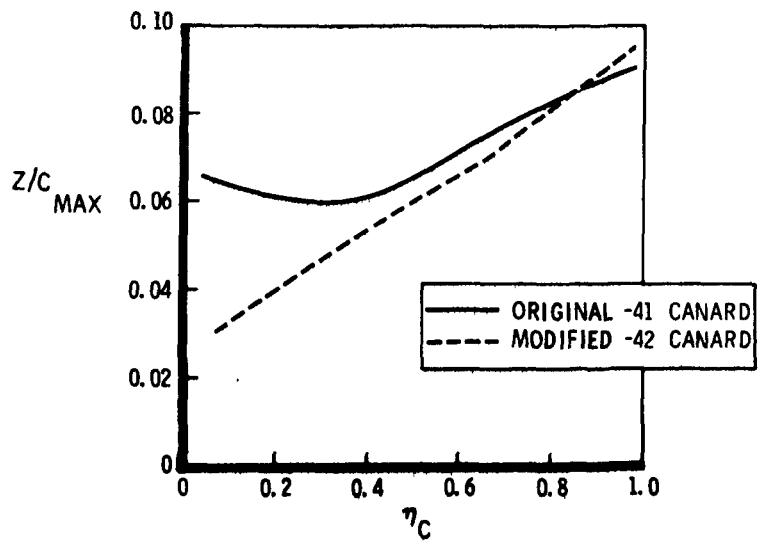

Figure 51. - Spanwise variation of maximum canard camber.

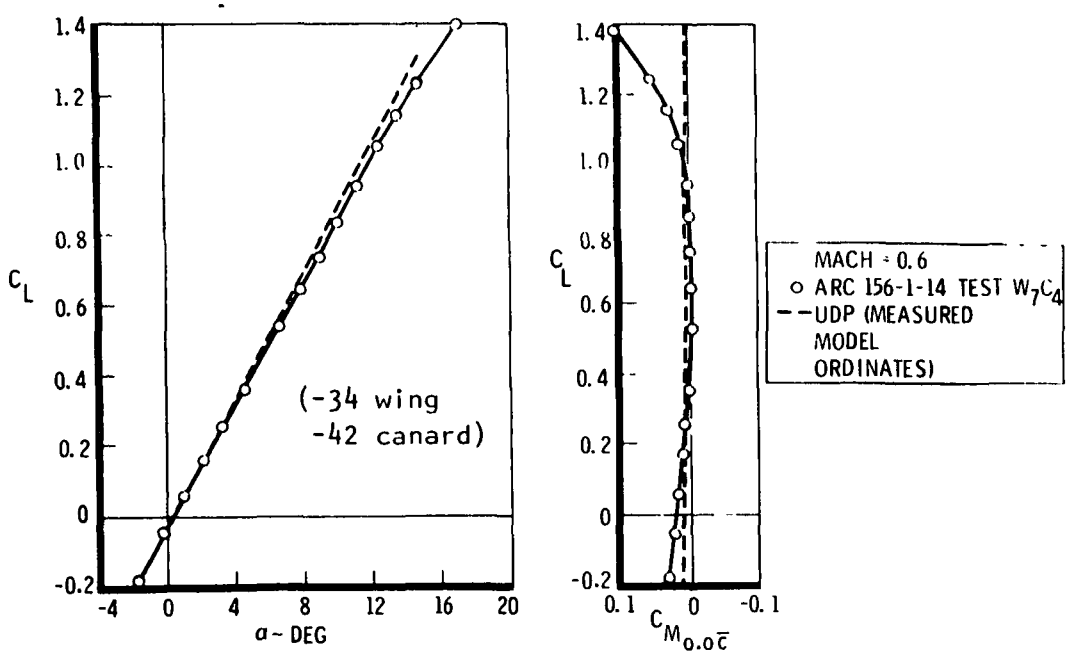

Figure 52. - Modified maneuver configuration longitudinal characteristics.

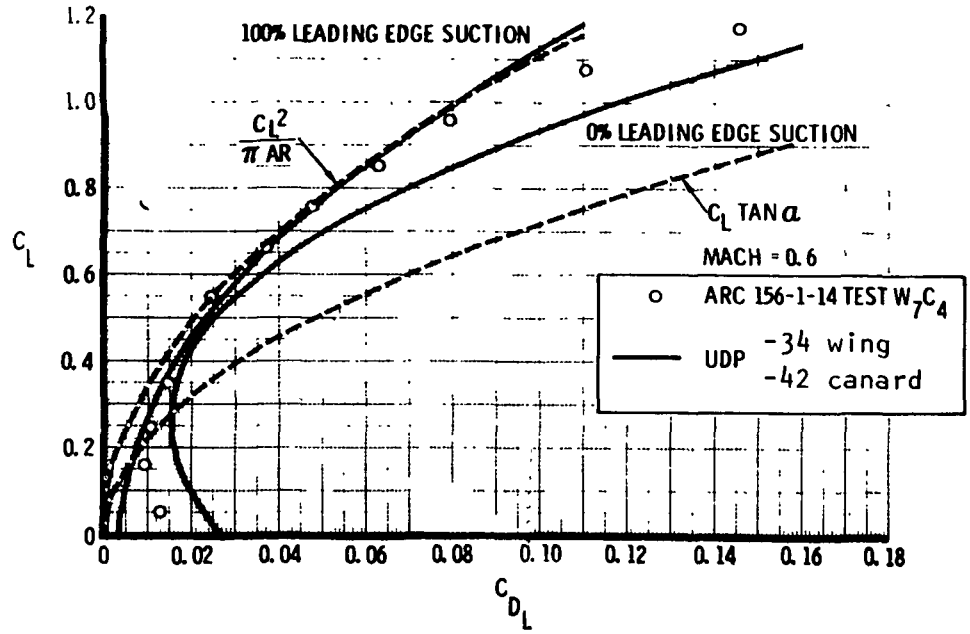

Figure 53. - Modified maneuver configuration drag due to lift.

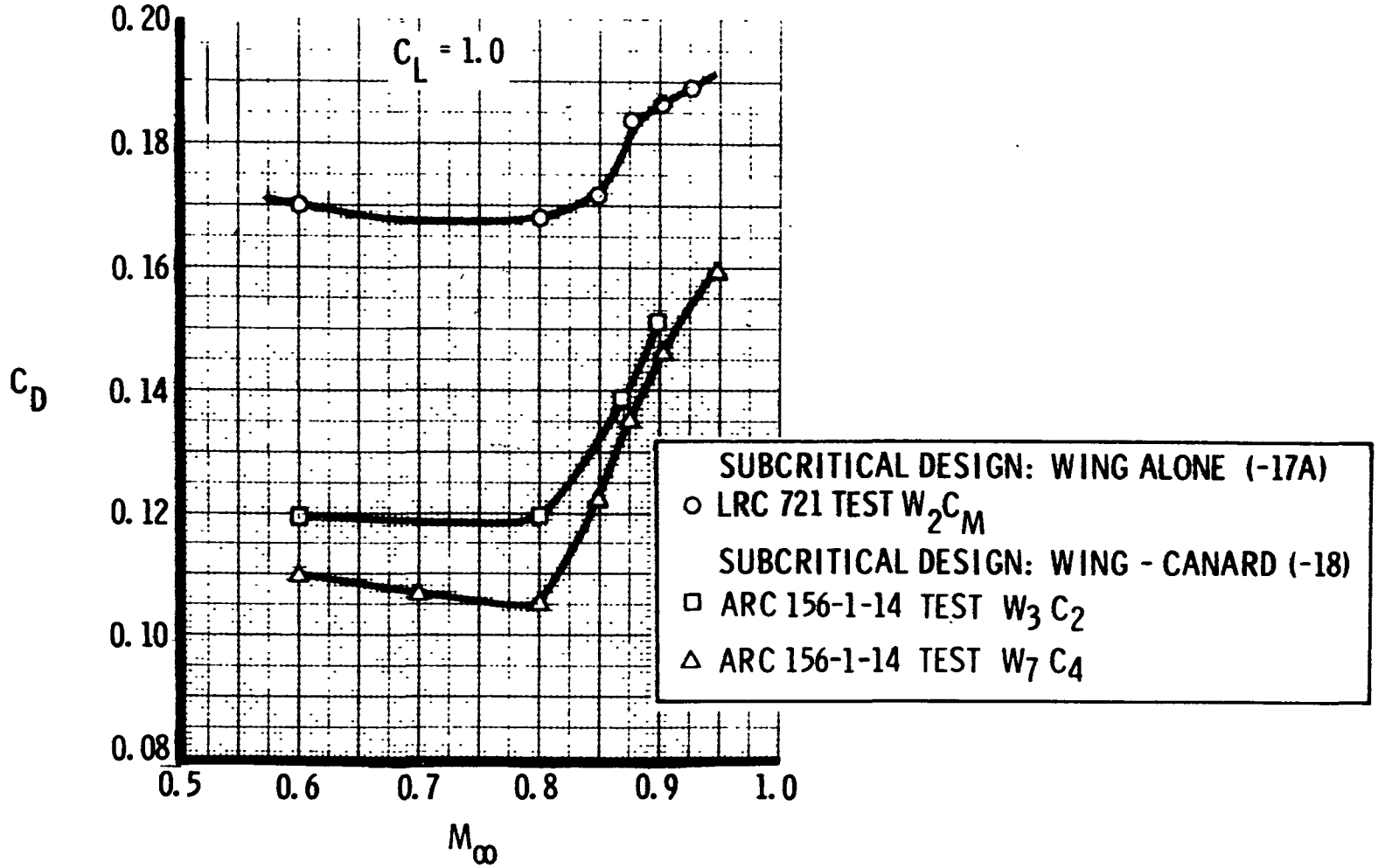

Figure 54. - Maneuver configuration drag rise.

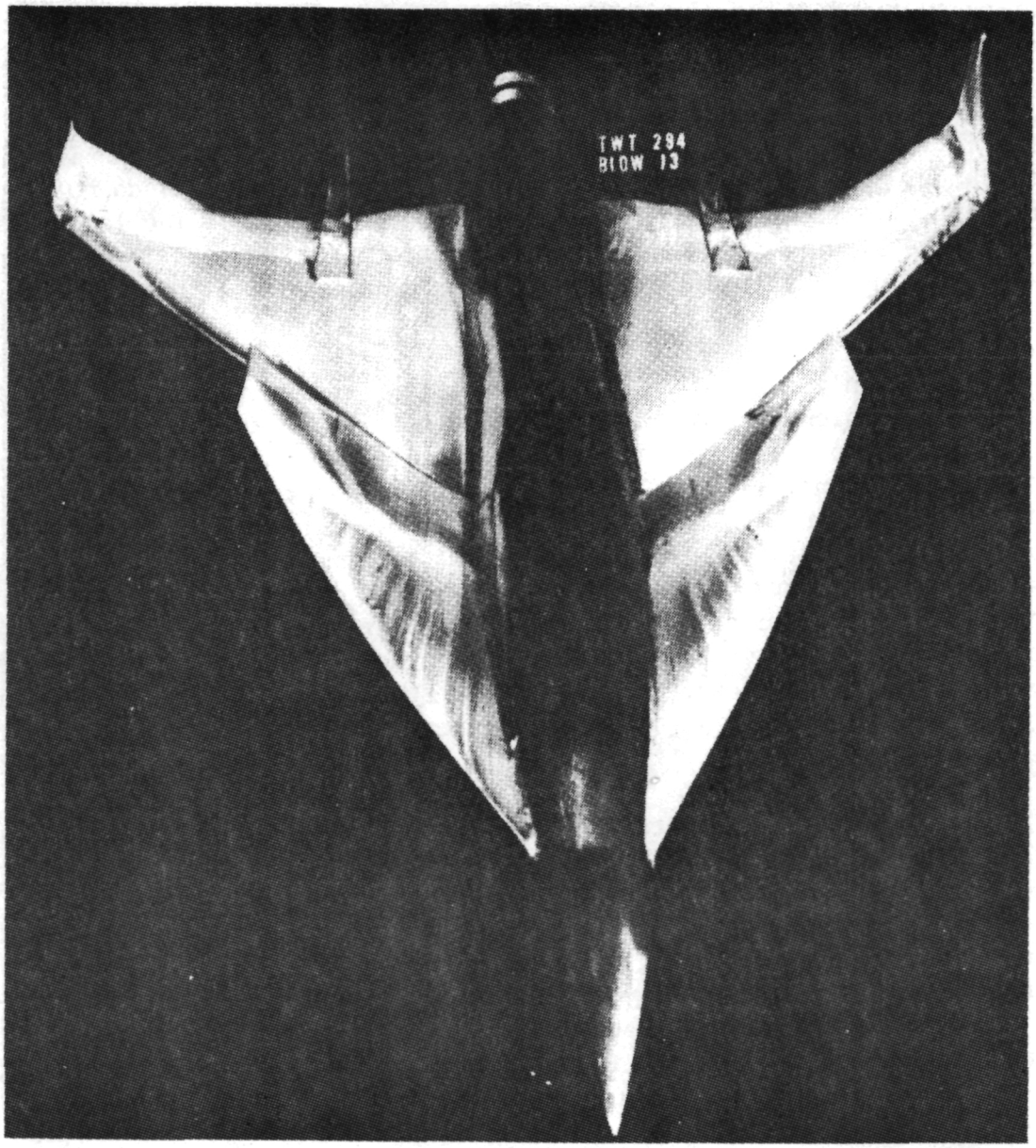

Figure 55. - Oil flow of subcritical design maneuver configuration, TWT 294 Test W_7C_4, M = 0.9, α = 11.7°.

The revised design (-34 wing, -42 canard) was analyzed with a slender body simulation at $M_\infty = 0.7$. The simulations differed with respect to the lifting surface attachment points, with the slender body slightly wider than the flat-plate body. Neither simulation is considered preferable for this geometry. The effect of the slender body solution on the span load shape at $C_L = 0.545$ is illustrated in figure 56, and reflects the body-induced upwash and the lift loss on the body. The 0% and 100% suction drag polars (figure 57) do not differ substantially from the pure lifting surface simulation. The load redistribution for the slender body configuration counteracts the loss in efficiency associated with wing-body interference so that a net reduction in vortex drag results.

Because the span load constraints are violated, the section lift predicted at $C_L = 1.0$ for the slender body simulation exceeds the design goal of $C_\ell < 0.75$. The section lift for the design solution and the body/lifting surface analysis are shown in figure 58. Because of the slight differences in the geometric simulation, the actual lift will be between these values but closer to the upper limit. The test data indicate, though, that the upper limit was exceeded without any appreciable separation at subcritical conditions. The value set for the section lift limit was based initially on experience with two and three-dimensional section characteristics as a function of Mach number and Reynolds number. Considering the available supercritical wing and airfoil technology and the design goals, it was concluded that no redesign was required at this time.

The preceding results indicate the importance of assuming a suitable load distribution consistent with wing-body interference effects. This is required when the design is initiated with a lifting surface simulation (flat-plate body) as was done here. Alternately, a slender-body/lifting surface inverse solution may be obtained. However, with the interference shell concept, the simulation for multi-surface configurations is generally inadequate. An extension of the linearized chord plane analysis is required for wing-body intersections which are not aligned with the free stream. This is preferable to the complexity involved in surface singularity methods for the purpose of evaluating several design options.

Canard Planform Modification

Between the subcritical and supercritical design phases the canard leading edge sweep was changed to 55° to improve low speed controllability. Previously the wing and canard strakes had been removed but the canard leading edge sweep was increased from 45° to 63° in an attempt to retain the vortex lift characteristics and $C_{L_{max}}$ of the earlier concepts.

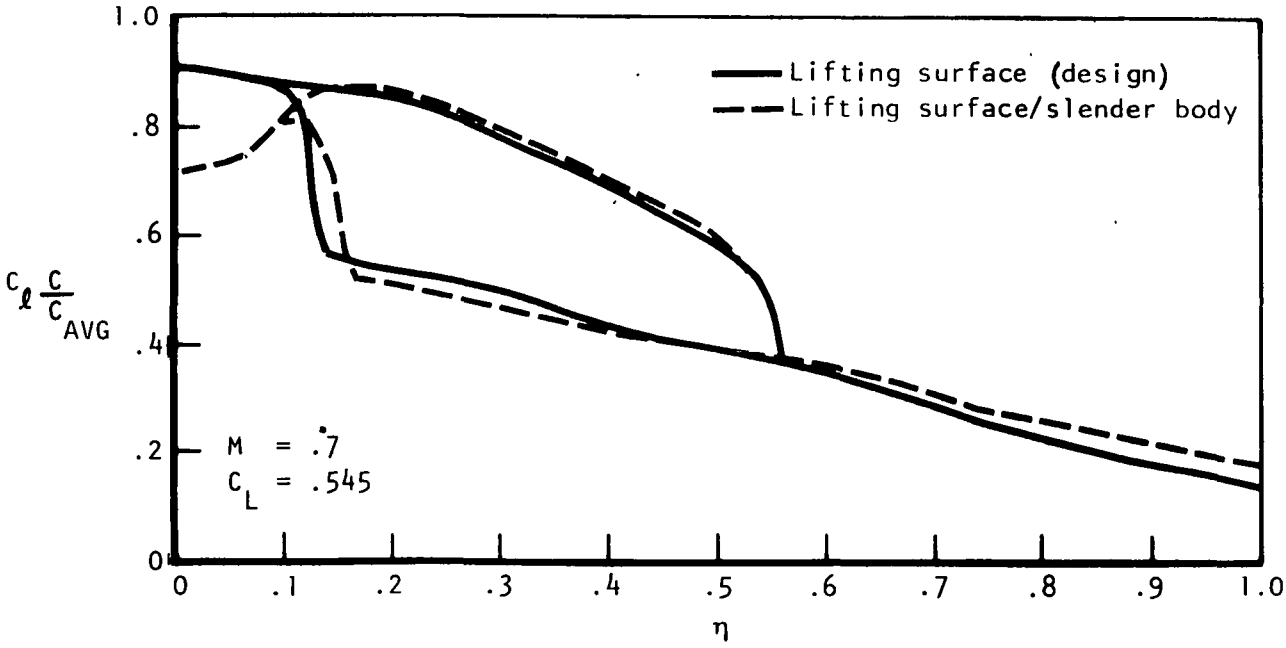

Figure 56. - Effect of slender-body simulation on span load.

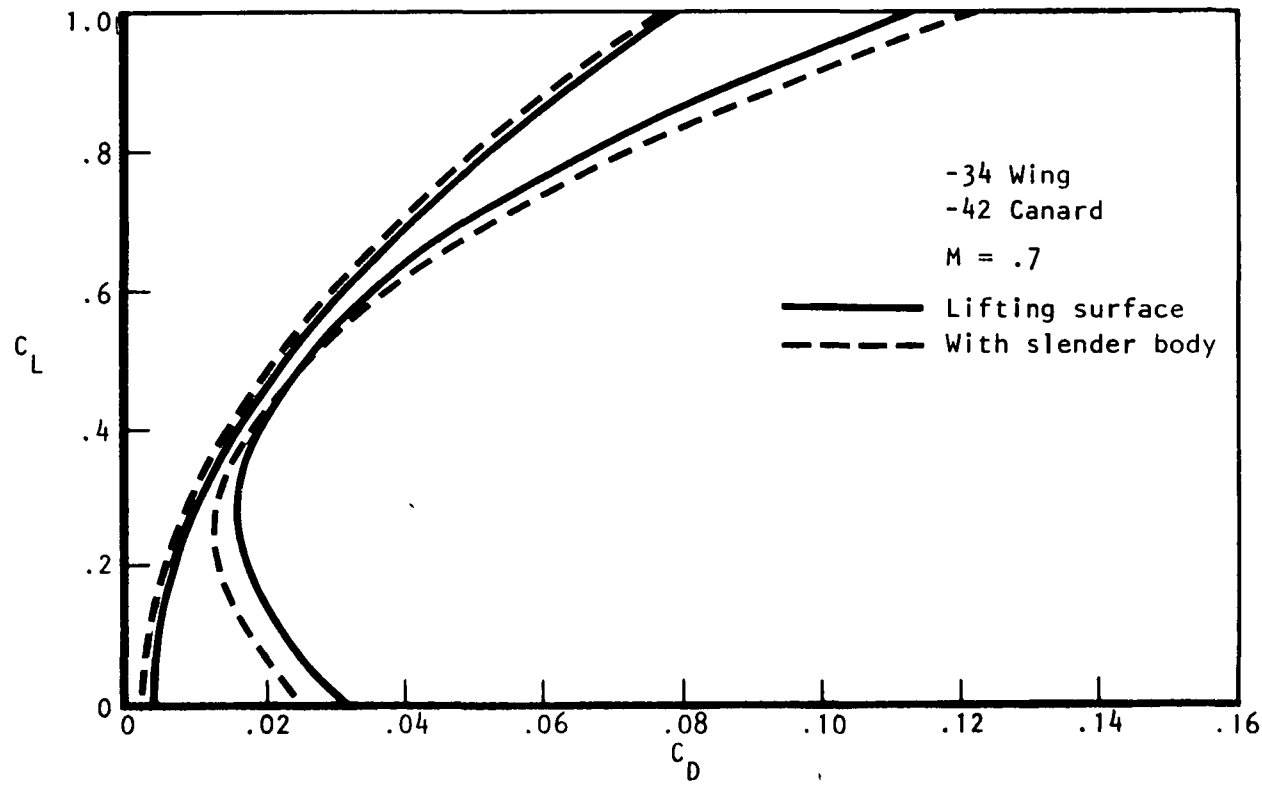

Figure 57. - Effect of slender-body simulation on drag due to lift.

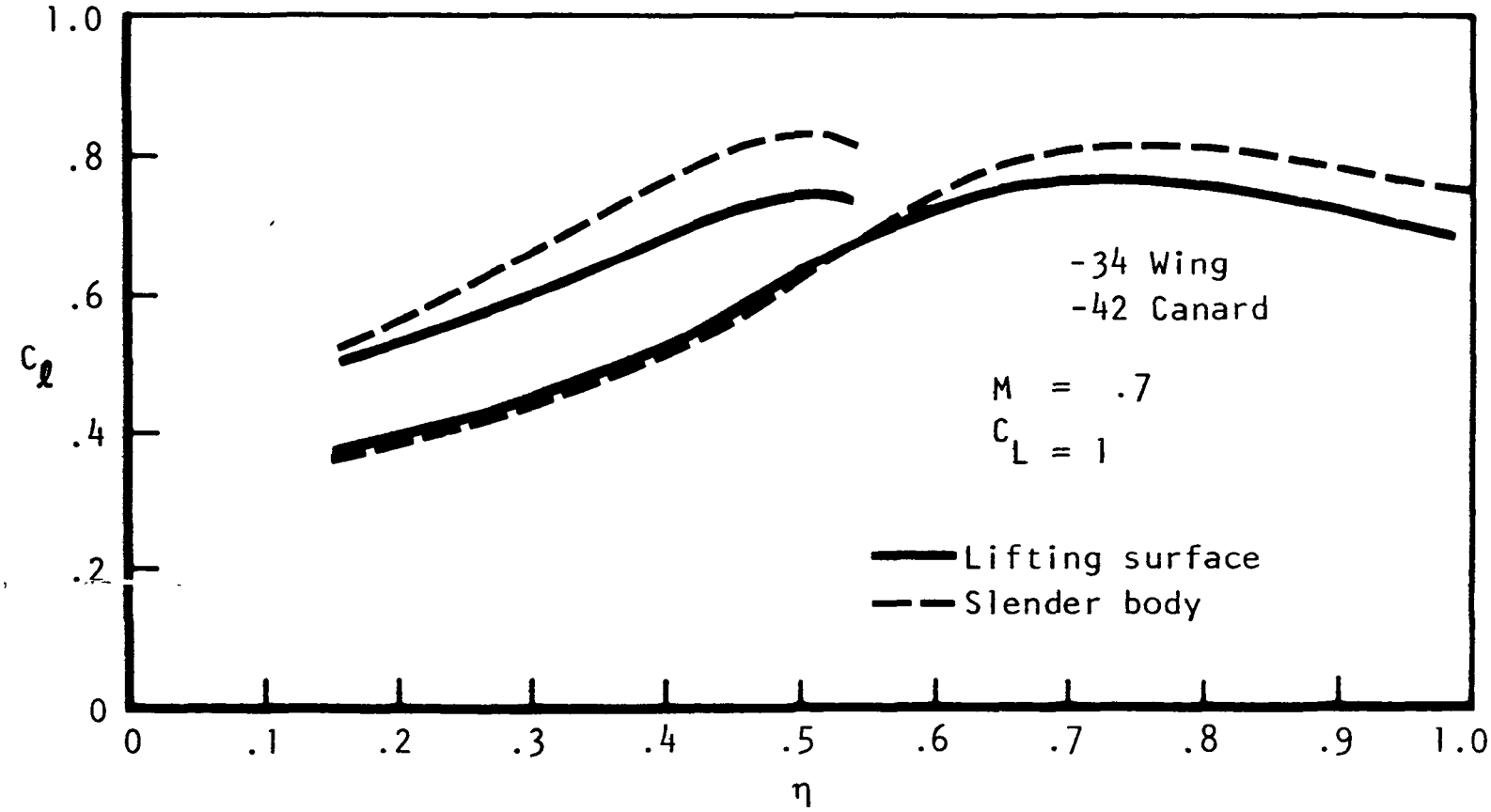

Figure 58. - Effect of slender body on section lift.

During the subcritical design/test cycle low speed tests were conducted to evaluate the $C_{L_{max}}$/controllability trade as a function of canard sweep. The results of these and subsequent tests are shown in figure 59. A compromise sweep of 55° was selected to maintain a $C_{L_{max}}$ of approximately 2.0. The canard planform change is shown in figure 59. The new configuration was analyzed with the camber and twist distributions derived for the 63° canard design. There were no substantial changes in the span loads, drag, or moment and a reoptimization was not pursued since the supercritical modifications were in progress.

The impact of the nonlinear moment characteristics associated with the development of vortex lift was not fully appreciated in the initial stages of the configuration development. As a result, sufficient control power was not available at high angles of attack in the low speed regime. It is necessary then to establish at an early stage the high angle of attack characteristics, trim requirements, and dynamic performance through analytical or experimental studies, or both. At present there are no analytical methods which have been demonstrated to give reliable predictions for the phenomena associated with leading edge vortices due to separation and their interaction with the flow field at large.

SUPERCRITICAL DESIGN

Before the first subcritical design/test cycle it was realized that the HiMAT configuration and design goals would require the development of capabilities for analysis at transonic conditions. The state of the art was (and is still) such that complicated configurations could not be analyzed. The recourse was to modify an existing method to the extent possible and prepare it for use as an engineering tool. The following discussion concerns the development of and experience with the transonic wing theory and the actual implementation of this and the other transonic analysis tools for the HiMAT configuration.

Small Disturbance Theory Experience

Cruise wing analysis. - The modifications to the Bailey-Ballhaus code included the addition of a vertical tip fin and the capability of specifying an irregular planform. Calculations with this nonlinear code were made for the first cruise wing (-17A) for a range of Mach numbers covering subcritical and supercritical conditions. Comparisons are made with linear theory at $M_\infty = 0.7$. The span load distribution and pressure distribution for the

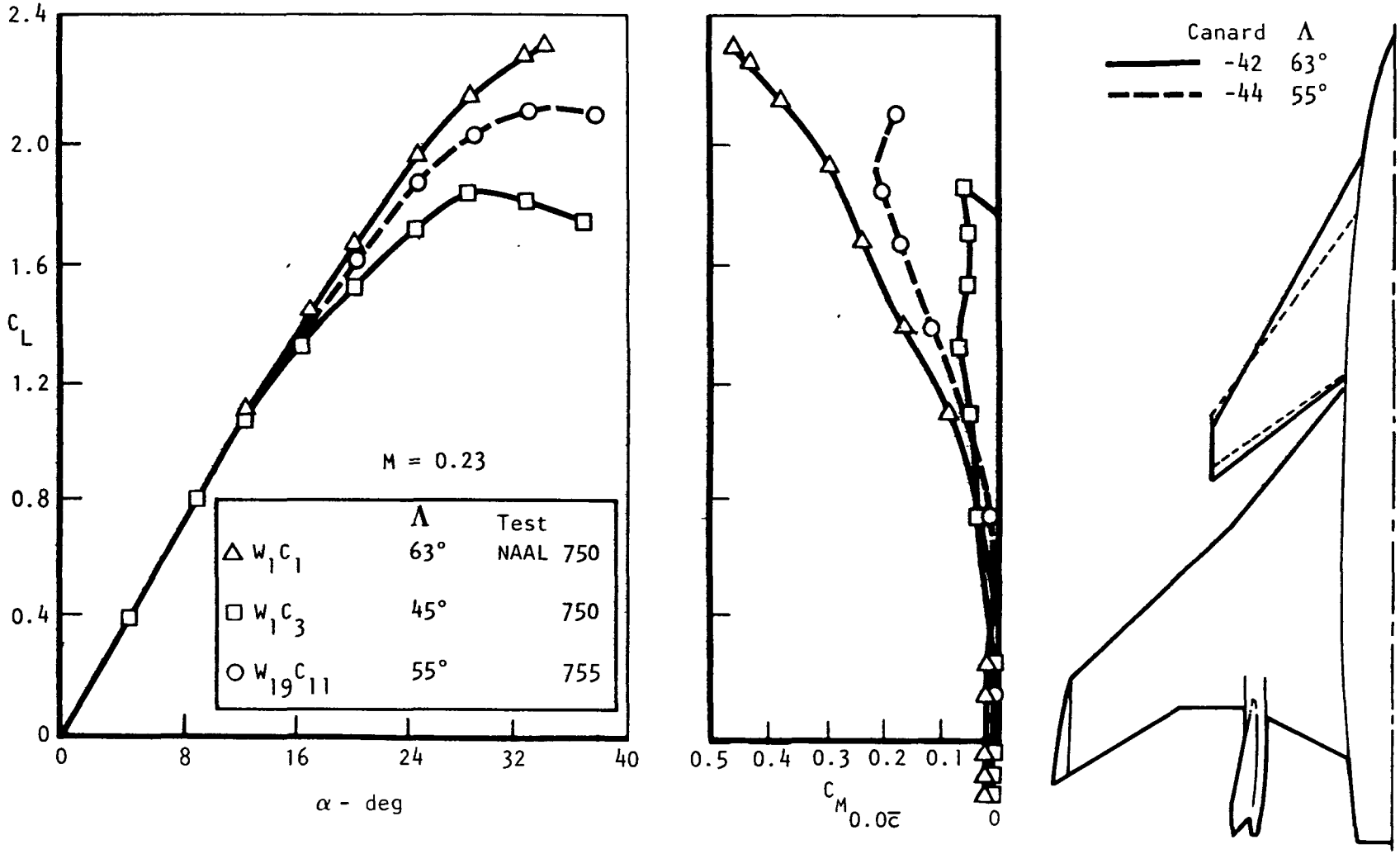

Figure 59. - Effect of canard leading edge sweep on low speed longitudinal characteristics.

region out of the influence of the tip fin are shown in figures 60 and 61. The agreement between the calculated pressure distributions at $\eta \sim 0.8$ is satisfactory, as shown in figure 61. Moreover, for the inboard region of this wing and for the entire surface of the wing without fin configuration, the agreement was similar.

The disparity between the two results concerning the tip fin was not resolved until much later. It was found that in the transonic small disturbance code a parameter operating on the fin boundary condition was not correct. The effect was to increase the fin slopes by a factor that is dependent on Mach number. The error was approximately 13% at M = 0.9 increasing to 40% at M = 0.7.

Maneuver wing analysis. - When the first subcritical wing-canard design was completed, the intent was to utilize the Bailey-Ballhaus code to analyze and modify the maneuver wing for low-drag supercritical flow. The following considerations affected the implementation of the transonic analysis. First, the simulation did not include the canard so that wing pressures would have to be treated in a qualitative manner. Second, the formulation was not well suited to capture swept shocks. With these points in mind there was initially some hesitation regarding the modification of the configuration until experimental pressure data were available. Nevertheless, some modifications were attempted, but they were minor in nature. The problem at this stage was implementing a trial and error procedure to obtain pressure distributions which would reflect the supercritical design philosophies described under "Transonic Design." As a result, the two subcritical configurations were tested essentially as designed. The results of the transonic analysis of these two designs are presented to illustrate the features of the transonic methodology and as a base point for later configuration modifications.

The first series of analysis and design attempts were done with a coarse solution grid for the -31 wing design. The conditions for which the small disturbance theory is applicable are not known a priori. At $M_\infty = 0.9$, the angle of attack corresponding to the subcritical intermediate design point was selected. The analysis later indicated that this was probably close to the limit where the theory was applicable. The upper surface pressures for the -31 wing are shown in figures 62 and 63. The formation of an unswept shock extending outboard to $\eta \sim 0.7$ is indicated. The solution with a fine grid is shown in figure 64. With the increased grid density, the shock near the trailing edge was resolved (figure 64 (a)) but no shocks were indicated on the outboard wing (figure 64 (b)). With a relaxation solution there is always the question of the required number of iterations for convergence. The previous fine grid results were obtained with 450 iterations from a

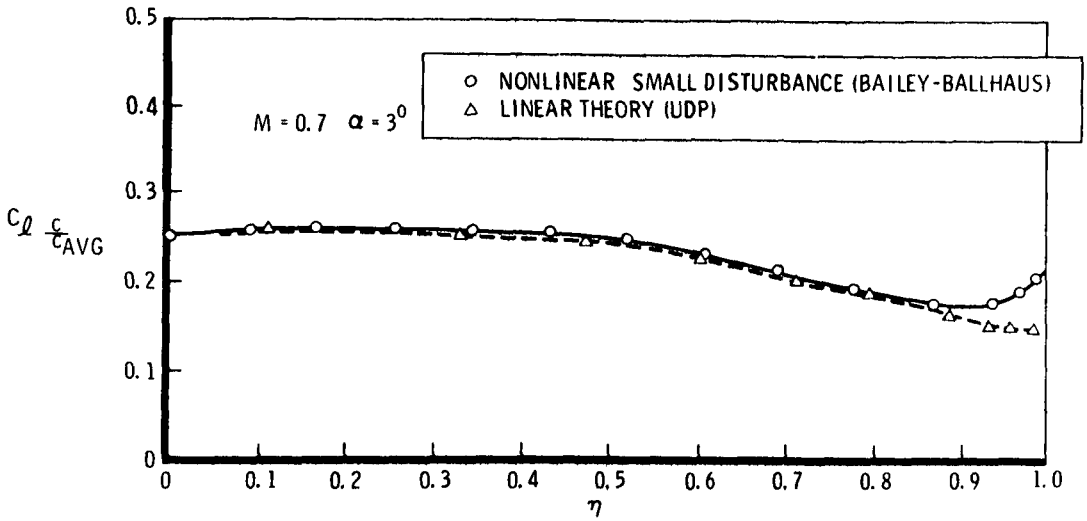

Figure 60. - Calculated cruise wing (-17A) span load.

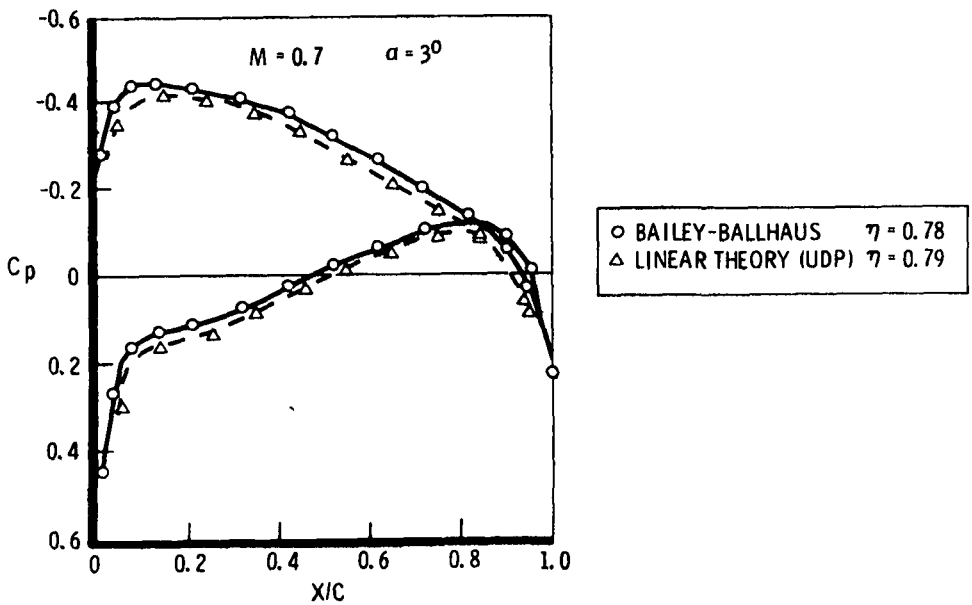

Figure 61. - Calculated cruise wing (-17A) pressure distribution.

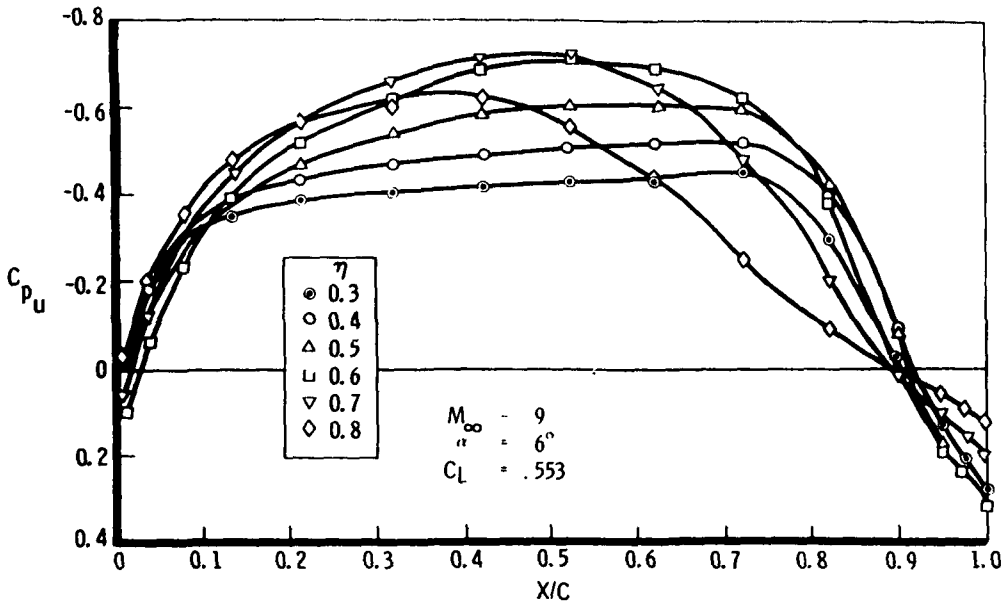

Figure 62. - Crude grid theoretical pressures for -31 maneuver wing.

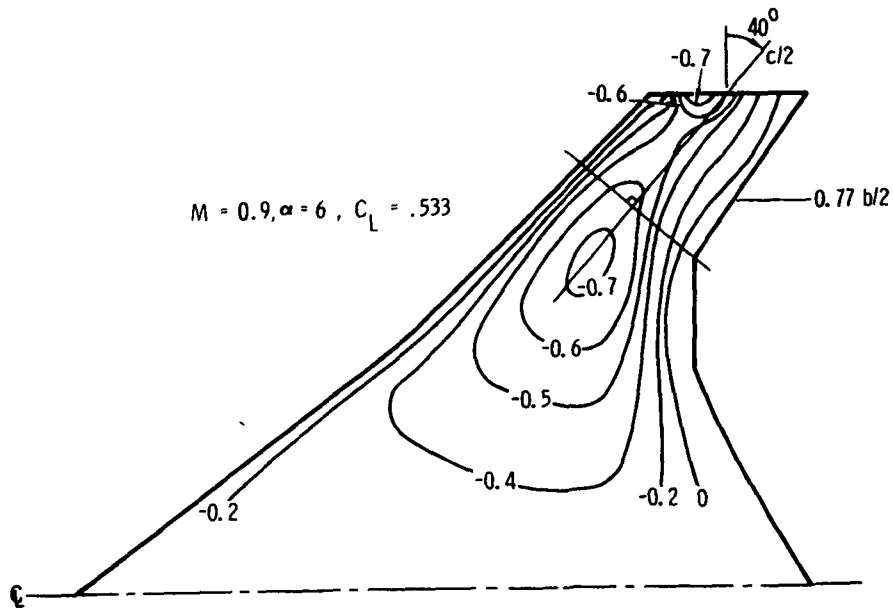

Figure 63. - Crude grid upper surface isobars for -31 maneuver wing.

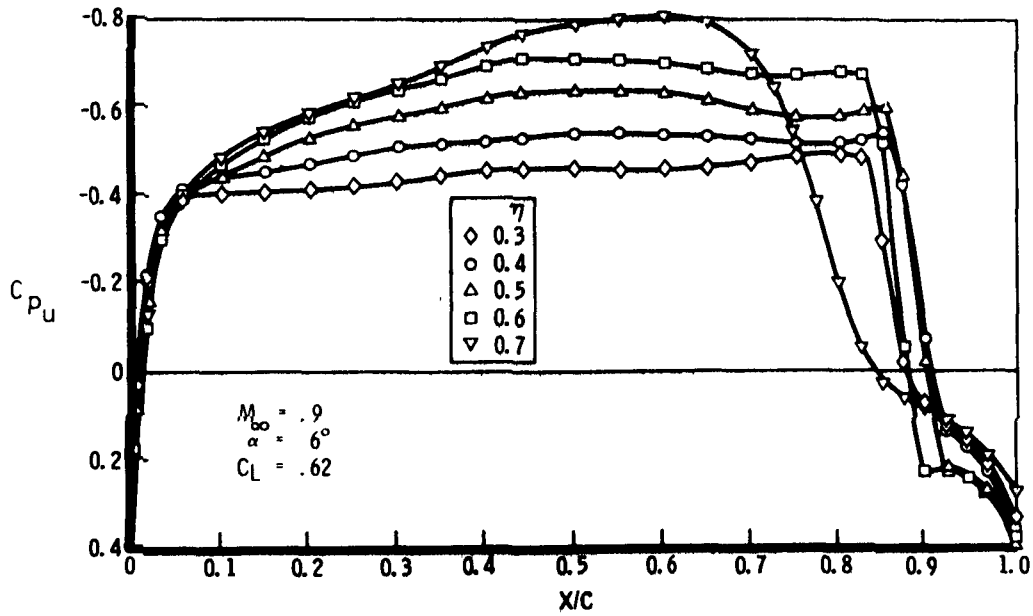

(a) Inboard wing.

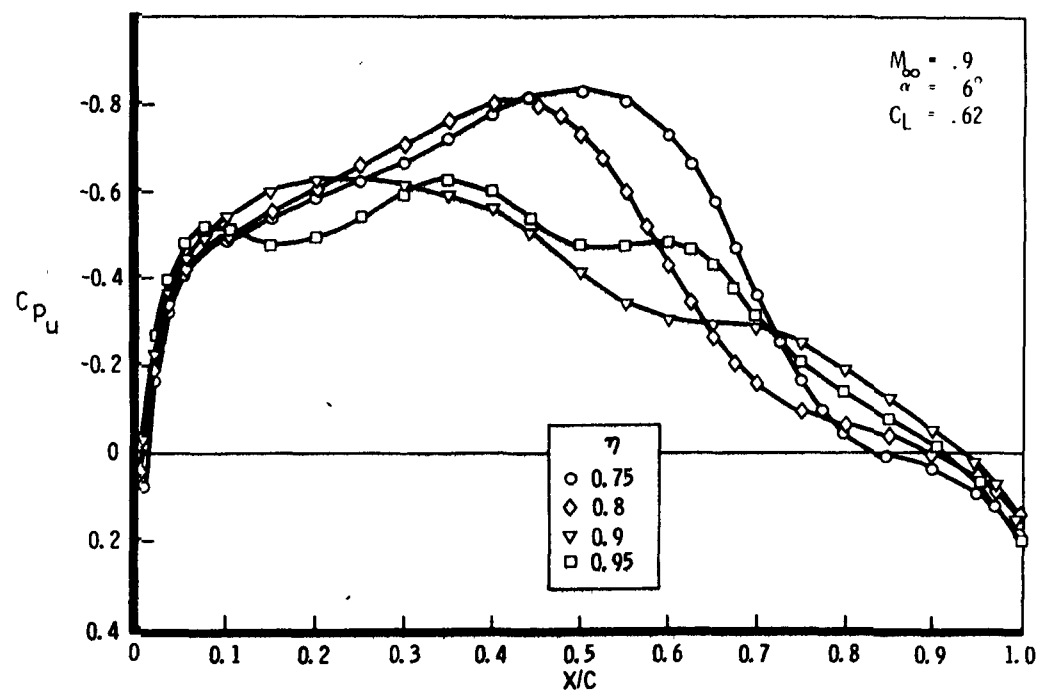

(b) Outboard wing.

Figure 64. - Fine grid theoretical pressures for -31 maneuver wing.

coarse grid solution. Results for two spanwise stations after 2000 additional iterations are presented in figure 65. The qualitative nature is unchanged.

The second subcritical design (-34 wing) was not analyzed in detail because of the short duration of the design/test cycle for this configuration. The results, however, did not differ appreciably from those of the previous wing.

Comparison of theory and test. - To resolve the configuration deficiencies at transonic conditions and provide some guidelines for the implementation of the Bailey-Ballhaus analysis, a follow-up test was conducted (TWT 294), after the Ames series (ARC Test 156-1-14), to measure upper surface pressure distributions.

The model coordinates were measured and a fine grid solution was obtained at $\alpha = 5°$ for comparison with the data. The theoretical calculation (figure 66) indicates the same qualitative behavior as the -31 subcritical design, specifically, a strong upswept shock inboard of 70% span and no shocks on the outboard region. For two spanwise stations the calculations were compared with canard-off measured pressures. At 55% span (figure 67 (a)) the agreement, allowing for viscous effects, is satisfactory with regard to the shock location. However, for the outboard wing (figure 67 (b)) the shock is not captured. Oil flow results indicated a swept shock and attached flow at $\alpha = 5°$. The inability of the method to adequately capture swept shocks has been noted previously. The slower convergence of the solution for this region may account for some portion of the difference but, based on earlier results, it was concluded that no shock would be predicted with further iterations.

Some proposed modifications to the method similar to those of reference 10 were considered. These involved additional terms in the governing equation and revisions to the differencing scheme. However, at the time, no modification was available to impact the design effort.

Conclusions. - The nonlinear analysis did validate the early -17A subcritical cruise design. The design and analysis were made for the wing-alone configuration. The results at M = 0.9 indicated a slightly supercritical rooftop distribution in agreement with the design philosophy.

For the maneuver point the disparity in the experimental and calculated results for the highly loaded outboard wing will limit the analysis and design capability for the present small disturbance formulation. This fact, along with the inability to account for the canard, requires additional testing within the design cycle.

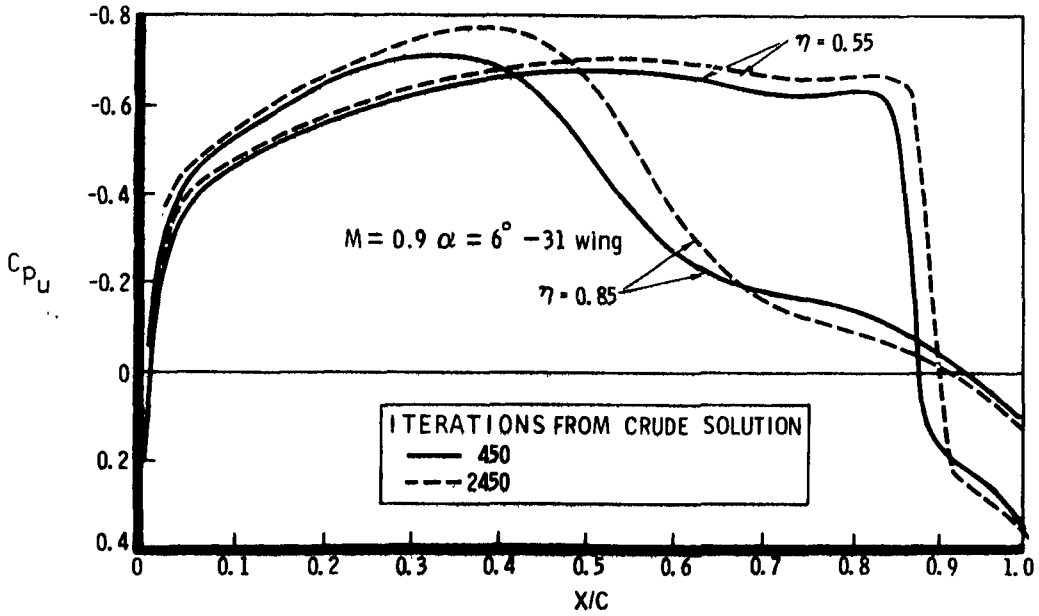

Figure 65. - Bailey-Ballhaus fine grid solution convergence.

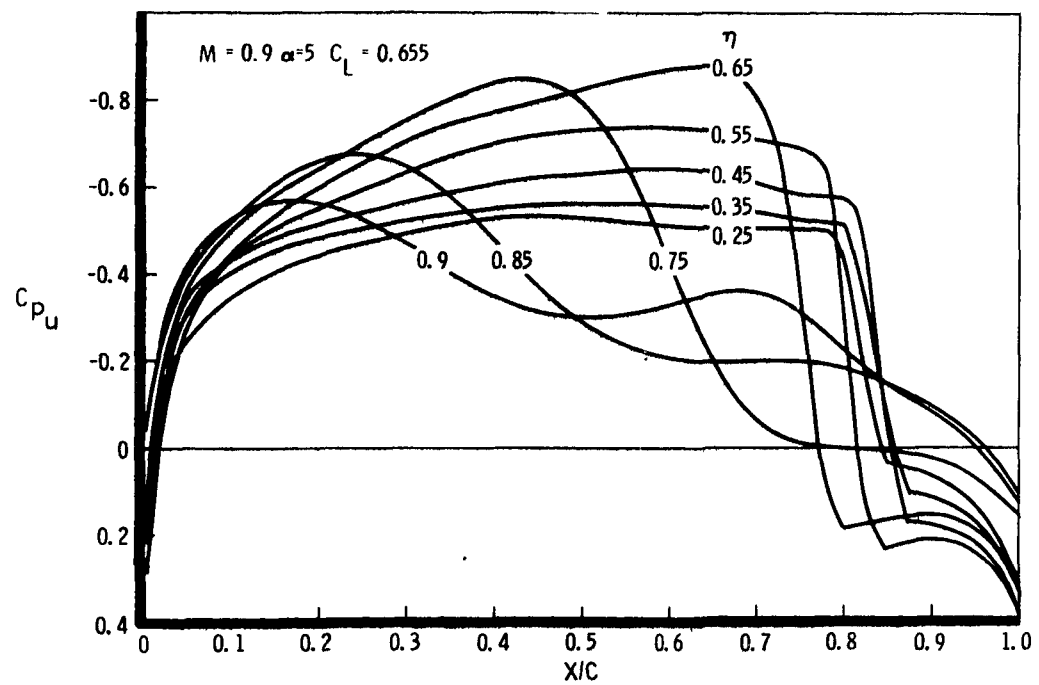

Figure 66. - Fine grid theoretical pressures for -34 maneuver wing, measured model coordinates.

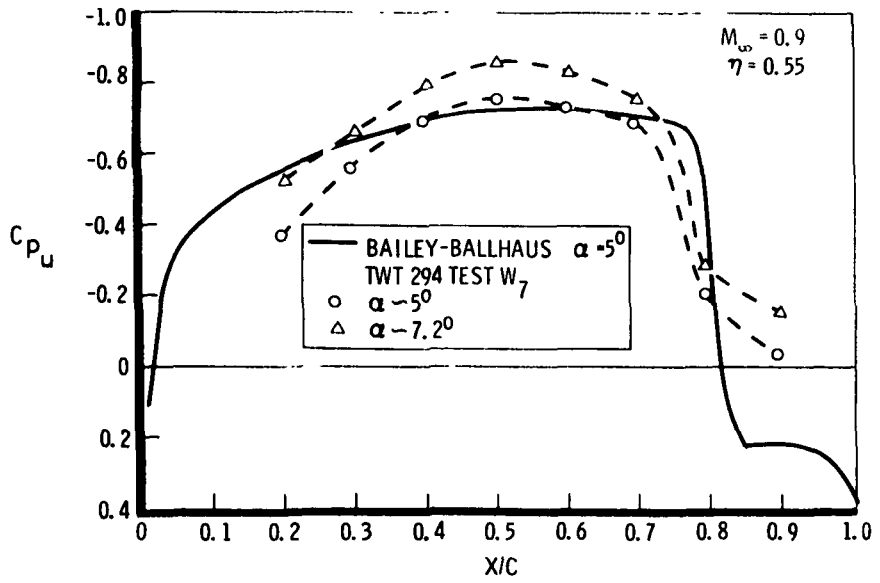

(a) Inboard wing.

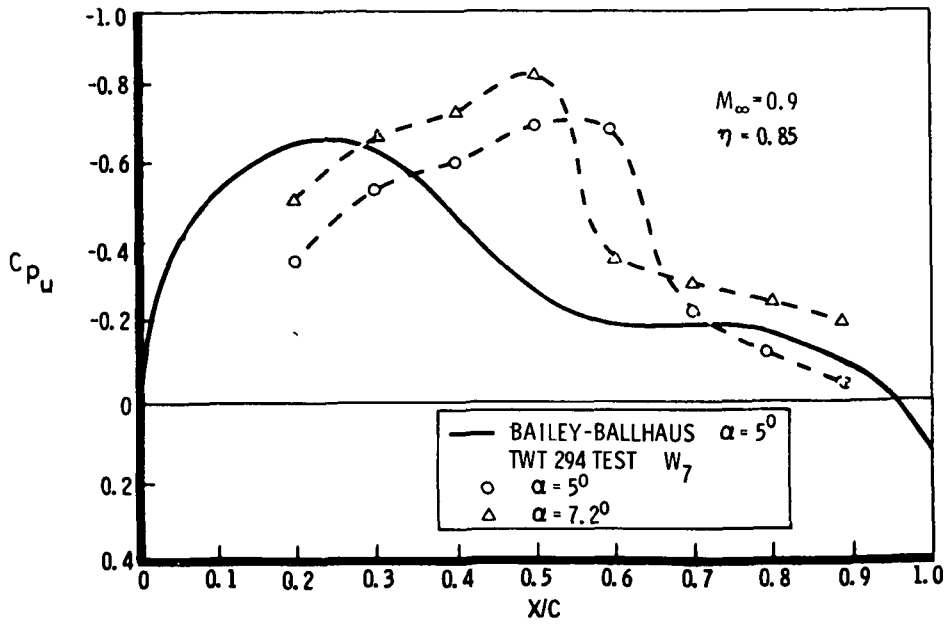

(b) Outboard wing.

Figure 67. - Calculated and measured canard-bff -34 wing pressures.

Three-Dimensional Transonic Maneuver Design

Based on the preceding transonic calculations and test analysis, the redesign of the HiMAT configuration was divided into two phases. The first was to improve the characteristics of the maneuver wing through application of the nonlinear small disturbance theory in an iterative manner. The second phase involved the design of those regions where the existing small disturbance formulation was not adequate - that is, the outboard wing and the canard. This section describes efforts relating to the first phase.

Design objective. - For the inboard and center regions of the wing ($\eta < 0.7$) the primary design objective was to reshape the sections to weaken the shock near the trailing edge. For this region, where the generator sweep is varying considerably, the design criteria outlined under "Aerodynamic Design Approach" prescribes a triangular-type upper surface pressure distribution. The distribution must be such that at higher lifts ($C_L \sim 1$) only a series of weak shocks occur.

Wing design implementation. - The Bailey-Ballhaus transonic analysis was used in a trial and error manner to reshape the pressure distribution. If a triangular-type upper surface pressure distribution is prescribed, the possibility exists that in reality weak swept shocks may form which will not be captured with the analysis.

To redesign the inboard and center wing sections, the camber was modified so that the load would be moved toward the leading edge. The wing was analyzed and based on these results the upper surface was varied in a trial and error process until an acceptable pressure distribution was obtained. The lower surface was then modified to produce a camber distribution which would retain the subcritical maneuver performance at high lifts.

The results of the first series of modifications are shown in figure 68 for 60% span. All calculations were made with the fine grid to properly resolve the shocks. Additional reshaping was not successful in further weakening the shock. The span load distribution prescribed in the subcritical design was generally maintained. The section lift coefficient increased across the span until about $\eta = 0.7$. The center third was thus more critical than the inboard region. To further weaken the shock in this center region, the trailing edge sweep was increased. The wing sections were modified slightly to assure that the proper isobar sweep was maintained. The planform modification and the resulting change in the pressure distribution at 60% span are shown in figure 69. The wing section at 60% span for the supercritical design (-35 wing) is compared to the -34 wing section in figure 70.

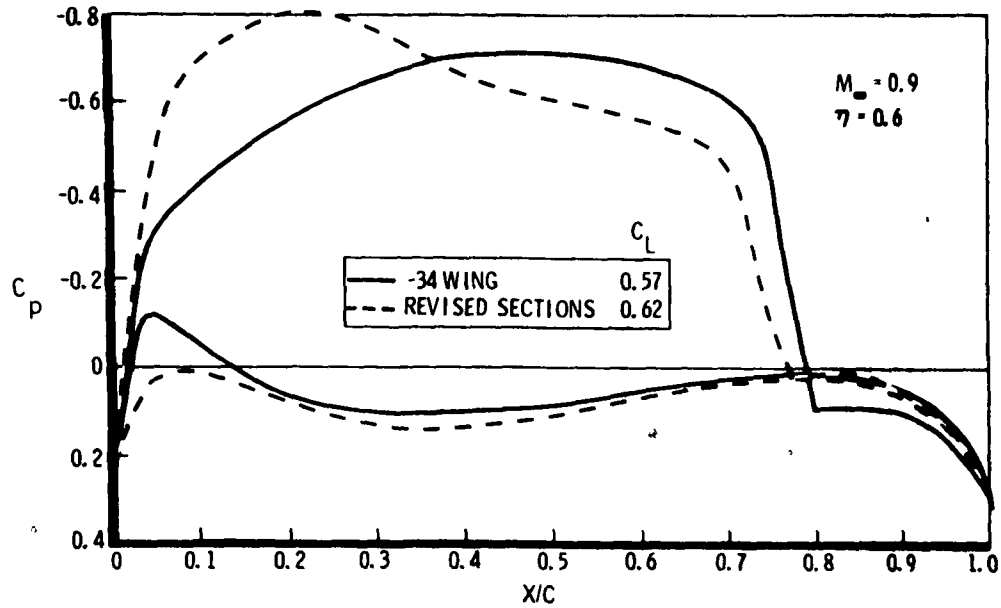

Figure 68. - Three-dimensional transonic design - effect of section modification.

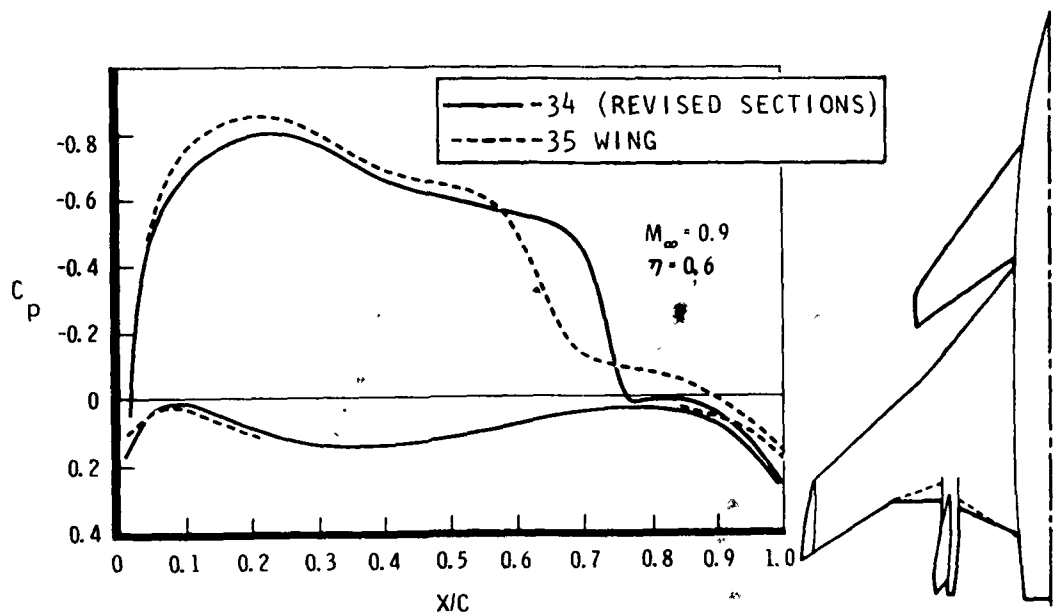

Figure 69. - Transonic wing design - effect of planform modification.

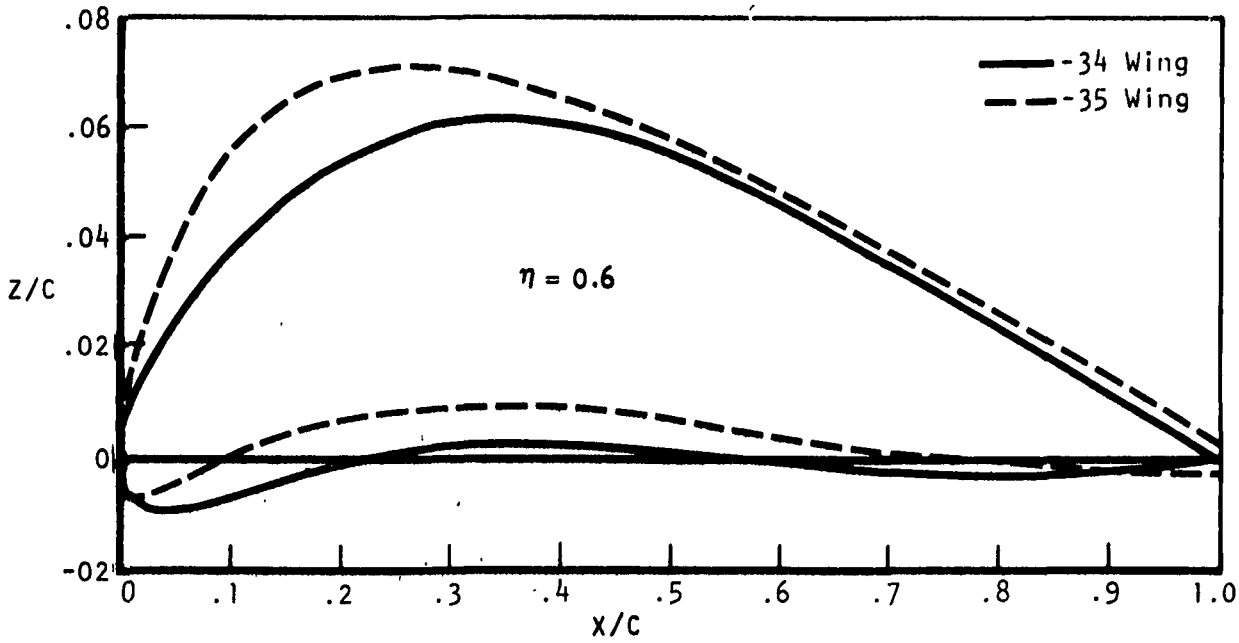

Figure 70. - Wing section modification.

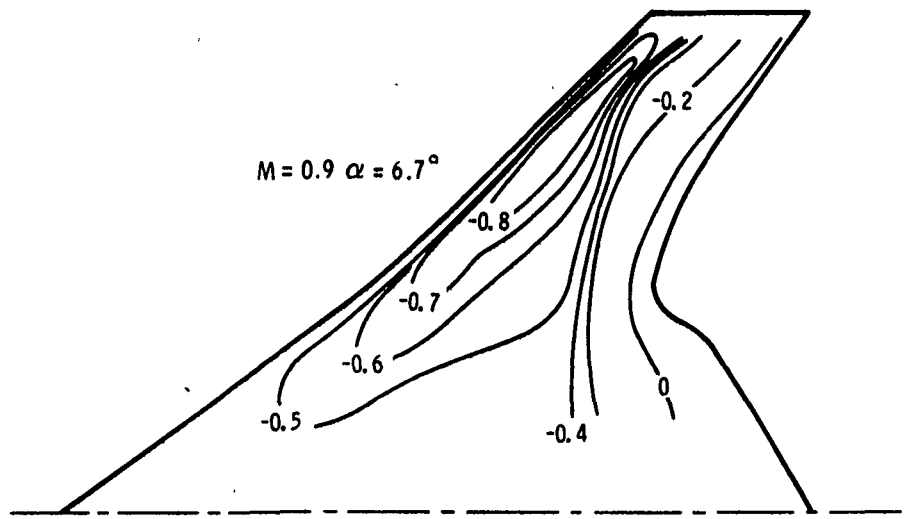

Figure 71. - Fine grid theoretical upper surface isobars for transonic design -35 wing.

The upper surface isobars for the -35 wing are shown in figure 71. It is noted at this point that the outboard wing was not considered in the preceding design cycle. The wing sections were obtained by extrapolating those in the center region. The solution for the outboard wing is probably not reliable for the reasons discussed earlier regarding swept shock capture. The resulting unsweeping of the isobars is thus considered to be exaggerated. The influence on the center wing region is such that the shock strength is probably less than indicated in figure 69, or in other words, the recompression is smoother.

At this point in the development of the configuration a single winglet was proposed rather than a variable camber system. The cruise winglet was selected as a baseline in order to reduce supersonic pressure drag. This choice did not preclude modifications for efficient transonic operation at the maneuver condition. The limitations of the three-dimensional transonic analysis regarding swept shock capture indicated that a design/test cycle would be required for both the outboard wing and winglet.

Canard design implementation. - Because of a combination of high average sweep and high loading, the use of the Bailey-Ballhaus analysis for the canard proved unworkable. The previous (63°) canard was characterized by shock-induced separation well before the transonic design lift. To take proper advantage of the canard sweep, that is, higher critical velocity near the leading edge, the design would resemble the triangular-type pressure distribution prescribed for the center wing section. As a first approximation, this wing section was used for the inboard canard. The section was varied outboard to maintain the isobar sweep based on a subcritical analysis.

Subcritical analysis. - With the revised wing and canard sections a subcritical lifting surface analysis is required to verify that the subcritical performance is still acceptable. Since the transonic methodology cannot analyze the wing-canard interaction at high lift coefficients there is no guarantee that the transonic goal or even the subcritical goal will be met.

A wing-body linear theory analysis was made for the revised wing and canard sections. The drag due to lift was not substantially different from that of the previous subcritical design. However, the combined effect of the body inductions and the revised camber produced a section lift on the outboard canard that was higher than that on the outboard wing. A wing-body inverse solution was used to determine the additional canard twist required to meet the section lift goals. The additional twist distribution was approximated by a constant 1° negative deflection for the entire canard.

Test results. - The revised wing (-35) and 55° canard (-44) for the maneuver configuration were tested (TWT 296) to determine the effectiveness of the supercritical modifications and to provide additional pressure data for estimating the influence of the canard on the position and strength of the wing shocks.

The modifications were successful in weakening the center wing shock and eliminating shock-induced separation at the design point. Pressure distributions at 55% span are shown in figure 72. For this design there was a swept, weak shock at approximately 35% chord. Oil flow results indicated that the shock at 85% chord did not separate the boundary.

A comparison of the measured canard-off pressures and the Bailey-Ballhaus solution is shown for 25% span on figure 73. The agreement is quite satisfactory considering the neglect of viscosity and body effects. Farther outboard (η = 0.55) the agreement was not as good due to the development of the weak swept shock and the fact that the proper isobar sweep was not obtained in the calculations. The latter, as noted previously, was due to the deficiencies in the outboard wing solution.

As an indication of the extent to which the canard influences the design, comparisons of canard-on and canard-off pressure distributions are shown in figure 74 and two points are noted. First, the canard downwash unloads the inboard wing which in turn reduces the outboard wing loading. Thus, across the entire wing span separation is delayed in the presence of the canard. Second, for the critical portions of the wing, the supercritical design procedure considering the wing alone was adequate as a first approximation.

The experimental wing and canard upper surface isobars are shown in figure 75. At this condition, α = 7.6°, the wing isobar sweep indicated a satisfactory design. On the canard an unswept shock developed but from the pressure data the conclusion was that the flow remained attached well above this condition - in fact, to α~10°. The canard modification of course was not rigorous but it was in the right direction. Well before separation was present on the canard, shock-induced separation occurred near the leading edge of the outboard wing. This is illustrated in the oil flow of figure 76. As a result no improvement was made in the transonic drag due to lift. The oil flow does, however, indicate the improvements made with the supercritical design process for the inboard and center wing regions.

In this series of tests, force data were available for two configurations, W_8C_5 and W_9C_5. The latter included the change in canard twist described under the preceding heading "Subcritical analysis." Instead of deflecting the canard, the wing was rigged with a positive 1° incidence. For subcritical

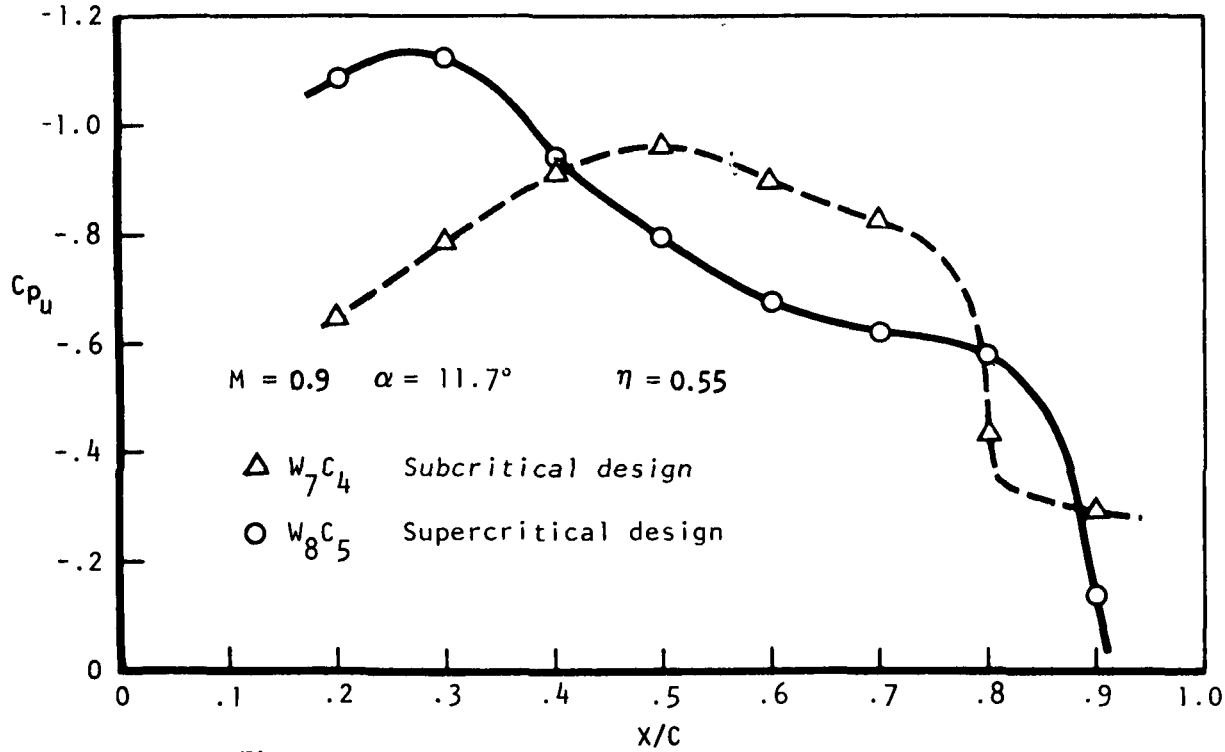

Figure 72. - Verification of weakened shock by transonic design/analysis cycle.

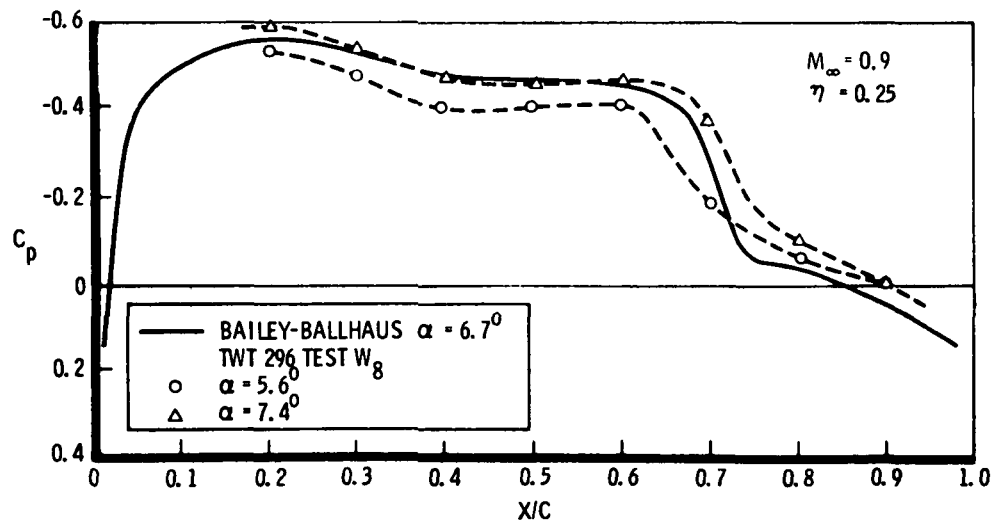

Figure 73. - Calculated and measured canard-off -35 wing pressures.

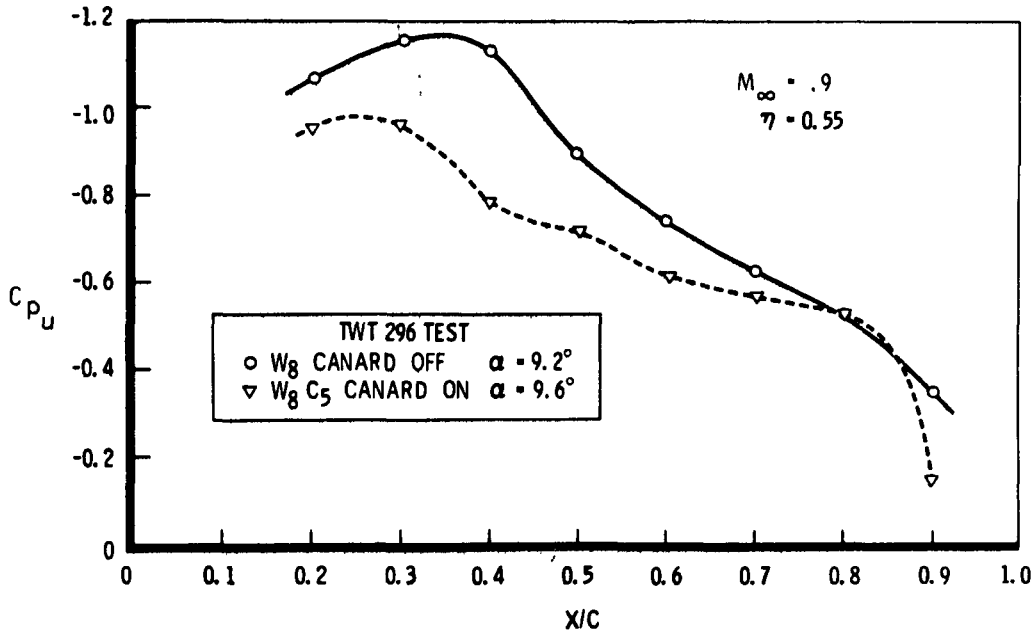

(a) Inboard wing.

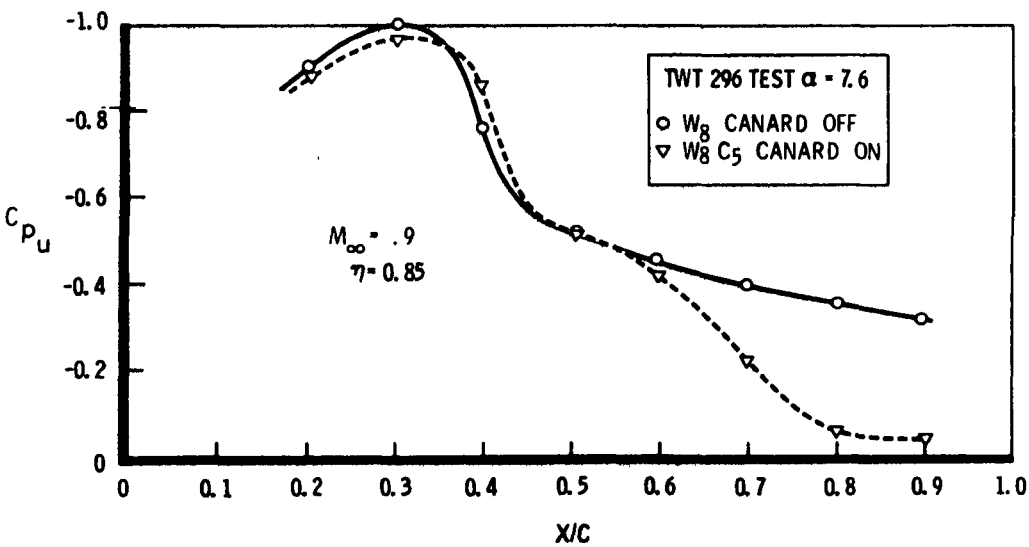

(b) Outboard wing.

Figure 74. - Effect of canard on wing upper surface pressures.

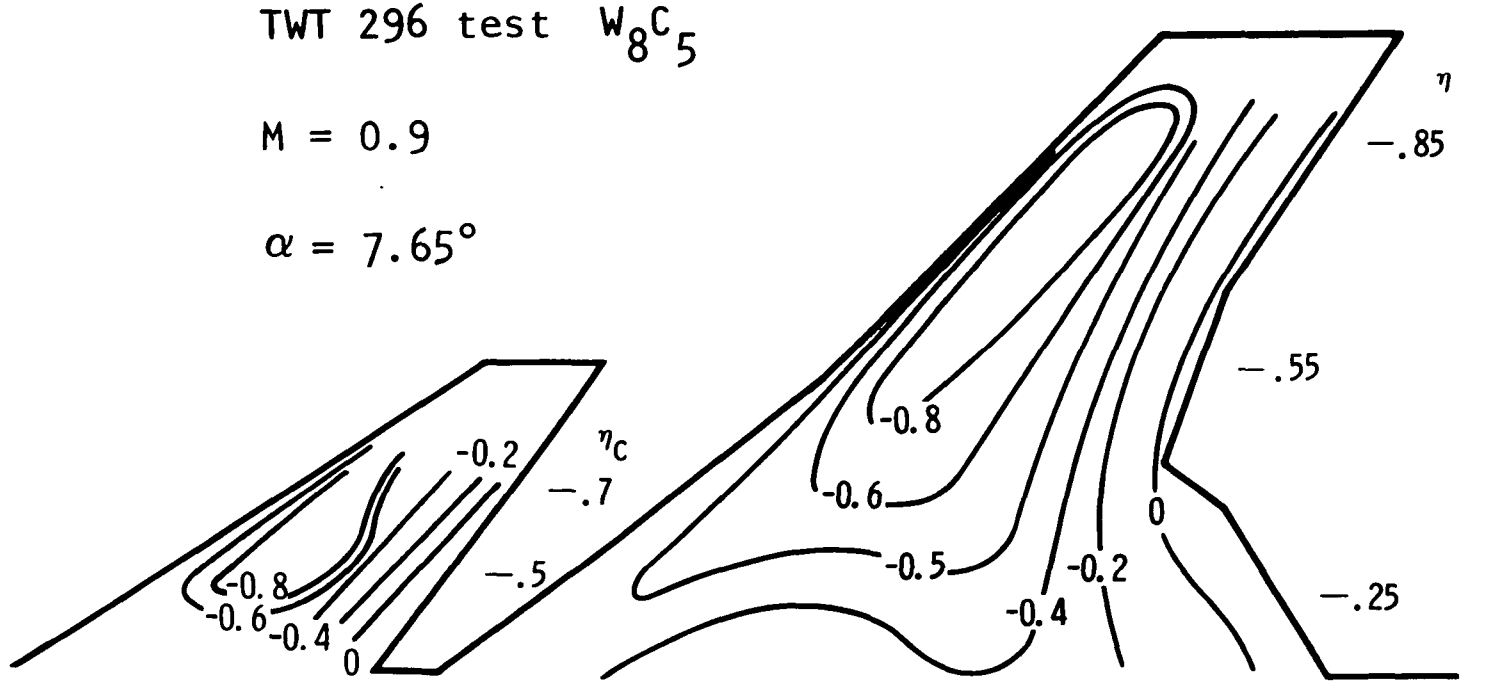

Figure 75. - Upper surface isobars for transonic design configuration.

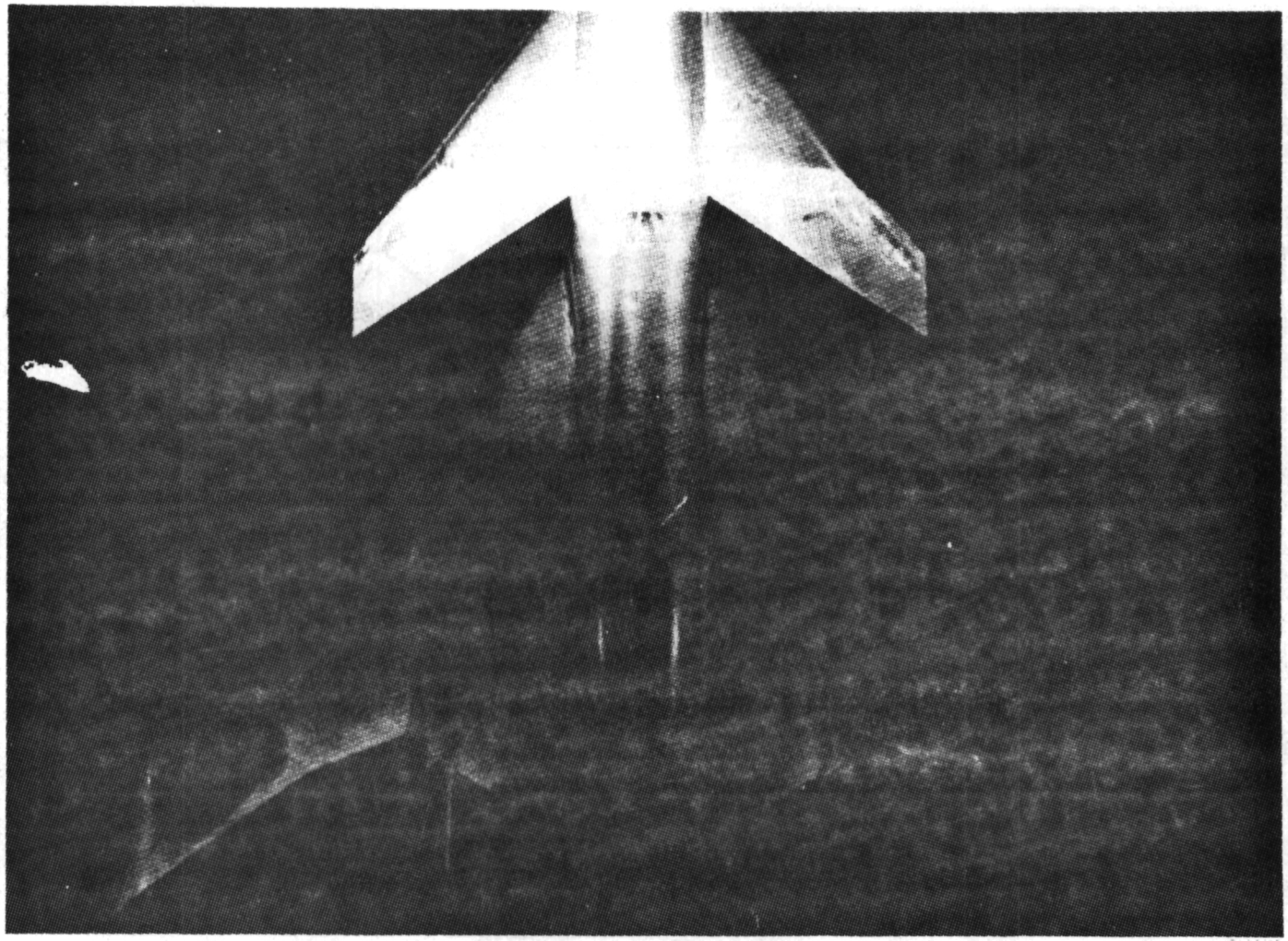

Figure 76. - Oil flow of three-dimensional transonic design, TWT 296 test, α = 10.1°, M = 0.9, C_L = 0.94.

conditions, the effect of the wing incidence change was to reduce the drag due to lift by 5% at $C_L = 1.0$. There was no change at M = 0.9 because of the separated flow on the outboard wing for both configurations. However, for later tests with an improved wing, the same reduction in drag was achieved at transonic speeds.

Conclusions. - The utilization of the Bailey-Ballhaus nonlinear small disturbance analysis was successful in satisfying the design objectives for the wing alone. The unswept shock was essentially eliminated over the inboard 70% of the wing. This shock was replaced by a series of weak, swept shocks. Near the wing root the unswept shock remained, as expected. The experimental pressure data indicated that the shock strength at the wing root was moderate at the design condition - local Mach number before the shock of 1.2.

The design objectives were generally maintained in the presence of the canard. The effect of the canard downwash over the center wing section did not change the weak, swept shock pattern. For the inboard wing near the body the effect of canard was not apparently equivalent to an angle of attack change. The pressure distribution indicated a slight expansion approaching the trailing edge shock whereas the wing alone pressure distribution was nearly flat until the shock.

Since the outboard wing was not included in this first design phase, the results for this region were not unexpected. To correct the deficiencies associated with both the outboard wing and the canard requires implementation of a higher order theory or empirical modifications in the wind tunnel. Higher order theory would encompass a full potential solution, reference 18, or appropriate modifications to small disturbance theory (for example, reference 19).

Outboard Wing Design

The inapplicablity of the small disturbance analysis for the highly swept outboard wing required the utilization of a two-dimensional/sweep theory design cycle. A higher order three-dimensional solution (ref. 18) would be preferable but could not be implemented in the time span required. The intent was to use two-dimensional section results and sweep theory to arrive at an appropriate upper surface pressure distribution for the relatively low taper outboard wing. Then, if the wing can be shaped to reproduce the two-dimensional result, the two-dimensional design goals can be met.

Design objectives. - The primary objective was to eliminate the shock-induced separation at the design point. At or near the design condition a

shockless or weak shock solution would be sought. Some trailing edge separation would be admitted. Additionally, the section thickness ratio must be compatible with the allowable supersonic pressure drag.

Design implementation. - First, the approximate two-dimensional section requirements were established. With a linear theory analysis and a correction based on the change in the spanwise variation of loading from the nonlinear analysis, an estimate of the section lift on the outboard wing was made for the existing configuration. A nominal design total lift coefficient of $C_L = 1.0$ was selected. This is still below the maneuver design point ($C_L \sim 1.1$), but, referring to figure 7, there is some allowance for decreased efficiency in the goal definition. The section lift requirements (figure 77) are still quite high but attempts to further constrain the outboard wing load would result in impractical twist requirements.

For this condition, using the midchord sweep ($\Lambda = 40°$), the required two-dimensional section lift C_ℓ is of the order $C_\ell = 1.2$ to 1.4. The normal Mach number is $M_\perp = 0.69$. Thus, if an airfoil section can be designed for efficient operation at these conditions, the corresponding pressure distribution, $C_p \cos^2\Lambda$, can be prescribed as a design goal for the finite yawed wing. The second problem is to reshape the outboard wing sections to produce infinite yawed wing conditions. This does not follow exactly for a tapered wing as is the case here. If the two-dimensional section and pressure distribution are assumed perpendicular to an element, then the streamwise section and pressure distribution will be distorted relative to the infinite yawed wing solution.

Some approaches to the first part, defining the airfoil section, are summarized as follows:

(1) Select an existing supercritical airfoil

(2) Transonically scale a known solution

(3) Develop a section with a design/analysis iteration such as in reference 14

(4) Design a shockless section with the inverse hodograph method (ref. 11)

Of these, (4) was beyond the scope of the present effort.

After a suitable inviscid pressure distribution is obtained, the displacement thickness for the yawed wing condition is removed from the section.

In a fully three-dimensional design, the streamwise inviscid design pressure distribution would be prescribed and the contour obtained with a transonic inverse solution as suggested by reference 19. A three-dimensional viscous calculation (for example, ref. 20) would then define the required displacement thickness to be removed. Here, though, an approximate approach was taken. After the streamwise section was defined, a linear theory analysis was made to assure that the sectional subcritical characteristics were nearly constant for the outboard wing region.

Shockless airfoil, off design. - Of the available supercritical sections, an airfoil reported in reference 16 came closest to the design requirements. The section is designated 65-14-08 where the sets of digits refer to nominal design Mach number, lift coefficient and thickness ratio. The shockless design pressure distribution is shown in figure 78, which is reproduced from reference 16. Also shown is the result obtained with the analysis program (ref. 11).

If this section is utilized directly, the design Mach number will be lower than required. At $M_\infty = 0.9$ ($M_\perp \sim 0.69$) the section will be operating off design and the advantages of the shockless approach will be lost. The section was analyzed at the appropriate two-dimensional conditions to determine the penalty due to the off-design operation. These results are shown in figure 79. Approaching the design point, shock-induced separation was predicted. The analysis for $C_\ell \sim 1.4$ of figure 79 is thus not realized.

These results were not encouraging since the design goal would not be achieved. However, the section was implemented to provide data relative to the applicability of sweep theory for the outboard wing region and because, even operating off design, it appeared to be an improvement over the previous configuration. For the corresponding streamwise section a subcritical analysis indicated that the existing twist distribution would maintain nearly constant section characteristics for the outboard wing.

The modified maneuver wing (-36) was tested (TWT 296) and pressure distributions at 85% span are presented in figure 80. The sweep theory analysis is shown to indicate predicted shock position and strength prior to separation. The drag rise characteristics for the configuration with the supercritical modifications described earlier and this first attempt at an outboard wing design are shown in figure 81. The test configuration identified as $W_{10}C_5$ was developed from the wing with the 1° incidence. The improvement relative to the best subcritical design is noted, but there is still a substantial reduction in drag required to meet the design goal.

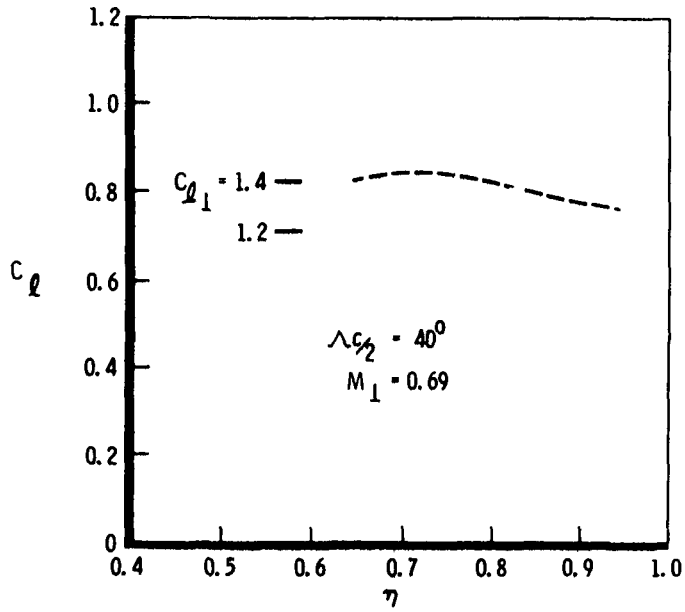

Figure 77. - Estimated section lift at $C_L \sim 1.0$, M = 0.9.

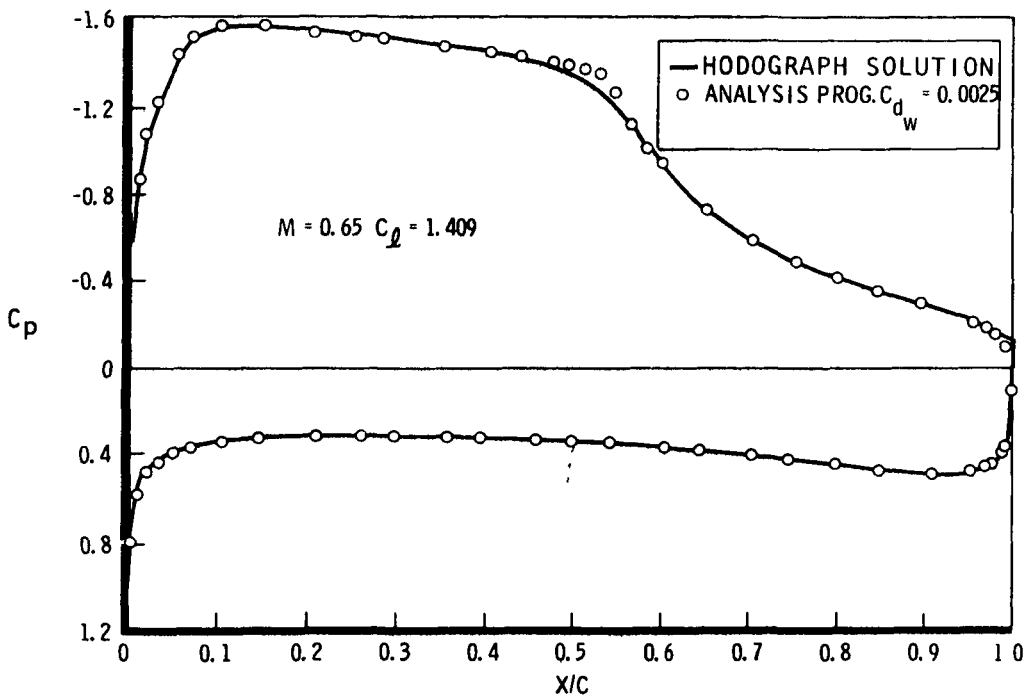

Figure 78. - Garabedian 65-14-08 airfoil inviscid design pressure distribution.

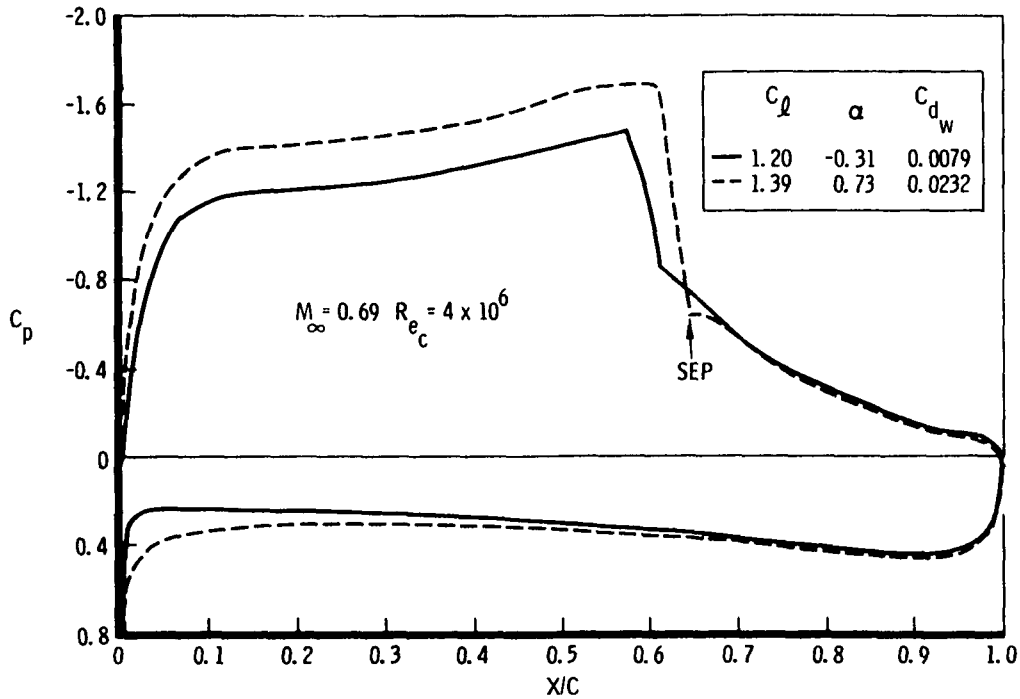

Figure 79. - 65-14-08 airfoil off-design performance.

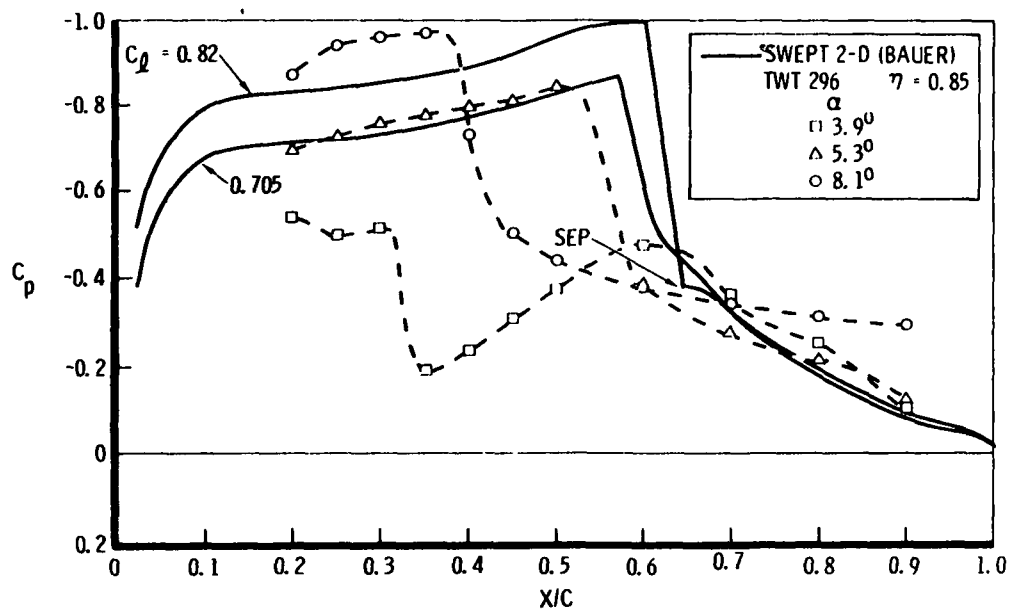

Figure 80. - Comparison of measured -36 wing pressures with sweep theory design.

The design pressure distribution shown in figure 79 is obviously unsatisfactory. There are two alternatives. The first is to use a section closer to the design Mach number while maintaining the prescribed section lift. The second is to select a sweep such that the characteristics of the 65-14-08 section can be more closely utilized. For example, a design sweep almost equal to the leading edge sweep of 45° will correspond to a perpendicular Mach number of $M_\perp = 0.65$. For a wing with taper, the design sweep is really indeterminate. Since the critical speed decreases from the leading edge to the trailing edge, a shock may be created when the adverse pressure gradient begins at a position where the isobar sweep is less than the design sweep. For proper operation of the 65-14-08 section, the design sweep then would correspond to a sweep less than or equal to that at midchord. It would have been desirable to examine analytically the effects of design sweep on the three-dimensional pressure distribution, but this was not possible. It was decided to maintain the design sweep at or aft of midchord and seek a solution by the first alternative.

Shockless airfoil, transonic scaling. - It was determined that the airfoil could be scaled with the Spreiter-type similarity rule and the general design features would be retained. The Garabedian 65-14-08 airfoil was scaled to a nominal design Mach number of $M_\infty = 0.7$. The section was analyzed at the scaled design point with the transonic method of reference 11. The pressure distribution is shown in figure 82. Although the similarity rule is based on a small perturbation analysis the results were very close to the predicted scaling. The design lift of course is reduced, so it is now necessary to operate the section off design with respect to lift instead of Mach number.

The actual section was obtained by removing the upper surface displacement thickness calculated for infinite yawed wing conditions. The displacement thickness for the model Reynolds number, which was used, and for a full-scale configuration are shown in figure 83. The lower surface displacement thickness correction could be similarly applied and a linear rotation (ref. 14) would be used to adjust the trailing edge thickness. Instead, to retain the minimum thickness for supersonic pressure drag considerations, the lower surface was modified as shown in figure 84.

The section was then analyzed to assess the off-design performance with increasing lift. The Bauer analysis (ref. 16) did not include a yawed wing boundary layer method so the results must be viewed qualitatively. Pressure distributions at $C_\ell \sim 1.2$ and 1.4 are shown in figure 85. The upper surface expansion and thus the shock strength and wave drag have been reduced. However, shock-induced separation is still predicted at the higher lift coefficient.

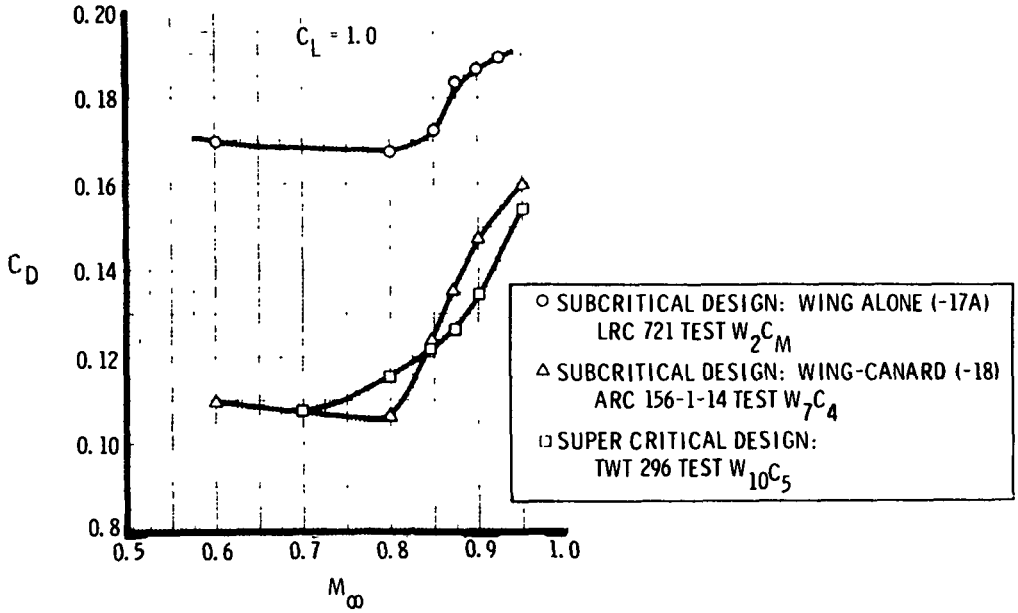

Figure 81. - Maneuver configuration drag rise.

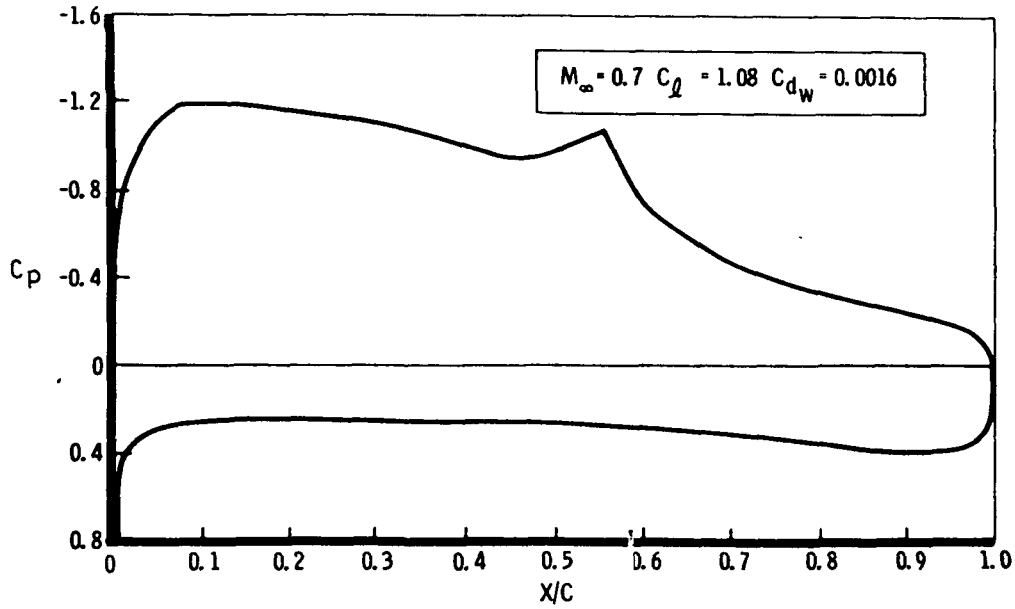

Figure 82. - Scaled Garabedian airfoil (70-11-06) at the inviscid design condition.

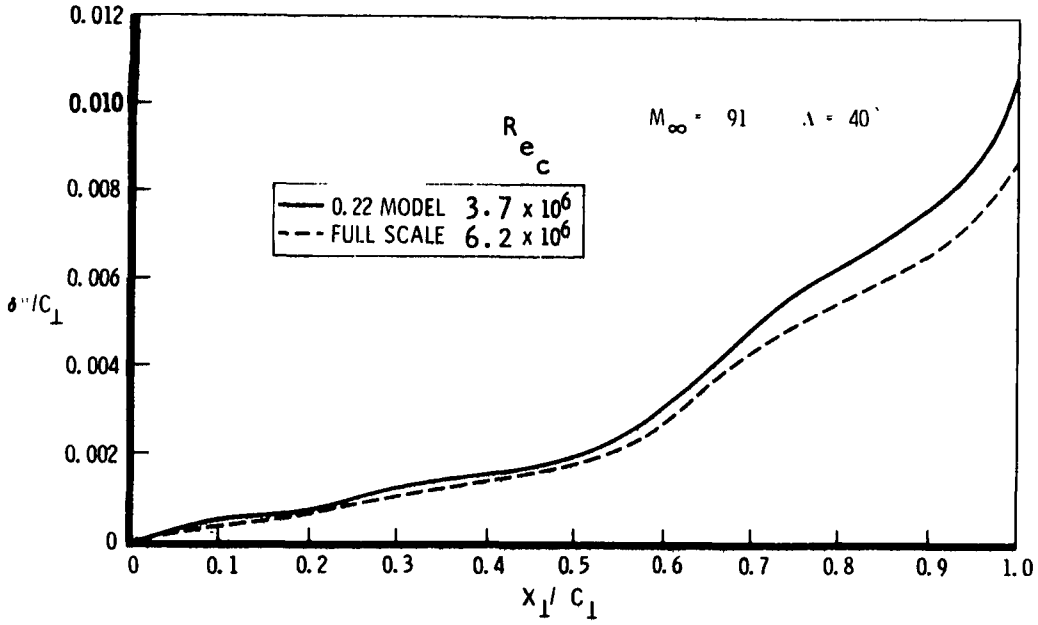

Figure 83. - Scaled Garabedian airfoil (70-11-06) upper surface displacement thickness.

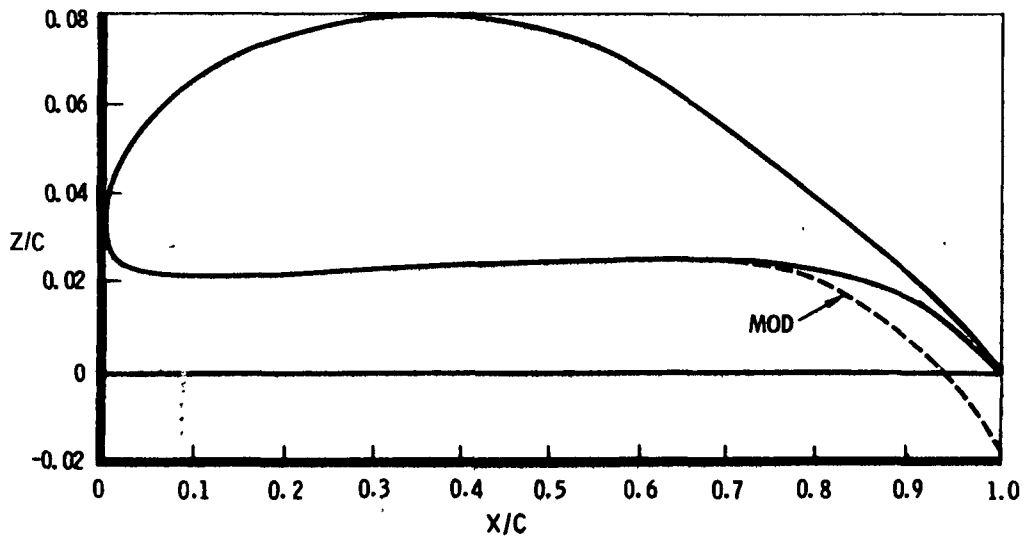

Figure 84. - Modified, scaled Garabedian airfoil (70-11-06M).

The section was adapted to the maneuver wing and the desired subcritical characteristics, constant section lift, verified. For the revised wing (-39), pressure and force data were obtained. The test configuration $W_{11}C_6$ also included a modification to the canard tip to reduce the maximum camber. This resulted in no change in drag due to lift. The effect of the outboard wing modification however, was to reduce the drag due to lift by 0.0070 at M = 0.9, C_L = 1.

Additional pressures were obtained at 70% span to examine the isobar pattern on the outboard wing. The results for 8° and 10° angle of attack are shown in figures 86 and 87, respectively. For the latter condition, which is still slightly below the nominal design point, shock-induced separation occurred outboard of 85% span. At α = 8° (figure 86) the isobars are unswept as expected for off-design operation. At α = 10°, the separation is consistent with the predictions in figure 85. It is probable that an inviscid calculation would indicate the required isobar sweep was attained. Inboard of 80% span the shock is swept higher than the 40° design sweep so that separation does not occur at this condition. The search for an acceptable two-dimensional pressure distribution was continued to eliminate the remaining shock-induced separation at the design point.

Weak shock airfoil. - The previous airfoils were operated off design so that the shockless airfoil philosophy was not given a fair test. Modifications would be required so that the required two-dimensional lift could be obtained without separation.

In a private communication from Richard T. Whitcomb of NASA Langley Research Center, an alternate supercritical philosophy was suggested where the final recompression is not initiated until approximately 80% chord. There may be one or more smaller recompressions preceding this and for supercritical flow weak shocks are accepted. This philosophy is illustrated in figure 88 for the LRC/Whitcomb 74-10-06 airfoil. The initial supercritical region is terminated in a shock. Following this is an expansion to a slightly supercritical flow and a shockless recompression. Although at the design point there is some wave drag, the off-design performance has been found, experimentally, to be usually better than that of the previous airfoils.

The 74-10-06 airfoil was analyzed at the design Reynolds number, the displacement thickness was added, and the section was scaled to a design Mach number of $M_\perp$ = 0.69. The inviscid pressure distribution was obtained at the scaled angle of attack and is shown in figure 88. The design lift, $C_\ell \sim 1.3$, was now much closer to the required value. The boundary layer characteristics for infinite yawed wing conditions, M_∞ = 0.9 and Λ = 40°, are presented in figure 89. Upper surface trailing edge separation occurred at approximately 95% chord. Several modifications to the contour

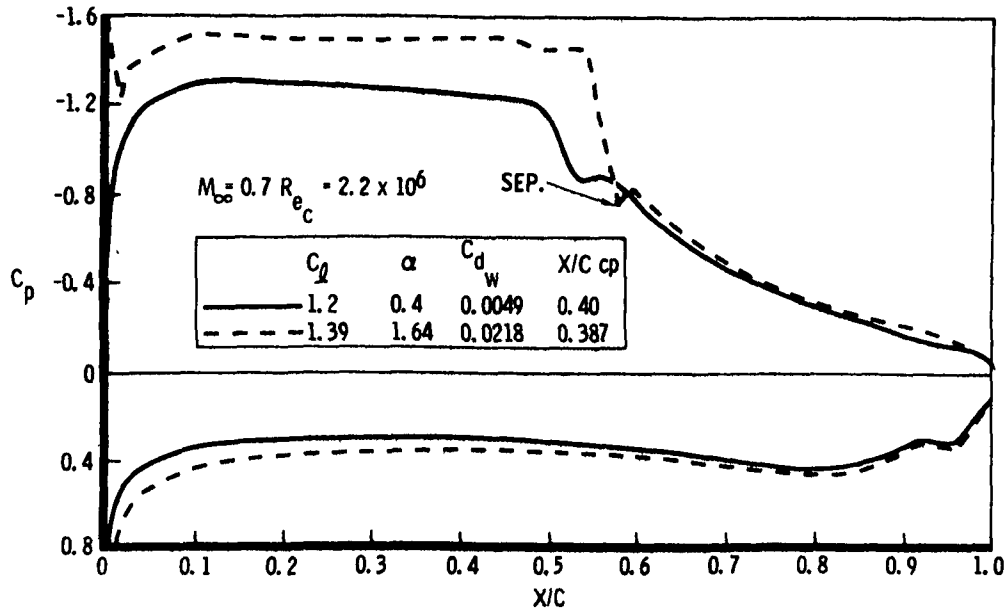

Figure 85. - Two-dimensional analysis of modified, scaled Garabedian airfoil (70-11-06M).

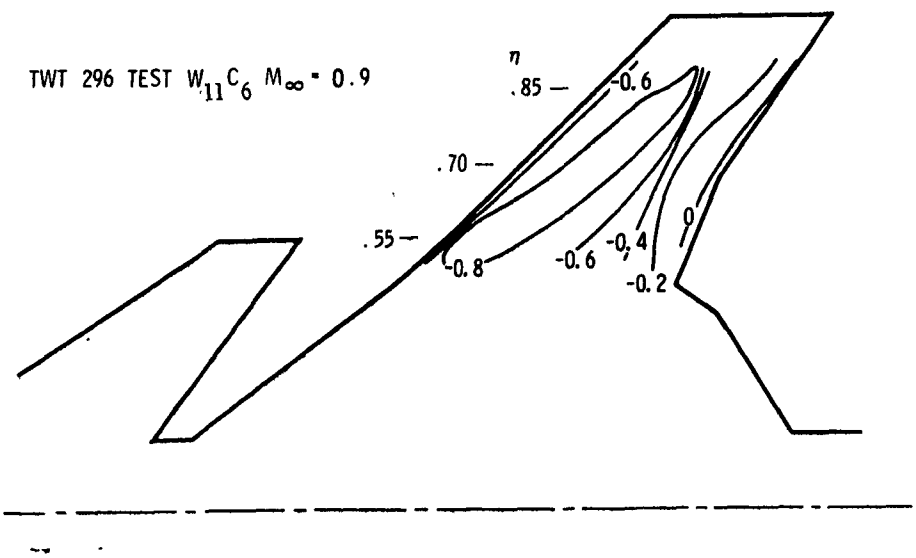

Figure 86. - Isobars at $\alpha = 8°$ for supercritical outboard wing design.

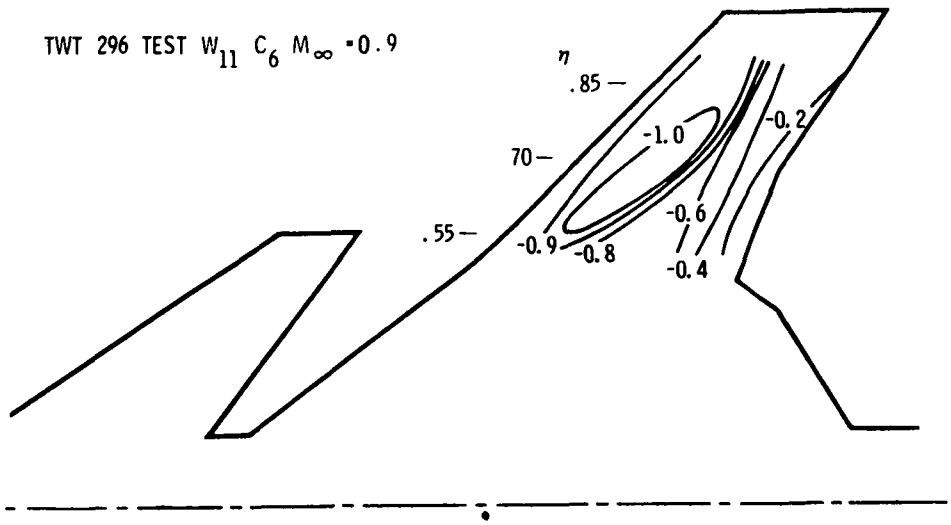

Figure 87. - Isobars at α = 10° for supercritical outboard wing design.

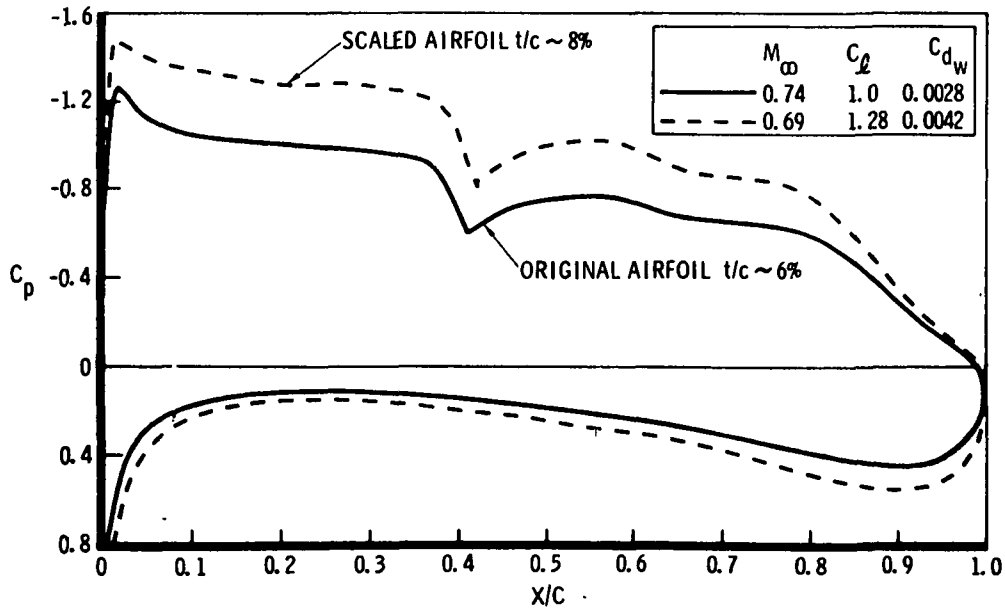

Figure 88. - Pressure distribution for scaled LRC/Whitcomb supercritical airfoil.

were attempted using the streamline curvature approach of reference 14, but the separation could not be eliminated. It was felt that some trailing edge separation could be tolerated if the existing shock-induced separation were delayed.

When the displacement thickness (figure 89) was removed from the inviscid shape the contours crossed before the trailing edge. The lower surface was rotated to provide a suitable thickness in the trailing edge region, but the thickness ratio was now almost 9% (7% in the free stream direction). A supersonic pressure drag analysis indicated a substantial penalty. By simply replacing the lower surface with the unmodified scaled Garabedian airfoil lower surface the thickness was reduced to 6%. The reduction in wave drag due to volume is shown in figure 90. The modified section, 69-13-06M was analyzed to assess its transonic performance. The results (figure 91) were applicable strictly for two-dimensional flow so they were used primarily for comparison with the previous transonic airfoils. At the lift corresponding to the nominal configuration design point ($C_\ell \sim 1.4$), no shock-induced separation was predicted. A comparison of the two-dimensional section drag polars for the airfoils considered is shown in figure 92. As a result of the higher design lift, the LRC/Whitcomb derivative is superior. However, starting from the pressure distributions at $C_\ell = 1.4$, both the 69-13-06M and scaled Garabedian sections could be improved.

The modified LRC/Whitcomb derivative was adapted to the outboard wing panel such that the isobar sweep would be maintained at the design condition. An oil flow for the revised wing (W_{17}) near the nominal design point is presented in figure 93. A weak swept shock on the outboard wing was achieved. Trailing edge separation is indicated, consistent with the analytical prediction. Pressure distributions will be presented in a subsequent section.

Conclusions. - The design pressure distribution selected for the outboard wing is characterized by a weak shock at the design condition in contrast to the shockless approach. The former seems to have better off-design characteristics. However, the latter has lower drag for a point design application. The weak-shock airfoil section was more successful for the present application because it more closely met the required design conditions. The Garabedian shockless airfoil approach would require additional modifications through a transonic two-dimensional design cycle in order to be equivalent with the LRC/Whitcomb airfoil.

The adaptation of the supercritical sections to the outboard wing was approximate because a three-dimensional design/analysis cycle was not possible for the highly swept region. A linear theory analysis was used to verify that constant sectional characteristics were maintained across the

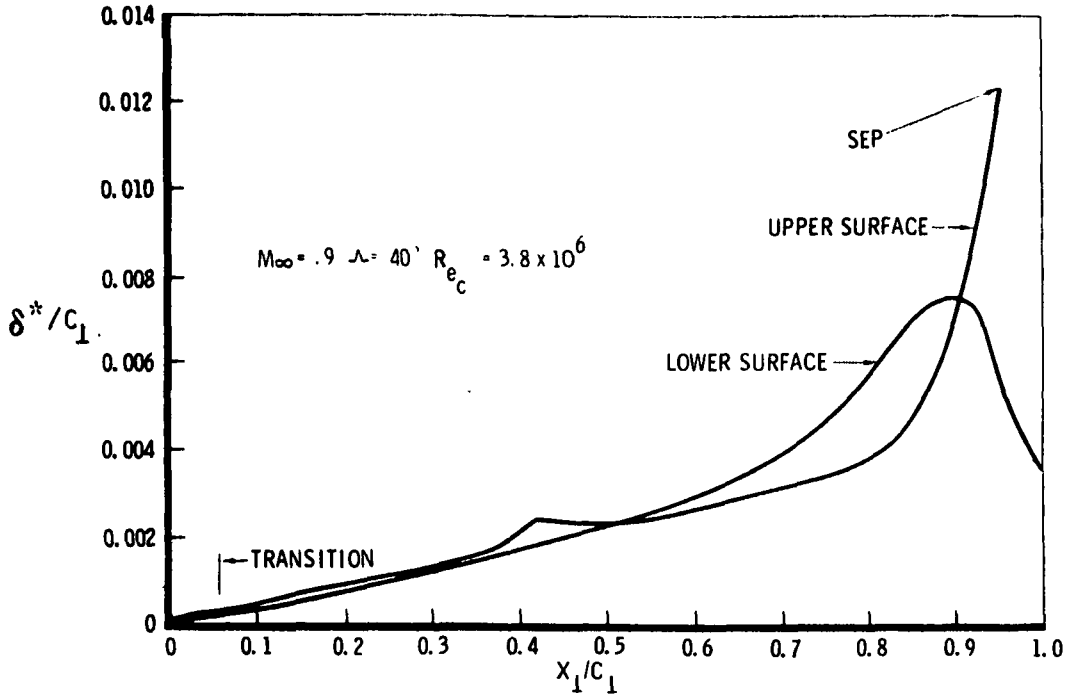

Figure 89. - Displacement thickness for design pressure distribution, LRC 69-13-08 airfoil.

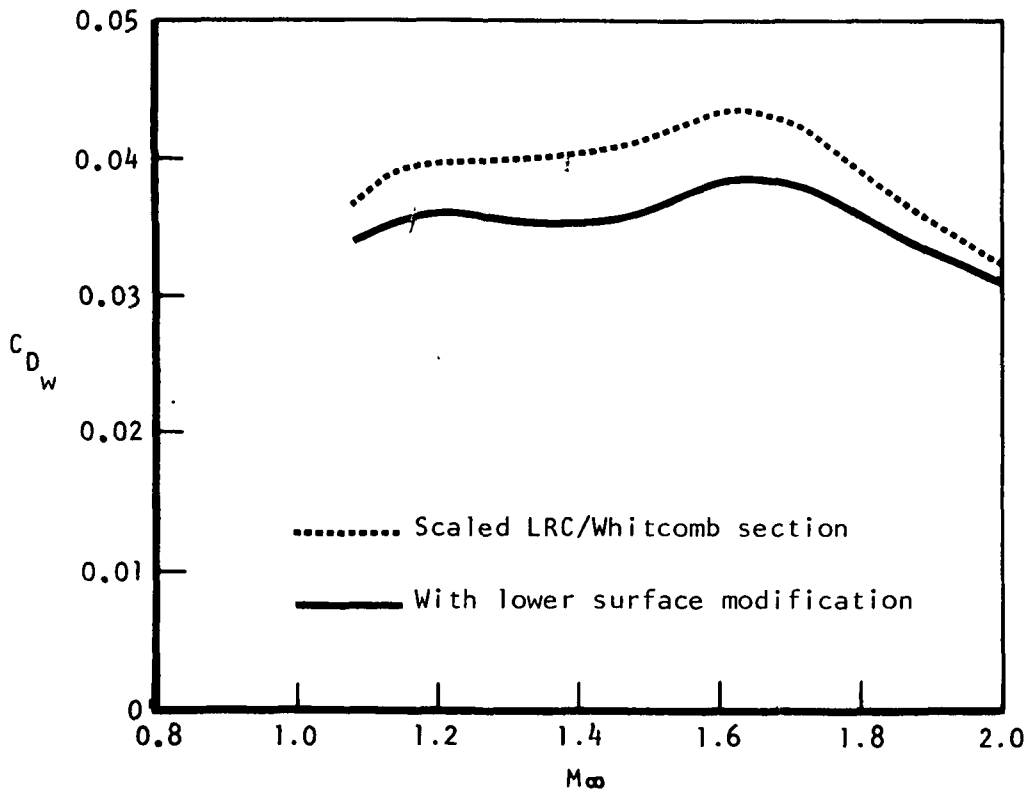

Figure 90. - Effect of outboard wing thickness on wave drag.

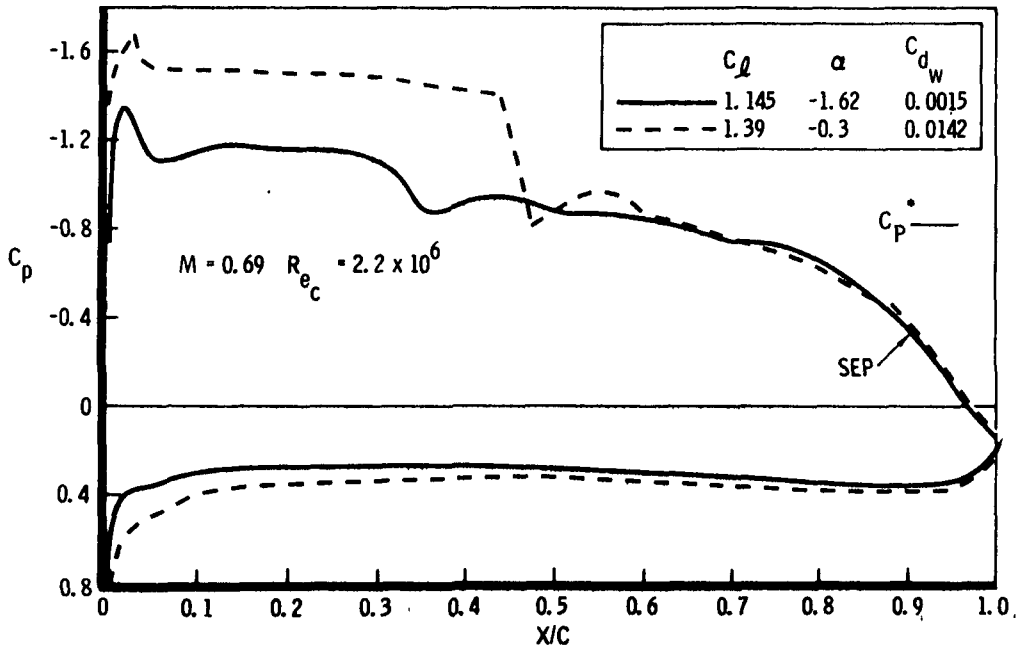

Figure 91. - Two-dimensional analysis of modified, scaled LRC/Whitcomb airfoil 69-13-06M.

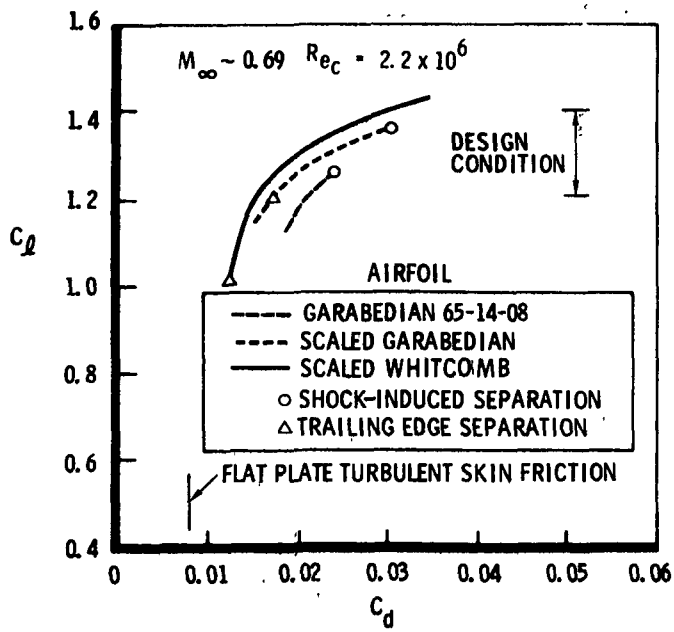

Figure 92. - Comparison of section drag polars for design airfoils.

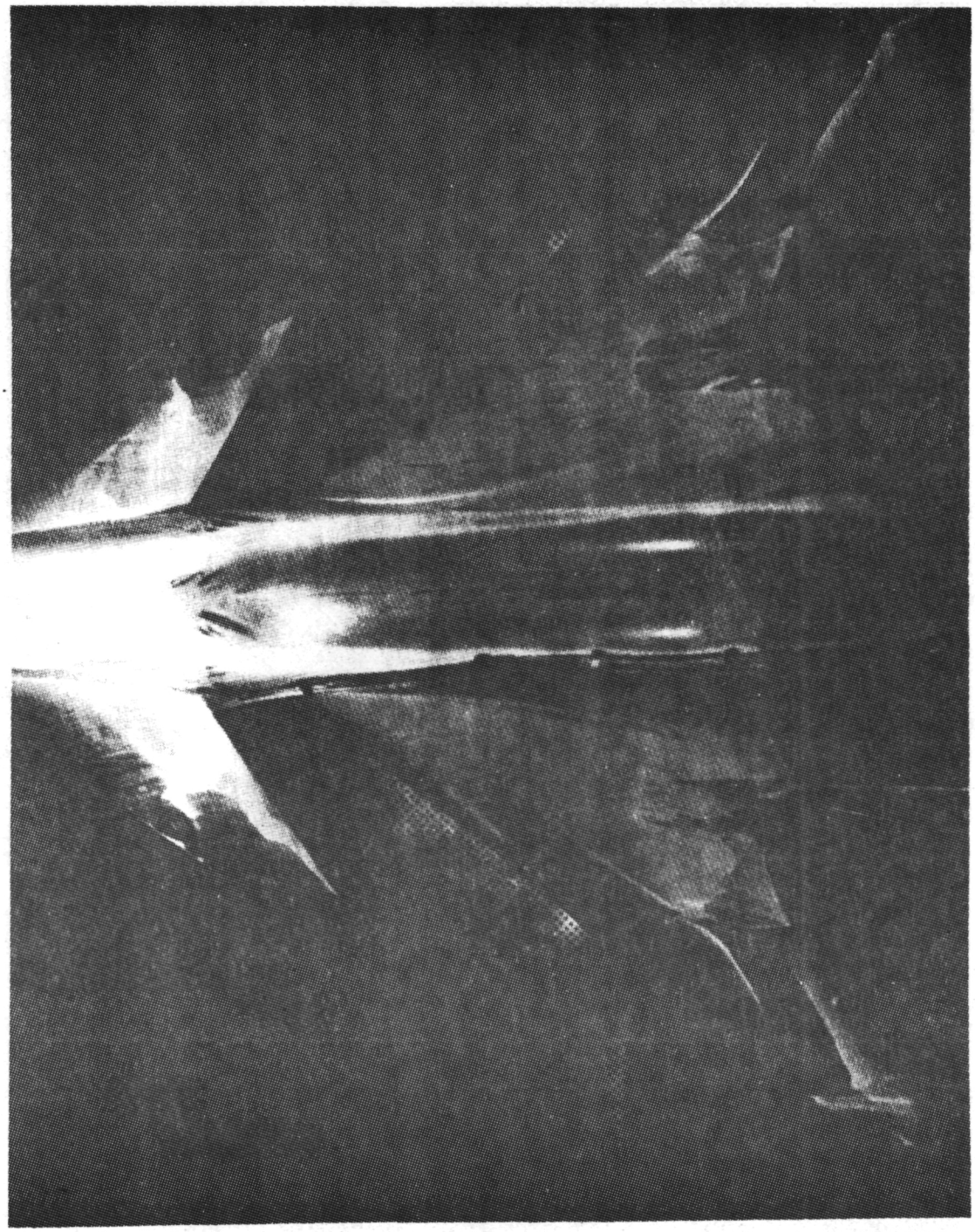

Figure 93. - Oil flow of maneuver configuration with scaled LRC/Whitcomb airfoil, TWT 296 test $W_{17}C_9$, $\alpha = 10°$, $M = 0.9$, $C_L = 0.93$.

span at an equivalent subcritical condition, but no modifications for the effects of the inboard wing or the winglet on the outboard wing flow field at transonic conditions were possible.

The winglet should have been modified with a sweep theory initialization but priority was given to the wing and, later, the canard and no redesign of the winglet eventuated. Pressure data from later tests indicated that the winglet stalled prior to the wing and adversely affected the outboard wing. Contributing to this adverse effect is the unsweeping of the isobars near the intersection which results in shock-induced separation. This characteristic of the winglet concept can only be moderated with a full three-dimensional analysis/design cycle. Although the shock is normal to the free stream in this region, the position is determined by the swept shocks on the wing and winglet. The problem was thus not amenable to analysis with the transonic wing code.

Canard Section Development

Through examination of experimental pressure data, it was concluded that the inboard region of the canard was satisfactory. The outboard area was characterized by a weak swept and strong unswept shock system. The objective was to replace this with a single weak shock.

A subcritical analysis with the body for the 55° canard design indicated a nearly constant section lift distribution could be prescribed without substantial variations in the existing twist distribution. A two-dimensional design was considered appropriate as an initialization but was complicated by the large amount of taper (generator sweep of 55° to 35° from leading edge to trailing edge). Pressure distributions derived under two-dimensional assumptions (C_p* constant) are not necessarily optimum due to this large sweep variation. However, since the three-dimensional transonic code was unworkable at the design conditions, a sweep theory implementation was pursued. The required section lift was, by design, the same as that for the outboard wing.

The parameters pertinent to the sweep theory/transonic scaling solution are summarized in figure 94 for two airfoils. If the midchord sweep is selected, the required lift is obtained with either a Garabedian 65-14-08 or LRC 74-10-06 derivative.

Scaling of the shockless airfoil (65-14-08) was the appropriate choice based on the design conditions. Because of the possibility of large three-dimensional effects due to the high taper of the canard, the section might

be required to operate substantially off design. Based on the previous experience with the outboard wing, scaling of the LRC 74-10-06 airfoil was pursued instead. As a first approximation, and to provide a practical thickness, the perpendicular section designed for the wing (69-13-06M) was utilized. With this section normal to the element line having a sweep of 40°, the canard streamwise section was constructed.

The revised canard, C_{10}, pressure distribution at 70% span is compared to the previous design in figure 95. The strong shock was eliminated but the extent of trailing edge separation estimated from the oil flow results was greater than predicted. Additionally, allowing for distortion of the two-dimensional shape of the pressure distribution due to taper effects, the leading edge peak was higher than anticipated. The overall performance, measured by the transonic drag due to lift, was only slightly better than the previous configuration.

The choice of 40° as the design sweep was arbitrary. It is possible that another design sweep (midchord or greater) would have been more appropriate, but for the highly tapered canard modifications with a higher order theory would seem to be required to eliminate the three-dimensional effects. These residual three-dimensional effects were apparent from the oil flows and pressure data which indicated unsweeping of the isobars on the outboard canard.

Fuselage Modifications

Due to a structural requirement, the fuselage cross-section near the wing leading edge was modified, resulting in an increased body width. The downstream fairing was then to be defined such that the minimum drag-due-to-lift penalty was incurred. Adverse pressure gradients on both the wing and body near the intersection were to be minimized.

The transonic wing-body code was not operational in an engineering sense. Therefore, the analysis was conducted with the linearized theory wing-body methodology. The downstream fairing (figure 96) was designed so that the wing adverse pressure gradient was unaffected as indicated in figure 96. On the body near the intersection increased velocities are thus unavoidable, but the peak occurs at a longitudinal station such that the isobar sweep is maintained (figure 97).

Drag polars at M = 0.7 and 0.9 from the TWT 296 test are presented in figure 98 indicating that the effect of the fuselage modification was negligible at M = 0.9. This may be fortuitous, since no transonic design was attempted.

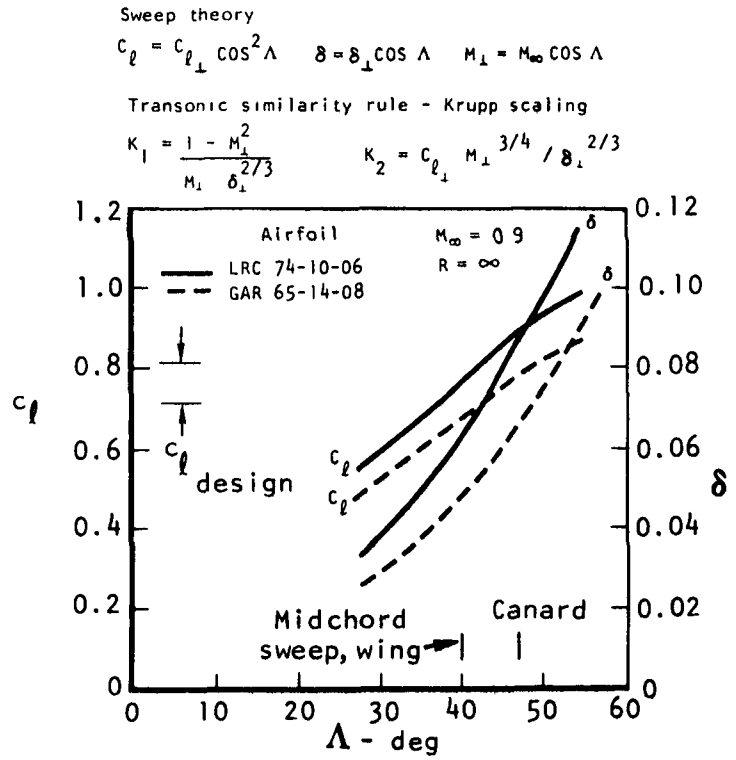

Figure 94. - Transonic similarity scaling/sweep theory design.

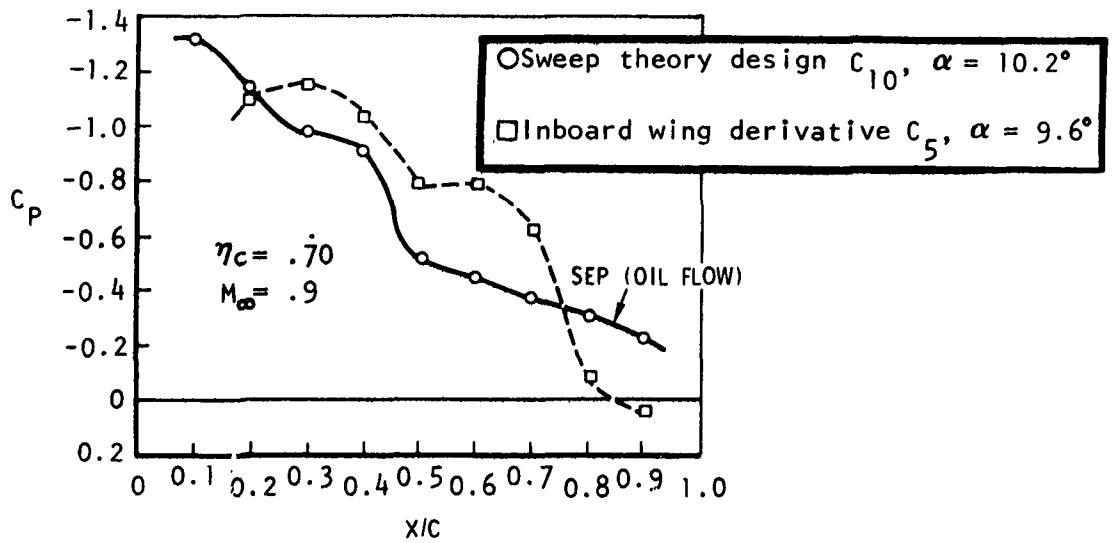

Figure 95. - Outboard canard upper surface pressure distribution.

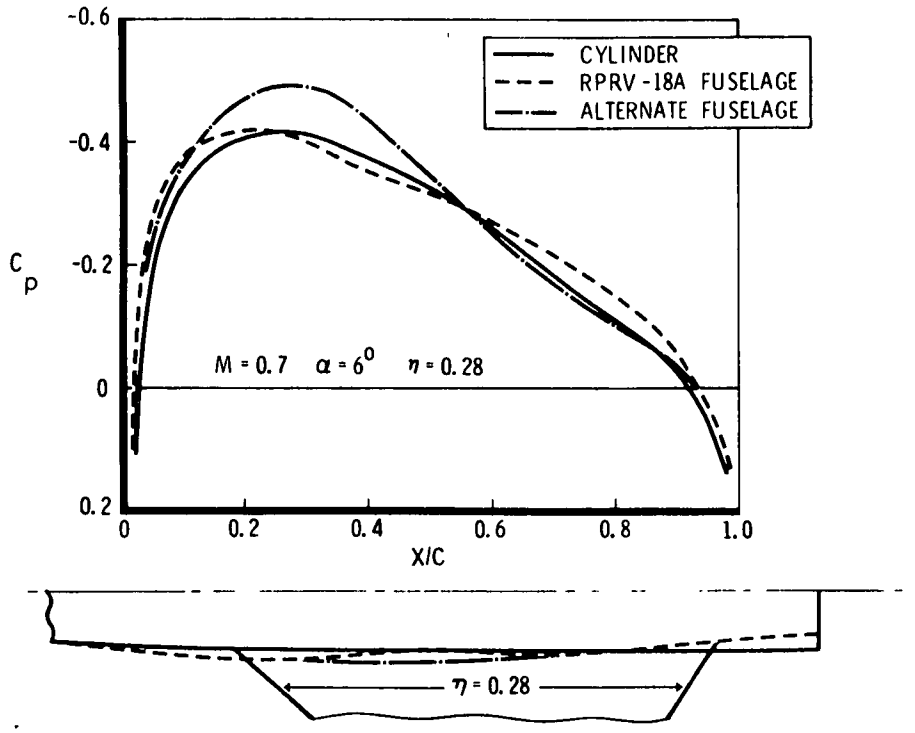

Figure 96. - Effect of body on inboard wing flow, linear theory calculation.

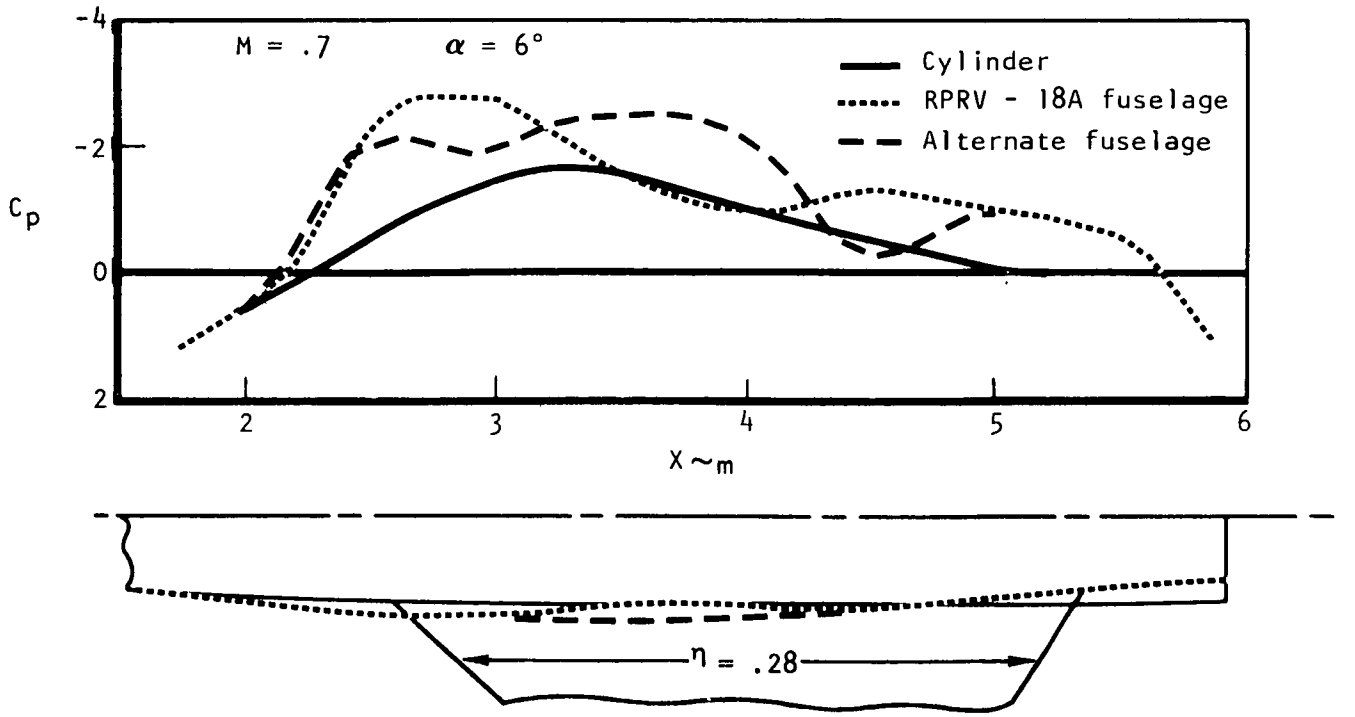

Figure 97. - Linear theory calculation of fuselage pressure distribution at wing intersection.

Supercritical Design Evolution

The drag rise characteristics for the maneuver configuration are summarized in figure 99. The two later configurations $W_{13}C_6$ and $W_{17}C_{10}$ include the revised fuselage whose impact was described previously. At $M = 0.9$ the major drag reduction resulted from the three-dimensional inboard wing design. The drag was progressively lowered through refinements in the outboard wing design. The trimmed performance goal at $M = 0.9$ and $C_L = 1.0$ is $C_D = 0.11$ using the estimated skin friction drag for the tunnel Reynolds number $R_{e\bar{c}} = 6.2$ million. The flight Reynolds number at the design condition is $R_{e\bar{c}} = 11$ million. A wind tunnel goal of $C_D \sim 0.120$ was set to allow for the anticipated favorable trim effects. Trimming the $W_{17}C_{10}$ configuration did not affect the $M = 0.9$ drag level at $C_L = 1.0$. The reduction in transonic drag due to lift with favorable trim was less than originally anticipated. As a result of the transonic flow nonlinearities (aft center of pressure movement with increasing lift) and the need to provide satisfactory low-speed characteristics with regard to stability and control, the moment to be trimmed with the trailing edge flap was small at the maneuver design point.

The data of figure 99 are for the wing rigged at 1° incidence relative to the canard. This was determined analytically with linear theory, and verified experimentally for transonic conditions, to be the optimum with respect to the wing-canard load balance. However, for the RPRV, the addition of the landing gear fairing resulted in a supersonic trim drag penalty for the cruise wing. Thus, the final wing was rigged at 0° incidence. At the transonic maneuver condition, the canard then carries more load, increasing the section lift above the original design constraint. A penalty for the untrimmed maneuver ($W_{18}C_{10}$) configuration resulted at $M = 0.9$. When the configuration was trimmed, no drag penalty was incurred relative to the $W_{17}C_{10}$ results due to the redistribution of the load from the canard to the inboard wing.

CRUISE DEFINITION

The cruise configuration is defined by deforming the maneuver shape so that satisfactory performance is obtained for transonic and supersonic cruise. The ideal situation would be a configuration that produced a nearly optimum loading with minimum viscous and wave drag as, for example, the subcritical cruise design described earlier. Designing primarily for maneuver performance will limit the freedom to design an optimum cruise configuration.

Variable Camber System Requirements

The variable camber system concept is based on obtaining optimum performance at two or more design conditions through a combined mechanical

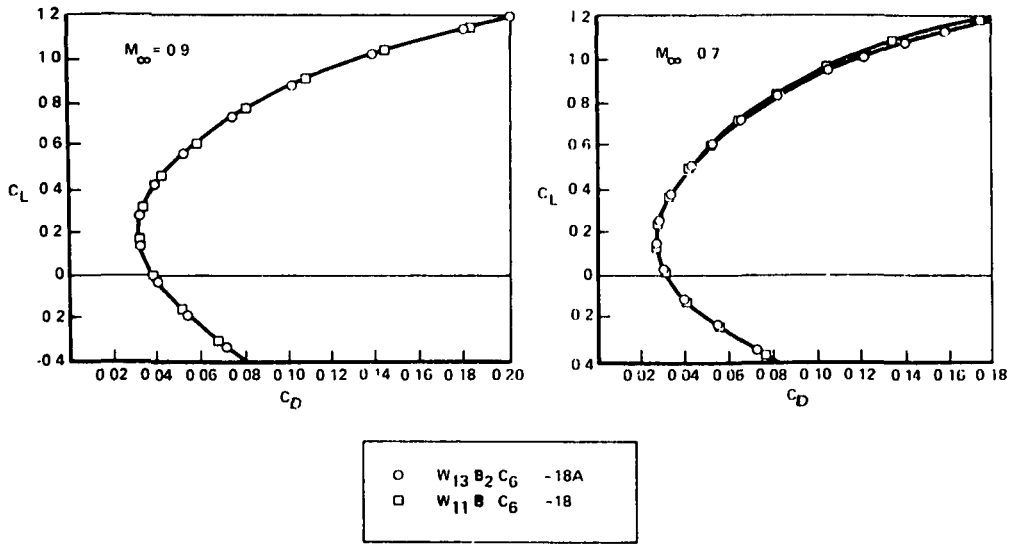

Figure 98. - Effect of fuselage modification on drag.

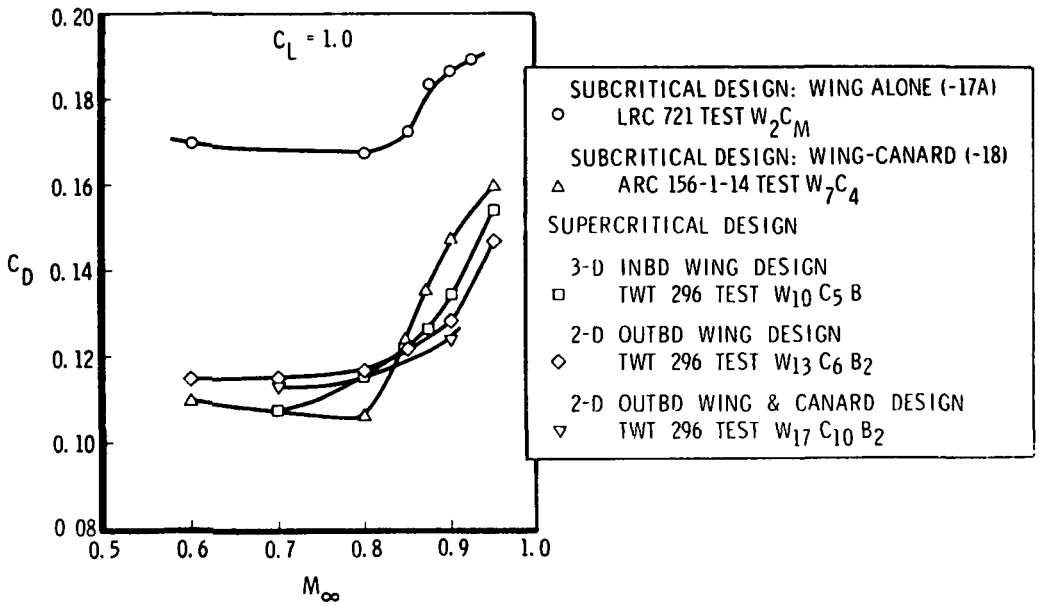

Figure 99. - Maneuver configuration drag rise.

and aeroelastic deflection. Once the maneuver configuration is defined, the cruise shape is determined by iteration. Given a leading edge variable camber system and an unspecified twist increment due to structural bending, a linear or nonlinear analysis, or combination of both, is used to define the best cruise shape with the geometric constraints of the supercritical maneuver design. These constraints limit, obviously, the number of section shapes that can be defined and so a compromise between the span load shape and the upper surface pressure distribution may be required. The design is thus an iterative process, guided by the results of earlier optimum cruise designs.

Subcritical Design Background

The -18 subcritical wing canard cruise design was used to initialize the variable camber system requirements. This design, described in "Wing Canard Design," was tested in the Ames 14-Foot Transonic Wind Tunnel with the maneuver configurations. The drag due to lift for the cruise design, W_1C_1, is compared with the goal in figure 100. The M = 0.9 cruise goal was met indicating the linearized theory design was adequate for the lightly loaded condition. This design was used as a basepoint to compare analytically and experimentally with later cruise configurations deformed from the supercritical maneuver configuration.

Cruise Compromise

The performance compromise which arose in the cruise configuration was due to the supercritical modifications associated with the maneuver design and the constraint imposed on the aeroelastic increment. The increment in spanwise twist was initialized with the first subcritical -18 design and subsequently modified for the revised subcritical maneuver design. At this point, the aeroelastic twist increment goal was set so that the structural development could proceed in parallel with the aerodynamic development.

A cruise configuration was defined for the design with the scaled Garabedian section on the outboard wing. This section was characteristic of aft-cambered supercritical airfoils and presented several difficulties in the derivation of the cruise wing. First, the available leading edge deflection from maneuver to cruise position was less than either the earlier subcritical sections or the inboard wing sections which had forward maximum camber locations. Second, the trailing edge cusp would, if utilized in the maneuver position, result in a transonic and supersonic camber drag penalty. The impact of the leading edge deflection capability was not as critical as the situation regarding the trailing edge camber. The latter was dependent on the assumed aeroelastic deformation. That is, if the

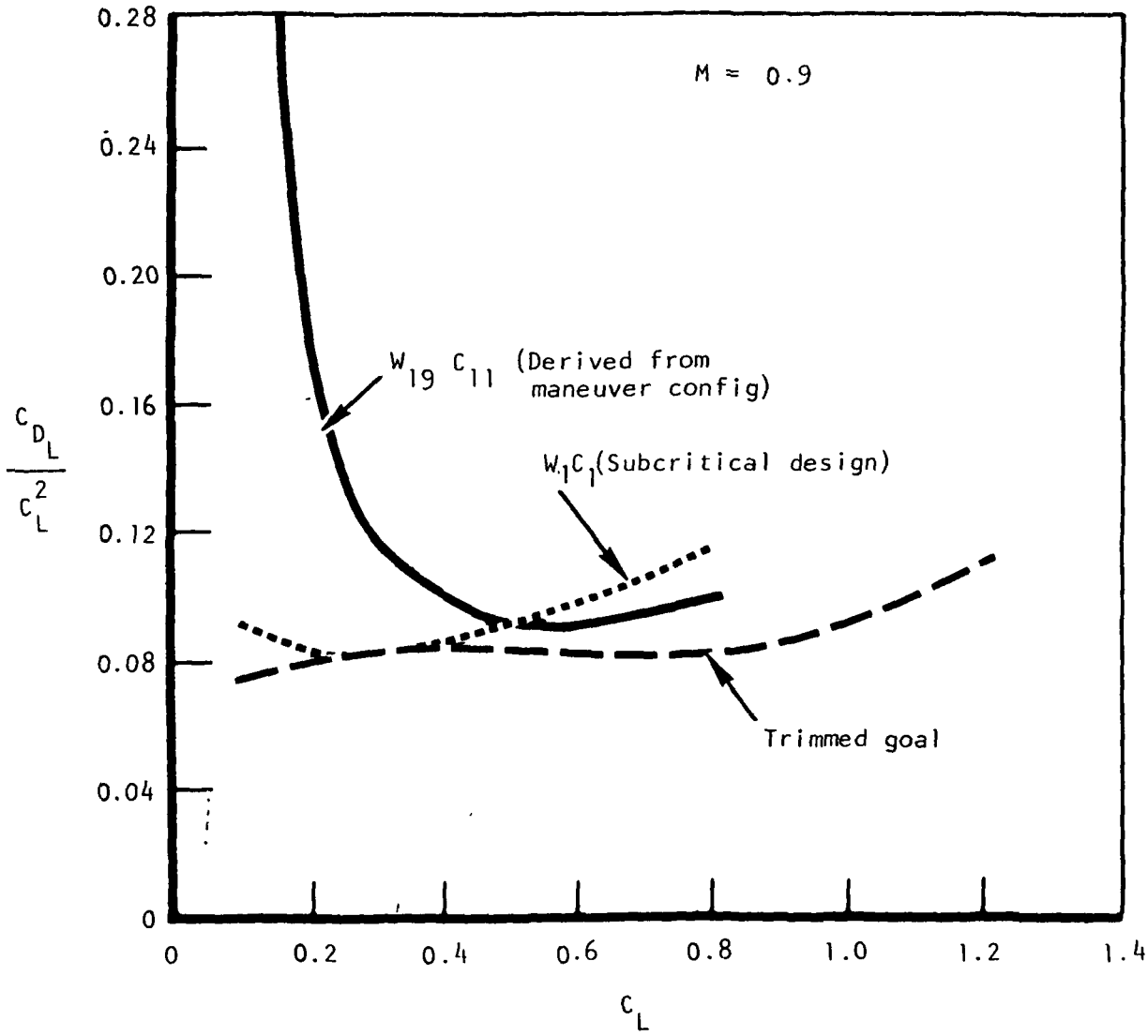

Figure 100. - Cruise wing trimmed drag due to lift.

aileron was deflected up, moderating the effect of the trailing edge cusp, the net result on the drag due to lift would be small if the twist could be reduced by additional aeroelastic deformation. As noted, the maximum twist increment was set prior to this point in the development. Therefore a subcritical analysis was performed to define the best compromise between trailing edge (aileron) deflection and twist distribution. The compromise is between average camber (twist) and local camber (trailing edge deflection).

The wing twist distribution for the compromise design is shown in figure 101. This distribution resulted from a 4° aileron deflection utilized to cancel the supercritical maneuver trailing edge camber. As a result of the constraint on available aeroelastic twist increment, the design of figure 101 results in an effective increase in the design lift and a drag-due-to-lift penalty at the nominal cruise condition, $C_L = 0.15$. The test results for this cruise configuration, $W_{15}C_8$, are not presented since they were indistinguishable from the later cruise design.

The final cruise definition was based on deformations of the LRC/Whitcomb supercritical airfoil on the outboard wing and canard. The wing twist was the same as the previous cruise wing since the general characteristics of the supercritical section were unchanged. For the canard the same difficulty existed but there was an additional consideration. The relative twist increment between maneuver and cruise at the canard-body intersection was larger than the available leading edge camber increment. For a variable camber system confined to one surface the twist can always be reindexed for the maneuver or cruise point. However, for a two-surface variable camber system, the possibility exists that one surface may require an unrealistic twist increment at the root between maneuver and cruise if the other is indexed for compatibility. This is what transpired for the HiMAT since the wing twist requirements were compatible while those for the canard root section were not.

The cruise compromise for the canard then considered the root section twist compatibility and the outboard variable camber system for the supercritical section. The aeroelastic increment was not as firmly fixed as in the case of the wing, so additional latitude was available. The final design, which evolved in order to satisfy all the pertinent constraints, is shown in figure 102.

The drag due to lift for the cruise configuration $W_{19}C_{11}$ is compared to the subcritical design, W_1C_1, and the goal in figure 100. The effective increase in design C_L resulted in a substantial penalty at low lift coefficients. The test results for the earlier cruise definition (based on the maneuver design) indicated the penalty was associated primarily with the wing.

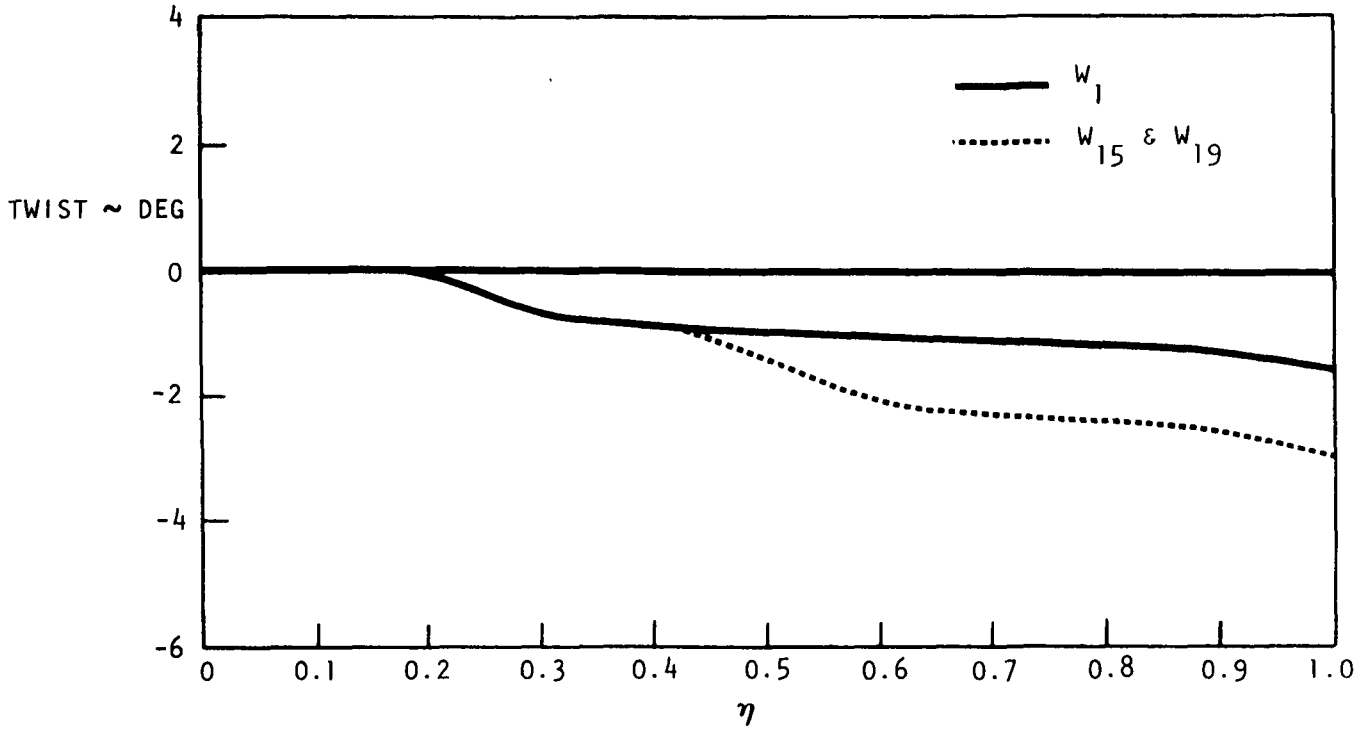

Figure 101. - Cruise wing twist compromise.

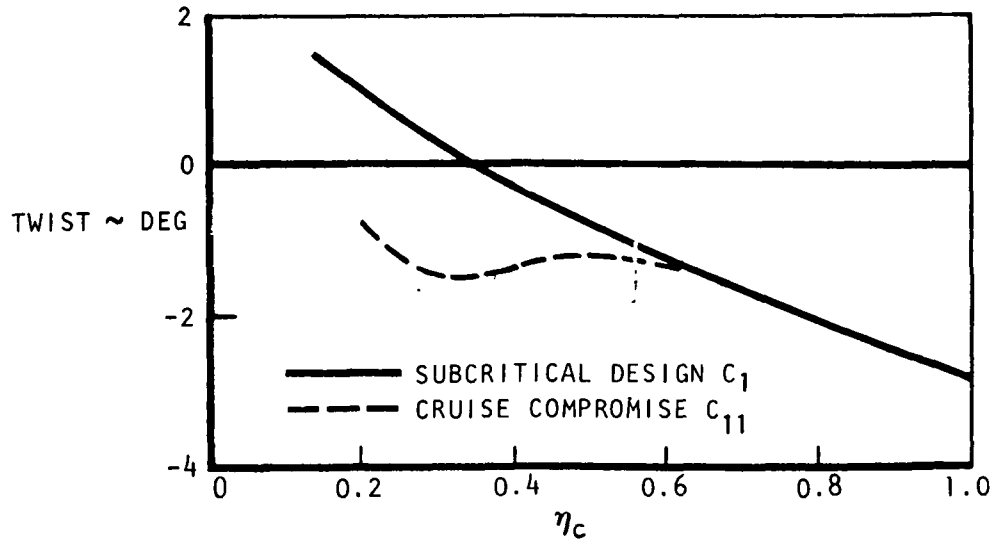

Figure 102. - Cruise canard twist distribution.

EVOLVED CONFIGURATION AND PERFORMANCE

The final configuration presented at the preliminary design review (PDR) and the performance status relative to the goals are presented in this section.

Baseline Description

Additional configuration modifications progressing from the -18A to -19 designs included: (1) an enlarged vertical tail and the addition of lower surface winglets for improved lateral-directional stability; and (2) mass balances at the wingtips for flutter suppression. The PDR baseline configuration for the RPRV concept is shown in figure 103.

The maneuver wing and canard sections are those corresponding to the test configuration $W_{18}C_{10}$. The cruise design tested, $W_{19}C_{11}$, was derived from the maneuver design assuming the aeroelastic goals would be met. The latter stages of the aerodynamic development are indicated in figure 8. The wing and canard cruise twist distributions were presented in figures 101 and 102.

The final maneuver design twist requirements were unchanged from those of figures 48 and 50. The intermediate definition with the wing rigged at 1° relative to the canard was, as noted previously, not selected for the RPRV. The 0° rigging definition produced moment characteristics which resulted in a smaller supersonic trim drag.

Configuration Characteristics

Transonic maneuver point. - Pressure distributions for the maneuver configuration at $M_\infty = 0.9$ are presented in figures 104(a) through 104(f). At 55% of the wing span the swept shock is indicated at high angles of attack. The shock near the trailing edge is not definite and does not separate the boundary layer. Further outboard, the shock moves aft and stabilizes at a constant percent chord. At 85% span, $\alpha = 9°$, the pressure distribution closely resembles the design objective (figure 91). There is insufficient data to properly characterize the flow on the canard. The midchord shock appears to strengthen moving outboard due to the unsweeping of the isobars.

The experimental isobars for $M = 0.9$, $\alpha = 10°$, are shown in figure 105. This condition corresponds to a C_L of 0.91. It is estimated that shock-induced

TOGW*	1528.6 kg
T/W LAUNCH	1.36
W/S LAUNCH	2837 N/m^2
STRUCTURE LIMIT	12g
FUEL*	286 kg
CG, $\%\bar{c}$	8.13

*TARGET

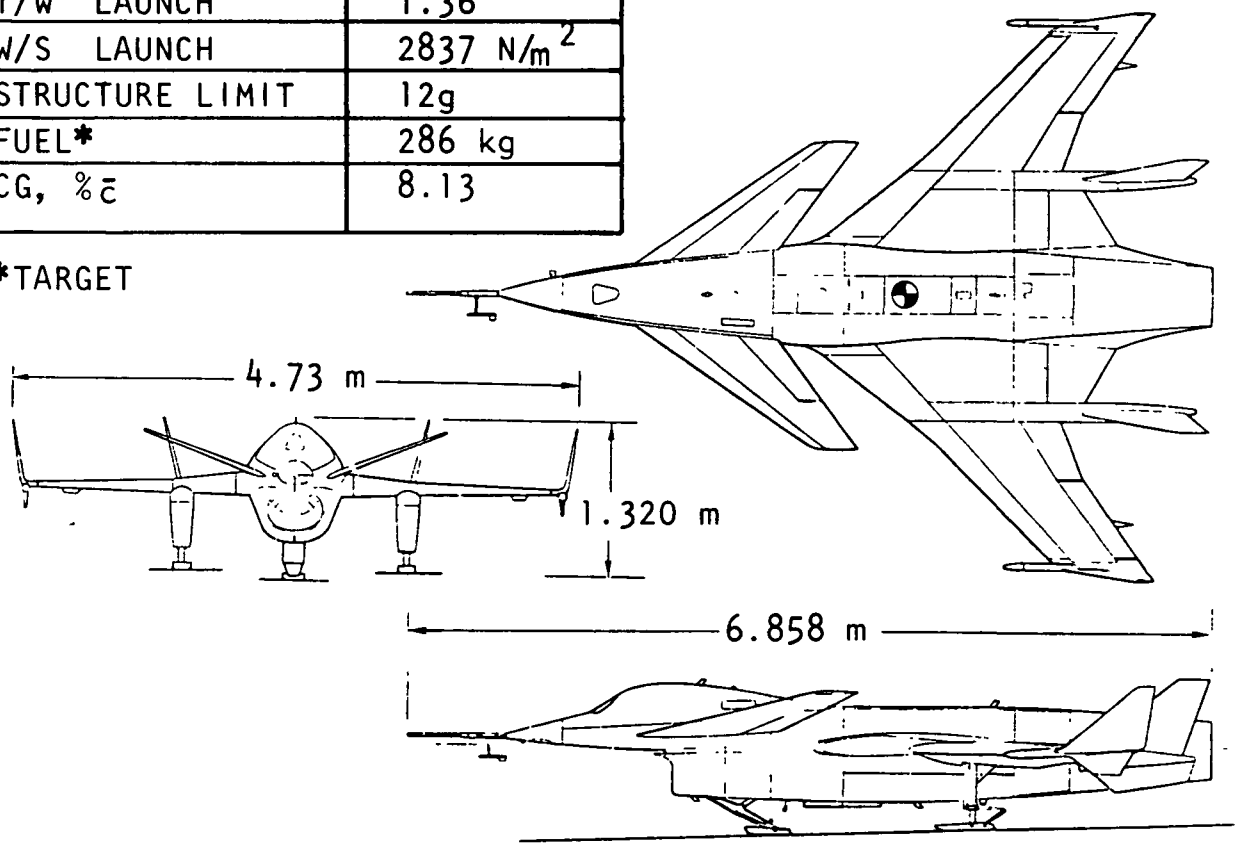

Figure 103. - PDR baseline - 19 model.

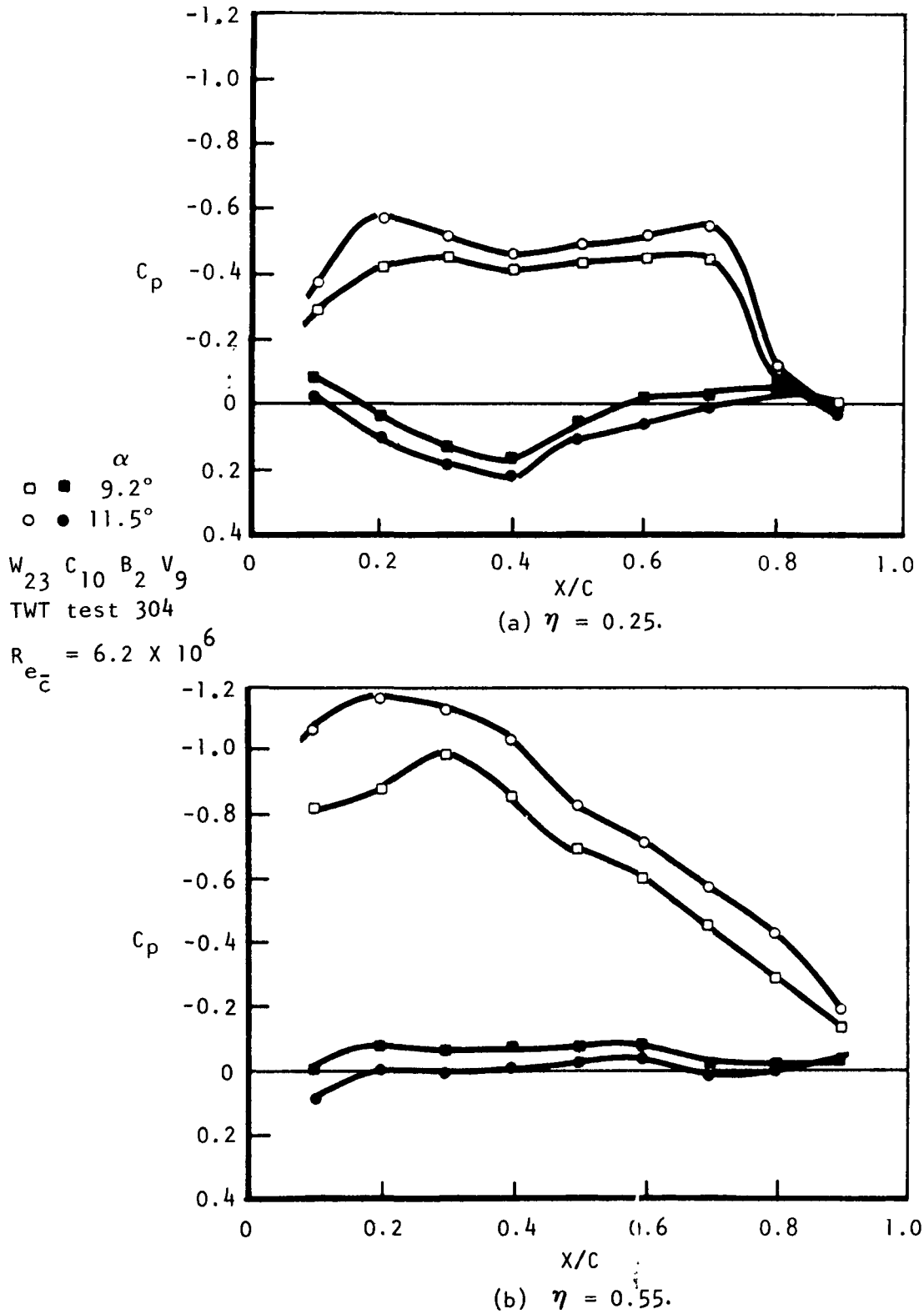

Figure 104. Maneuver configuration pressure distribution, M=0.9.

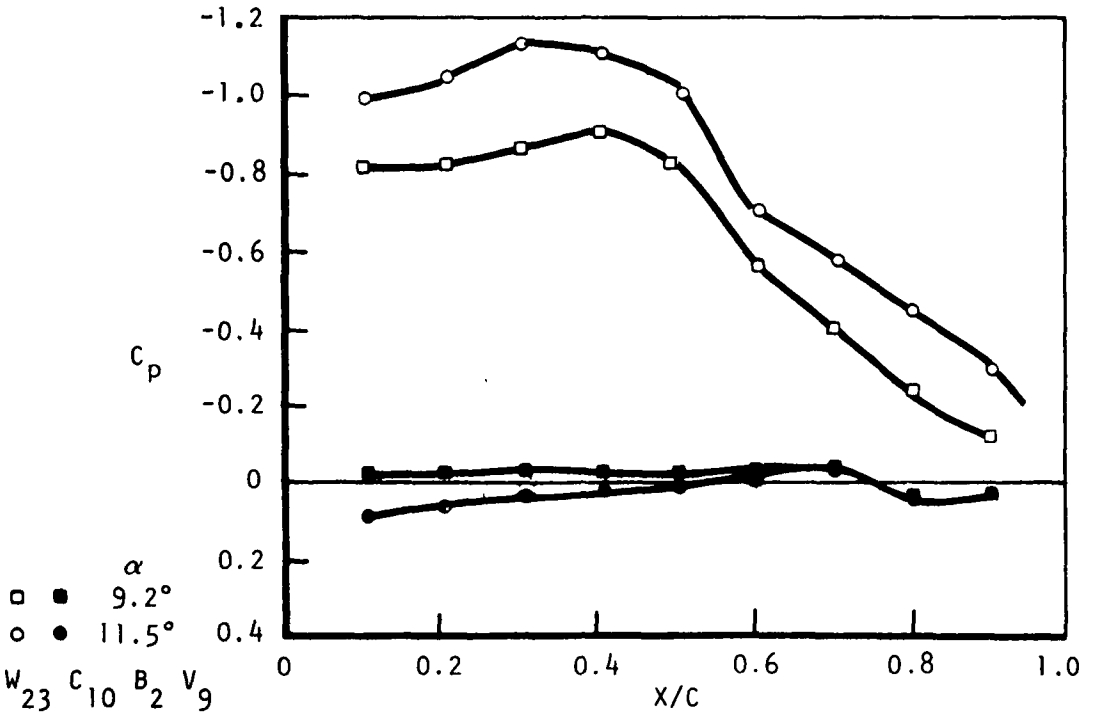

(c) η = 0.70.

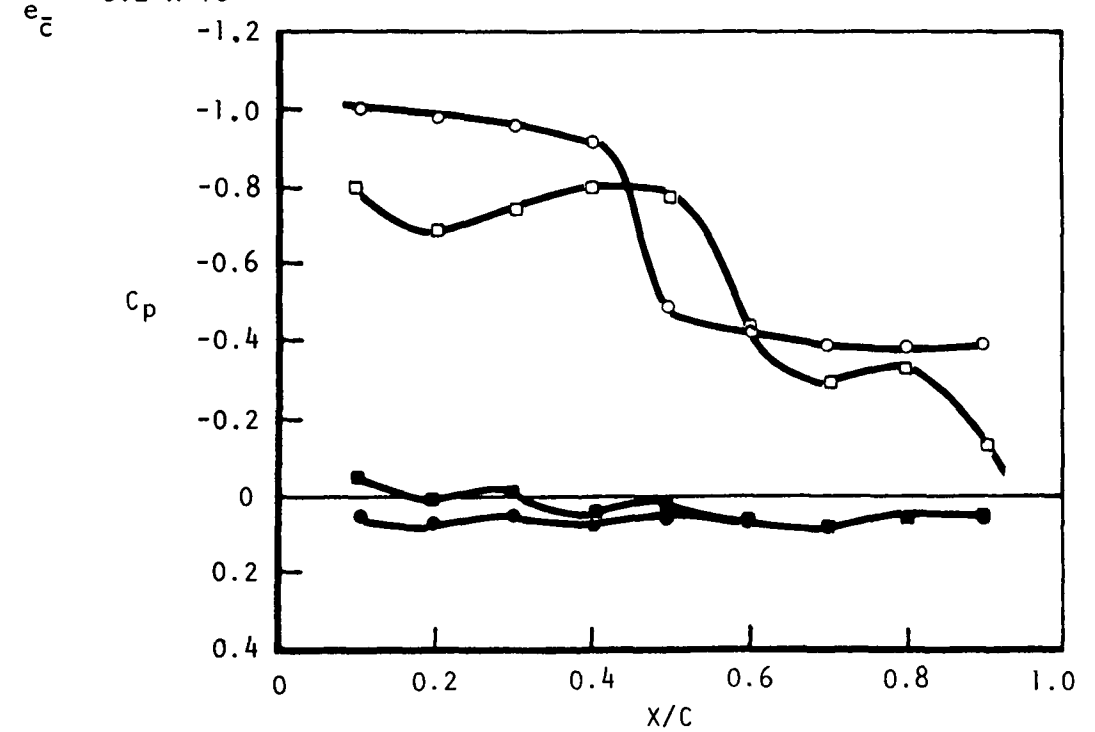

(d) η = 0.85.

Figure 104. - Continued.

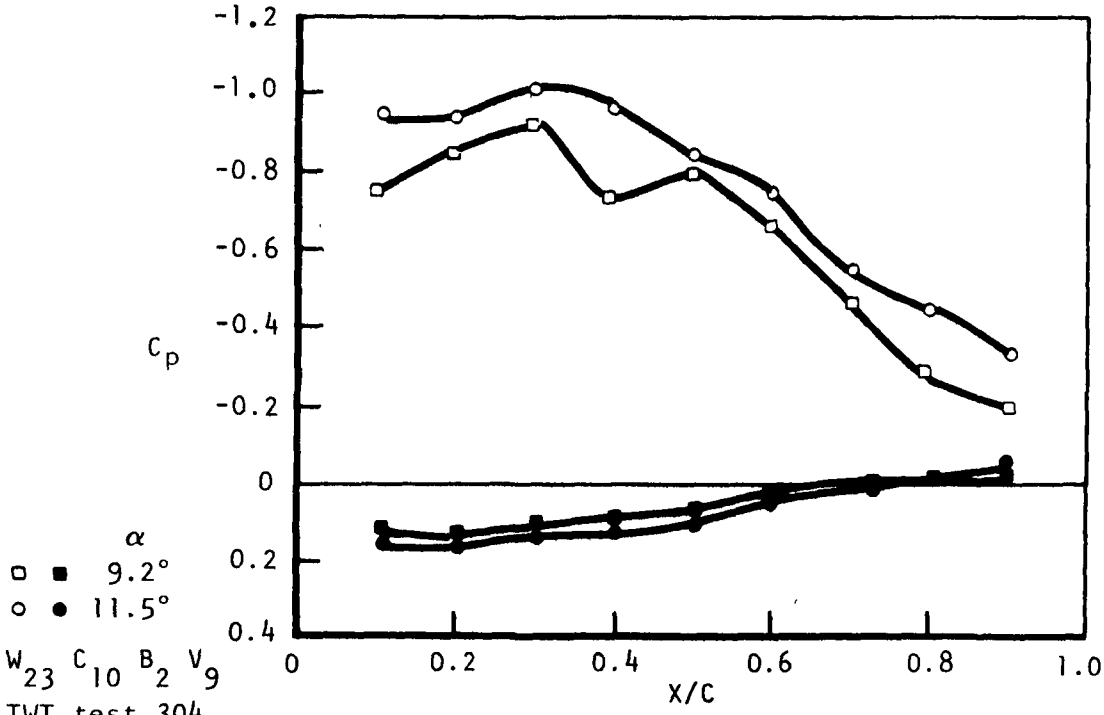

(e) $\eta_c = 0.50$.

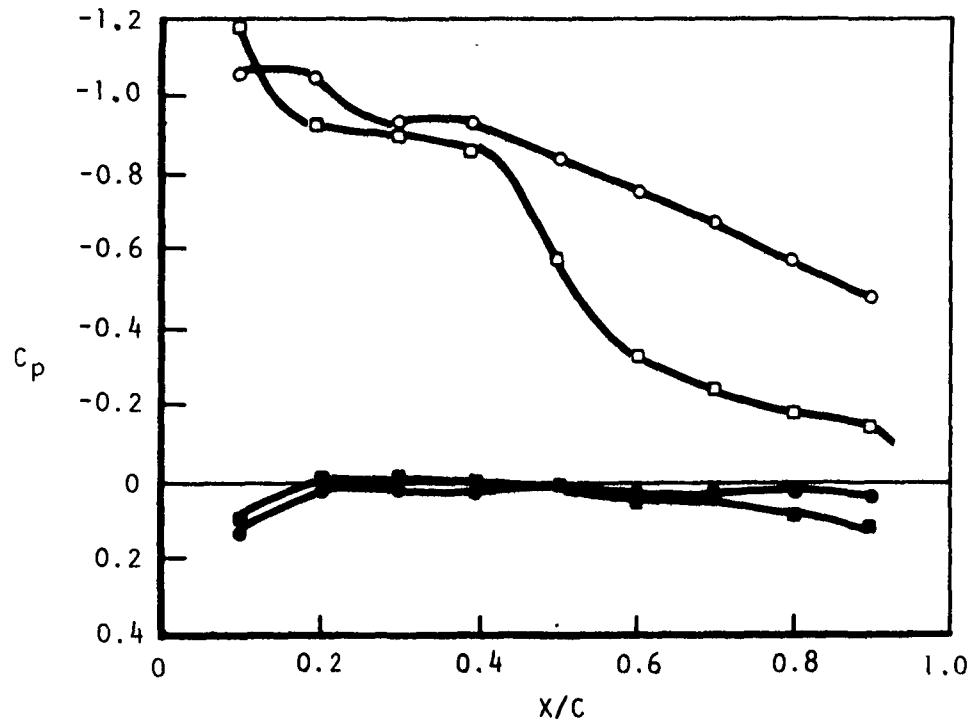

(f) $\eta_c = 0.70$.

Figure 104. Concluded.

separation occurs on the outboard wing at approximately $\alpha = 11°$. At a lift coefficient approaching 1, the pressure distribution on the wing appears to meet the prescribed design. It is difficult to assess the relation of the pressure distribution to the magnitude of drag. For example, at 25% span (figure 104) there is an unswept shock but the flow remains attached. The local Mach number before the shock is $M \sim 1.18$ at $\alpha = 9°$. This is within the range of current supercritical rooftop-type airfoils and the associated wave drag should not be large unless the volume of the shock (that is, the extent above the wing surface) is large.

Performance status.- Test results are presented in the following section to indicate the extent to which the design objectives have been met. The primary goal is the minimization of the transonic drag due to lift. In figures 106 through 108, trimmed and untrimmed drag due to lift is compared to the goal for Mach numbers of 0.6, 0.875, and 0.9. For subsonic conditions up to $M_\infty \sim 0.8$, the trimmed drag due to lift objective was achieved or exceeded for lift coefficients up to $C_L \sim 1.2$. At a lift coefficient of 1, the efficiency factor **e** is approximately 0.95 for subsonic conditions. For transonic operation, the trimmed objective was still not achieved (figures 107 and 108). At the nominal design point, $M = 0.9$ and $C_L \sim 1$, the drag-due-to-lift factor $C_{D_L}/C_L{}^2$ was 0.014 above the trimmed objective. Still, considerable progress in reducing the transonic drag had been made since, for the phase III baseline, the drag-due-to-lift factor was 0.07 above the objective.

The final configuration lateral-directional characteristics for the cruise configuration are shown in figure 109 versus Mach number. The modifications for improved lateral-directional stability, increased vertical tail volume and lower surface wingtip fin, occurred after the cruise and maneuver development tests. There was a slight reduction in drag due to lift as a result of incorporation of the lower winglets. As noted previously, the effectiveness of the winglets at $M = 0.9$ was unknown. The test results (figure 4) previously shown did indicate a reduction in drag due to lift at high-lift, transonic conditions. For subcritical conditions, the test results verified that the design successfully integrated the winglet. At transonic conditions, the results were fortuitous since no design efforts were conducted for the wing-winglet region of interference for transonic flow.

The low-speed, maximum lift goal was achieved. The maximum lift coefficient for the 55° canard configuration was $C_{L_{max}} \sim 2.1$ as previously shown in figure 59.

An objective of the advanced fighter concept was satisfactory supersonic acceleration. Wave drag of the order $C_{D_W} = 0.02$ to 0.025 was proposed for the fighter. An analysis with the total pressure drag theory was made for

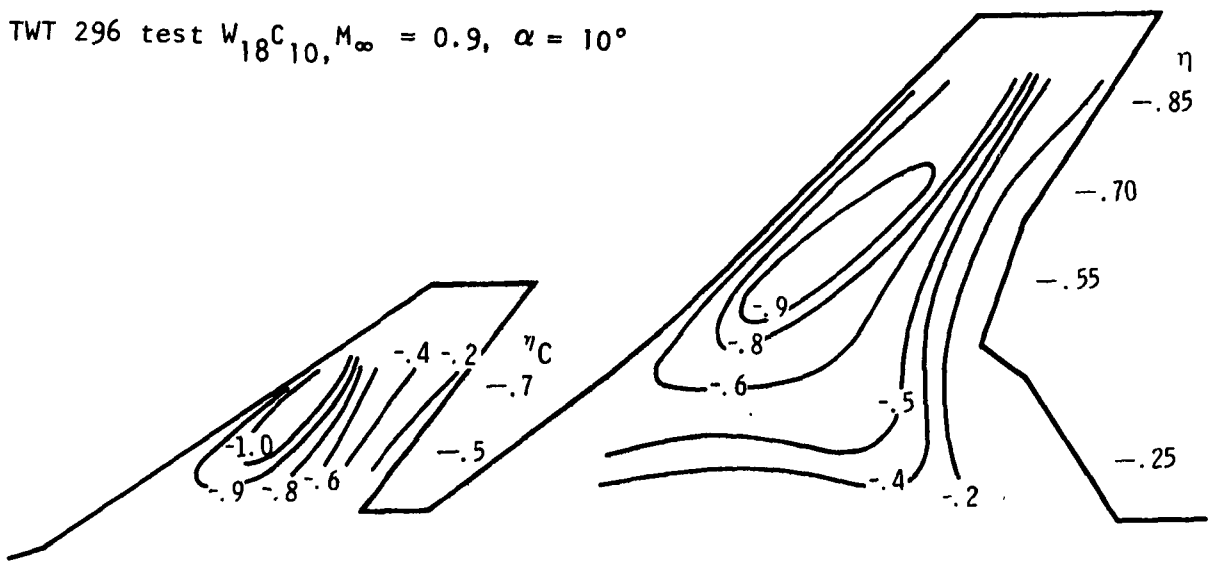

Figure 105. - Maneuver configuration upper surface isobars.

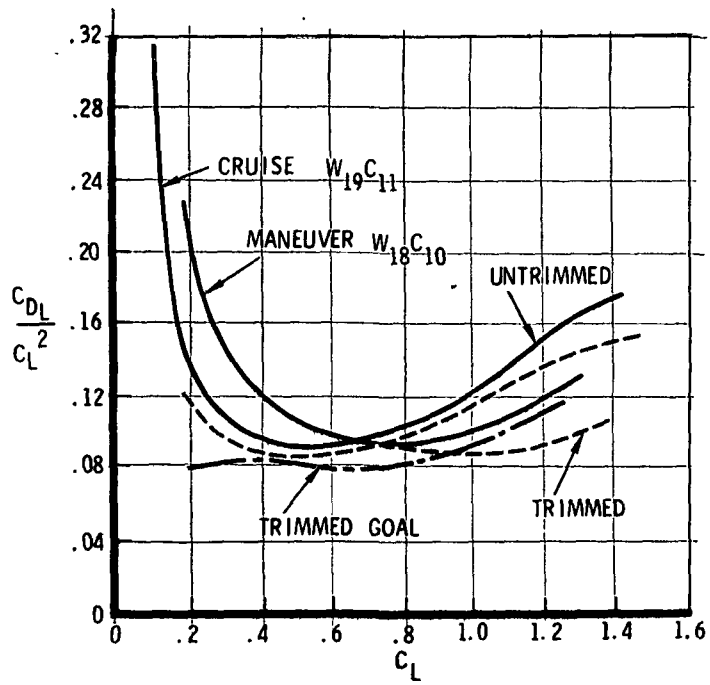

Figure 106. - Drag due to lift at M_∞ = 0.6.

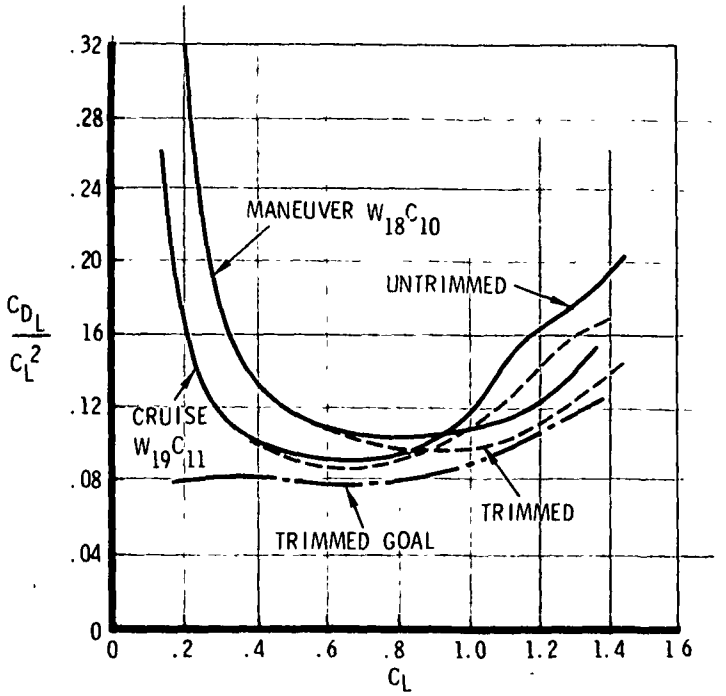

Figure 107. - Drag due to lift at M_∞ = 0.875.

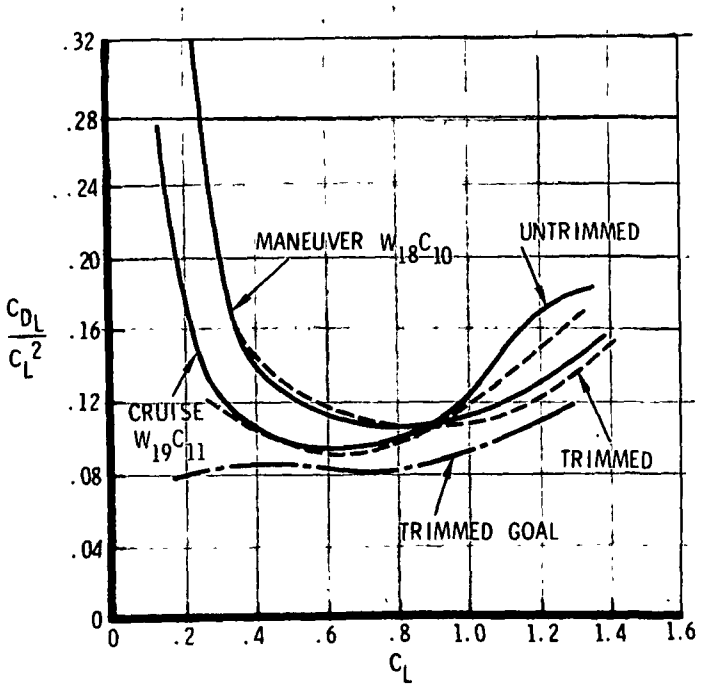

Figure 108. - Drag due to lift at M_∞ = 0.9.

the RPRV and the fighter to estimate the difference in wave drag due to the fuselage variations. After this correction was applied to the RPRV test data, the indication was that the fighter wave drag objective would be met.

For the RPRV vehicle, subsonic/transonic and supersonic maneuvering performance was estimated with the maneuver and cruise configuration test results, respectively. The static maneuvering performance for subsonic/transonic operation is shown in figure 110, and figure 111 presents the results for supersonic operation. The RPRV maneuvering goal is a normal load of $N_Z = 7.3$ for $P_S = 0$ at the design point of $M_\infty = 0.9$ and h = 9144m. The -19 RPRV configuration maneuvering performance status is $N_Z = 6.8$ for $P_S = 0$.

The characteristics and performance of the RPRV, as presented at the preliminary design review (PDR), are compared with the goals, set by the preliminary operating instructions (POI), in table III. A status versus goal evaluation of the fighter concept is also presented in table III.

CONCLUSIONS

The general conclusions of the HiMAT aerodynamic design experience are:

(1) The HiMAT configuration required several major rebaselining efforts partially as a result of the limited scope of the initial program phases in quantifying some of the off-design aspects of the various technologies. In particular, the canard planform changes illustrate the need to closely monitor the stability and control characteristics when integrating the vortex lift phenomena into the design. The wing was revised based upon detailed design investigations, which revealed the proper balance between constraints for viscous and transonic flow considerations and a practical structural requirement. The experience with the HiMAT configuration indicated that the necessary span load contraints should be fully investigated prior to the baseline definition. This requires at least a cursory examination of the circumstances for which low-drag transonic flow is practical, that is, the requirements of the pressure distribution.

(2) A substantial amount of the maneuver design effort involved linear theory. In the future, as more general transonic design and analysis techniques evolve, the extent of the linear theory design utilization should be diminished. At present though, linear theory provides a fast and efficient means of evaluating design requirements for preliminary and detailed design studies. The modifications to the computerized design procedure, necessitated

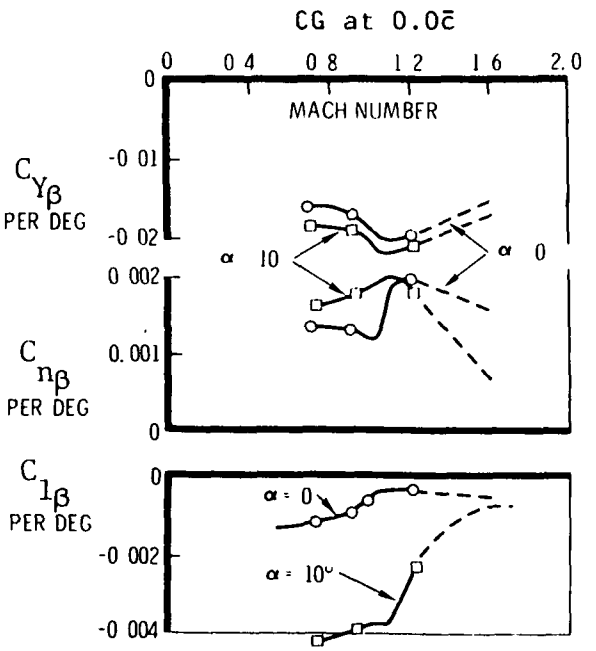

Figuare 109. - Cruise configuration (-19) lateral-directional stability.

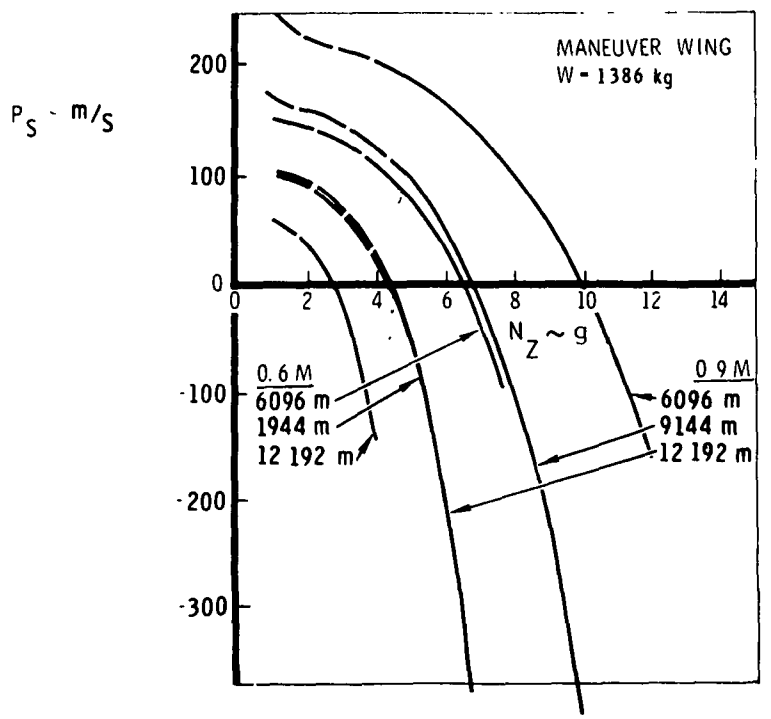

Figure 110. - Transonic maneuver performance.

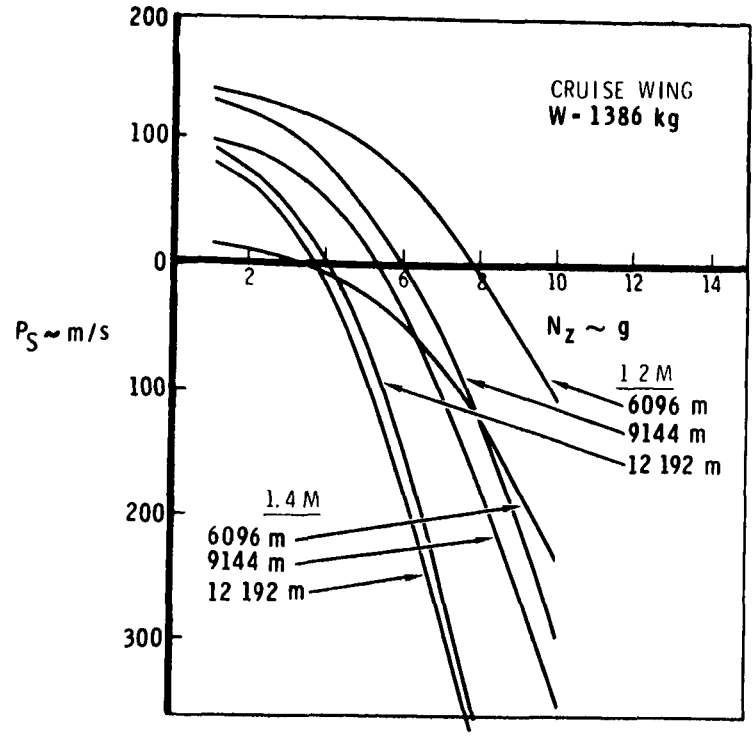

Figure 111. - Supersonic maneuver performance.

TABLE III. - PDR STATUS VERSUS GOAL PERFORMANCE

	Fighter		RPRV	
	Phase II	PDR status	POE (-17A)	PDR status
TOGW (kg)	7740.1	17067 7740.1	1528.6 3371	1528.6
Fuel (kg)	1787.6	3942 1787.6	285.8 630 (19%)	285.8
Combat/research		w/s (13%) 57		
W (kg)	6846.5	6846.5	1385.7	1385.7
W/S (N/m^2)	2423	2423	2525	2525
T/W	.828	.828	.824	.824
Engine	67.4% PW 74-20		100% J 85 GE 21	
T/W (sea level static)	9.11		7.50	
Nozzle type	vectoring 2-D		conventional	
Wetted area (m^2)	125.6	1390 129.1	27.87	30.10
S_{WET}/S_{REF}	4.54	4.66 S_{ref}=29.8ft²	5.17	5.59
Mission radius (n mi)	300	300	25 ✓	25
Research time (min)				
M_∞ = 1.4, h = 12 192 m	-	-	4.06	3.81
M_∞ = 0.9, h = 9144 m	-	-	4.49	4.16
Maneuver performance, h = 9144 m				
P_S at M_∞ = 0.9 8g (m/s)	0	-39.9	-68.6	-100.7
N_Z at M_∞ = 0.9 (g)	8	7.3	7.3	6.77
N_Z at M_∞ = 0.6 (g)	-	4.8	4.1	4.3

by the HiMAT configuration and design objectives, produced a means of properly initializing the maneuver design so that lifting surface efficiency, structural requirements, and off-design performance could be examined and varied in an efficient manner.

(3) The Bailey-Ballhaus transonic analysis, used in an iterative mode, was valuable in achieving the prescribed supercritical pressure distributions for regions of moderate shock sweep. The restrictions of the formulation were partially overcome by relying on a design/test cycle. This was necessary to account for the effects of the canard and evaluate conditions above the design point. The application of the transonic code was generally successful in weakening the shocks for the wing region inboard of 70 percent span. Further weakening of the root shock is desirable but the possible decrease in wave drag cannot be quantified with the present small disturbance formulation in order to evaluate the overall impact.

(4) The restrictions of the three-dimensional transonic analysis were most troublesome for the highly swept, highly loaded outer wing panel. Here the recourse was a two-dimensional/sweep theory initialization aided by a linear theory analysis to verify that constant sectional characteristics prevailed. The sweep theory design is a valid means of determining a pressure distribution that will produce attached flow for moderately tapered regions. Guidance for the transonic implementation of the sweep theory design was principally obtained through analysis of the test data. This was not the most effective design procedure. A more comprehensive set of methodology is required, which would include a multiple-surface transonic design and analysis capability, and a three-dimensional boundary layer analysis.

(5) The transonic drag rise was not entirely eliminated due to premature separation on the winglet and the resulting influence on the outboard wing flow field, and shock-induced separation on the outboard canard. The balancing of requirements for acceptable configuration characteristics at low speeds with the transonic maneuver design reduced the capability for favorable trim effects at the maneuver condition.

(6) For the cruise configuration, the consequences of the utilization of supercritical sections and variable camber was not fully resolved. This was due primarily to the imposed structural (twist) constraint and not a lack of inherent aerodynamic efficiency, although an arrangement without the structural constraints was not tested.

RECOMMENDATIONS

Relative to the design approach, linear theory is still recommended as the primary means of evaluating the design options. More general transonic codes should be developed for future concepts that involve complicated planforms and stringent maneuver goals. Sweep theory is appropriate for establishing a design pressure distribution for moderate taper regions, but a fully three-dimensional transonic solution is required for verification and the elimination of any residual three-dimensional effects.

Additional comparisons between the existing nonlinear codes must be made to examine the numerical solution characteristics to improve computation time and delineate the restrictions relative to flow conditions, geometry, and theoretical consistency. For example, most of the published modified small disturbance solutions are not self-consistent within the order of magnitude analysis from which they are derived.

For the HiMAT/RPRV configuration, the actions required to reduce the drag rise include redesign of the winglet, elimination of the unswept isobars on the canard, and reduction of the inboard wing-root shock for the trimmed condition. A modified small disturbance solution for a wing-winglet configuration similar to the Bailey-Ballhaus classical small disturbance analysis will be required in addition to a wing-canard solution. The latter is necessary to properly characterize the inboard wing-root shock although a wing-alone analysis would provide an approximate design technique if supplemented with test data. For all future analyses, first-order viscous corrections (displacement thickness) should be included.

APPENDIX

WIND TUNNEL MODEL NOMENCLATURE

Notation for the RPRV wind tunnel models is presented for the major configuration components (fuselage, wing, canard, and vertical stabilizer). The wing always includes the upper surface winglet unless stated otherwise.

0.147 Scale:

W_2	-17A maneuver wing, wing-alone design
C_M	-17A canard

0.22 Scale:

B	-18 fuselage, constant cross section at wing intersection
B_2	-18A, -19 contoured fuselage
W_1	-30 wing, subcritical wing-canard-winglet cruise design
W_3	-31 wing, subcritical wing-canard-winglet maneuver design
W_7	-34 wing, revised subcritical wing-canard-winglet maneuver design
W_8	-35 wing, inboard sections designed with three-dimensional transonic code, cruise winglet
W_9	W_8 with 1° incidence relative to body
W_{10}	-36 wing, Garabedian 65-14-08 section normal to midchord element, 1° incidence
W_{11}	-39 wing, scaled Garabedian section 70-11-06, 1° incidence
W_{12}	W_{11} with 0° incidence
W_{13}	W_{11} with outboard wing trailing edge deflected
W_{14}	W_{13} with 0° incidence
W_{15}	-39 cruise wing derived from W_{14}

W_{16}	W_{15} with 1° incidence
W_{17}	-310 maneuver wing with modified, scaled Whitcomb 69-13-08M section on outboard wing, 1° incidence
W_{18}	W_{17} with 0° incidence
W_{19}	-310 cruise wing, derived from W_{18}
W_{22}	-19 configuration cruise wing, W_{19} with lower surface winglets
W_{23}	-19 configuration maneuver wing, W_{18} with lower surface winglets
W_{24}	W_{18} without upper or lower surface winglets
C_1	-40 canard, subcritical wing-canard-winglet cruise design, 63° leading edge sweep
C_2	-41 canard, subcritical wing-canard-winglet maneuver design, 63° leading edge sweep
C_3	Uncambered 45° leading edge sweep canard for low-speed tests
C_4	-42 canard, revised subcritical wing-canard-winglet maneuver design
C_5	-44 maneuver canard, 55° leading edge sweep, -42 camber
C_6	C_5 with reduced outboard camber
C_8	-46 cruise canard derived from -44 maneuver canard
C_9	C_6 with modified outboard camber
C_{10}	-19 configuration maneuver canard (-48), Whitcomb 69-13-08M section normal to 40° sweep element on outboard canard
C_{11}	-19 configuration cruise canard (-48) derived from C_{10}
V	-18, -18A configuration vertical stabilizer
V_9	-19 configuration enlarged vertical stabilizer, NACA 64A004 section

REFERENCES

1. Gloss, B. B. and McKinney, L. W.: Canard Wing Lift Interference Related to Maneuvering Aircraft at Subsonic Speeds. NASA TM X-2897, 1974.

2. Henderson, W. P.: The Effect of Canard and Vertical Tails on the Aerodynamic Characteristics of a Model With a 59° Sweptback Wing at a Mach Number of 0.30. NASA TM X-3088, 1974.

3. Huffman, J. K.: Effect of Vertical-Tail Location on the Aerodynamic Characteristics at Subsonic Speeds of a Close-Coupled Canard Configuration. NASA TN D-7947, 1975.

4. Gloss, B. B.: Effect of Canard Location and Size on Canard-Wing Interference and Aerodynamic-Center Shift Related to Maneuvering Aircraft at Transonic Speeds. NASA TN D-7505, 1974.

5. Gloss, B. B.: The Effect of Canard Leading Edge Sweep and Dihedral Angle on the Longitudinal and Lateral Aerodynamic Characteristics of a Close-Coupled Canard-Wing Configuration. NASA TN D-7814, 1975.

6. Gloss, B. B.: Effect of Wing Planform and Canard Location and Geometry on the Longitudinal Aerodynamic Characteristics of a Close-Coupled Canard Wing Model at Subsonic Speeds. NASA TN D-7910, 1975.

7. Woodward, F. A.: Analysis and Design of Wing-Body Combinations at Subsonic and Supersonic Speeds. J. Aircraft; vol. 5, no. 6, 1968, pp. 528-534.

8. Bonner, E.: The Expanding Role of Potential Theory in the Design of Supersonic Aircraft. J. Aircraft; vol. 8, no. 5, May 1971, pp. 347-353.

9. Ballhaus, W. F. and Bailey, F. R.: Numerical Calculation of Transonic Flow About Swept Wings. AIAA Paper 72-667, June 1972.

10. Lomax, H., Bailey, F. R. and Ballhaus, W. F.: On the Numerical Simulation of Three-Dimensional Transonic Flow With Application to the C-141 Wing. NASA TN D-6933, 1973.

11. Garabedian, P. R. and Korn, D. G.: Analysis of Transonic Airfoils. Commun. Pure & Appl. Math; vol. XXIV, 1971, pp. 841-851.

REFERENCES (Continued)

12. Liepmann, H. W. and Roshko, A.: Elements of Gasdynamics. Wiley, New York, 1957.

13. Krupp, J. A. and Murman, E. M.: The Numerical Calculation of Steady Transonic Flows Past Thin Lifting Airfoils and Slender Bodies. AIAA Paper 71-566, June 1971.

14. Barger, R. L. and Brooks, C. W.: A Streamline Curvature Method for Design of Supercritical and Subcritical Airfoils. NASA TN D-7770, 1974.

15. Bradshaw, P.: Calculation of Three-Dimensional Turbulent Boundary Layers. J. Fluid Mechanics; vol. 46, part 3, 1971, pp. 417-445.

16. Bauer, F., Garabedian, P., Korn, D., and Jameson, A.: Supercritical Wing Sections II, Lecture Notes in Economics and Mathematical Systems. Springer-Verlag, New York, 1975.

17. Boppe, C. W.: Calculation of Transonic Wing Flows by Grid Embedding. AIAA Paper 77-207, January 1977.

18. Jameson, Antony.: Iterative Solution of Transonic Flows Over Airfoils and Wings, Including Flows at Mach 1. Commun. Pure & Appl. Math; vol. 27, 1974, pp. 283-309.

19. Schmidt, W.: Progress in Transonic Flow Computations Analysis and Design Methods for Three-Dimensional Flows. VKI Lecture Series 87: Computational Fluid Dynamics, von Karman Institute for Fluid Dynamics, Rhode-St.-Genese, Belgium, March 15-19, 1976.

20. Cebeci, T., Kaups, K., Ramsey, J., and Moser, A.: Calculation of Three-Dimensional Compressible Boundary Layers on Arbitrary Wings. Aerodynamic Analyses Requiring Advanced Computers Part I; NASA SP-347, 1975, p. 41.

~~G. Hyder A 241/33/23123~~ 10 SEP 796

17 MAR 80 ER Hudson Guthrie 345/26/Rm. 270

14 OCT 82 A ~~W. G. Price 345/32/2/255/36482~~ 16 SEP 33

R. L. Swengle 341/33/6

87 OCT 87 Kevin Keller 341/2708/2/425/21852 1989 JUL 28

9/20/90 Tom Lacey - 341/32/034380